Grant Agreement Number: 101014517
Project Acronym: AB4Rail
Project title: Alternative Bearers for Rail

DELIVERABLE D [2.4]
[Experimental assessment of the most promising ABs]

Project acronym:	AB4Rail
Starting date:	01-01-2021
Duration (in months):	24
Call (part) identifier:	S2R-OC-IP2-02-2020
Grant agreement no:	Number 101014517 – IP/ITD/CCA - IP2
Grant Amendments:	N/A
Due date of deliverable:	1-06-2022
Actual submission date:	12-08-2022
Coordinator:	Franco Mazzenga (RDL)
Lead Beneficiary:	Radiolabs (RDL)
Version:	0.1
Type:	Report
Sensitivity or Dissemination level[1]:	PU
Contribution to S2R TDs or WAs[2]	TD2.1
Taxonomy/keywords:	Adaptable Communication System; ACS; Alternative Bearers; Free Space Optics; Low Earth Orbit High Throughput Satellite; High Altitude Platform System; performance assessment.

---

[1] PU: Public; CO: Confidential, only for members of the consortium (including Commission Services)

[2] https://projects.shift2rail.org/s2r_matrixtd.aspx

Authors Table

Name	Affiliation	Contribution
Alessandro Vizzarri	Radiolabs (RDL)	Main contributor
Franco Mazzenga	Radiolabs (RDL)	Support on LEO analysis and simulation
Romeo Giuliano	Università degli Studi Guglielmo Marconi (USGM)	Support on HAPS analysis and simulation.
Anna Maria Vegni	Roma Tre University	Support on FSO analysis

The document history table provides a summary of all the changes in reverse chronological order (the latest version first).

Document history

Date	Name	Affiliation	Position/Project Role	Action/ Short Description
12 August 2022	Alessandro Vizzarri	Radiolabs (RDL)	Technical Manager	Description of experimental assessment for FSO, LEO Satellite and HAPS.

Disclaimer

The information in this document is provided "as is", and no guarantee or warranty is given that the information is fit for any particular purpose. The content of this document reflects only the author's view – the Shift2Rail Joint Undertaking is not responsible for any use that may be made of the information it contains. The users use the information at their sole risk and liability.

Table of Contents

Executive Summary

In this Deliverable D2.4 "Experimental assessment of the most promising ABs" of the "Alternative Bearer for Rail" (AB4Rail) project, we aim to provide the performance assessment of the eligible ABs, as defined in D2.3 i.e., FSO, HAPS, and LEO. We provide the main outcomes in case of static and dynamic railway scenarios, where different ABs take place. The document details the setup and results obtained from simulation and emulation of the eligible ABs using the tools in our labs.

For each of the eligible technology we considered its maturity and its availability of the market. FSO is mature for static environment, but many advances are required for dynamic scenarios. Concerning LEO, some devices are available but the subscription to a connectivity is required for performing tests on the field and operators do not guarantee the coverage in Europe or the service itself. Finally, HAPS deployment is limited to preliminary experimental settings and no one of them has been used to realize devices that could be used by one or more HAPS operators to start a commercial service. Then some simulations in lab have been conducted to their assessment. To this aim, we considered a realistic environment (also used in the D2.3) related to the mainline Rome-Florence with a real speed profile of the train. Specifically, FSO technology is the sole one that well fits into the static scenarios (i.e., the train station) due to its technical features and the impact on the railway sector. As main outcome, we can observe that shorter FSO links allow for achieving lower BER, as well as a degradation of link performance increases in case of additional attenuation losses. Finally, in case of dynamic scenarios i.e., mainline, regional, and freight, we will consider a fixed FSO source and a receiver moving following a path, so that variable FSO link lengths are achieved. A more realistic dynamic scenario has been investigated, comprised of a single and double beam model, where multiple FSO transmitters are accordingly deployed along the railway track. With these schemes, we can demonstrate more stable connectivity links that do not overcome fixed lengths, thus guaranteeing stable link performance. Regarding the LEO constellations, Starlink SpaceX and OneWeb constellations are considered. When the LEO satellite is visible from the ground station, a quite constant satellite service level is evidenced in all situations. It is fully compliant with the Network-as-a-Service (NaaS), already discussed in the previous D2.3 deliverable. For each LEO satellite beam, an aggregated traffic capacity of around 1 Gbps can be provided. This considerable amount of capacity is very important to manage a huge amount of data, as foreseen in specific ACS traffic classes, especially in tomorrow's situation (e.g., for video data application in uplink). This makes the LEO technology as a very interesting and competitive AB with the terrestrial communication technologies (e.g., 5G). Another important implication regards the possibility of assuring greater reliability of the connections, managing the corresponding QoS/QoE levels, and reducing the re-transmissions in case of failures, especially in the case of mission-critical applications. The HAPS is currently used as a physical asset hosting the LTE eNB, and in the future the 5G gNB. HAPS has a reduced altitude from the ground (at 19 km), and it can be assumed almost a static system (affected by a few oscillations). In the three different frequency bands (identified by the ITU-R P.528 propagation model), the traditional UE gives a poor performance in B1 (694–960 MHz) in terms of MCS adoption and the corresponding available spectral efficiency. From simulations, it emerges the opportunity to use a dedicated enhanced User Equipment (UE) with higher antenna gain and transmission power, able to use more efficient Modulation and Coding Schemes (MCS).

The results evidence the applicability of FSO, LEO, and HAPS to be used as ABs for ACS applications in railway scenarios. Their technical feasibility allows having a huge capacity for data transmission. This is very important, especially for the bandwidth-consuming ACS applications in tomorrow's railway scenarios.

List of abbreviations, acronyms, and definitions

Acronym	Definition
AB	Alternative Bearers
ACS	Adaptable Communication System
ATPC	Automatic Transmit Power Control
AWGN	additive white Gaussian noise
BER	Bit-Error-Rate
CCDF	Complementary Cumulative Distribution
CDF	Cumulative Density Function
DL	Downlink
DVB-S2	Digital Video Broadcasting - Satellite - Second Generation
EIRP	Effective Isotropic Radiated Power
eNB	Evolved Node B
FSO	Free Space Optics
FSPL	Free Space Path Loss
GG	Gamma-Gamma
GS	Ground Station
GSMA	Global System for Mobile Communications
GUI	Graphical User Interface
HAPS	High Altitude Platform System
HDTV	High-Definition TV
ITU	International Telecommunication Union
KPI	Key Performance Indicator
LEO	Low Earth Orbit
LN	Log-Normal
LoS	Line of Sight
MCS	Modulation and Coding Scheme
NORAD	North American Aerospace Defense Command
OOK	On Off Keying

QAM	Quadrature Amplitude Modulation
QoE	Quality of Experience
QoS	Quality of Service
RBC	Radio Block Center
RP	Reference Point
SINR	Signal to Interference & Noise Ratio
SNR	signal-to-noise-ratio
SNR	signal-to-noise ratio
TB	Traditional Bearer
TLE	Two Line Element
TRL	Technical Readiness Level
UE	User Equipment
UL	Uplink

List of Figures

List of Tables

1. Introduction

This document constitutes the Deliverable D2.4 "Experimental assessment of the most promising ABs" according to Shift2Rail Joint Undertaking programme of the project titled "Alternative Bearer for Rail" (Project Acronym: AB4Rail, Grant Agreement No 101014517 — IP/ITD/CCA — IP2). On 22nd July 2020, the European Commission awarded a grant to the AB4Rail consortium of the Shift2Rail / Horizon 2020 call (S2R-OC-IP2-02-2020). AB4Rail is a project connected to the development of a new Communication System planned within the Technical Demonstrator TD2.1 of the 2nd Innovation Programme (IP2) of Shift2Rail JU: Advanced Traffic Management & Control Systems.

The IP2 "Advanced Traffic Management & Control Systems" is one of the five asset-specific Innovation Programmes (IPs), covering all the different structural (technical) and functional (process) sub-systems related to control, command, and communication of railway systems.

1.1 Purpose and scope of the document

This document aims to provide an experimental assessment of the eligible ABs, as defined in D2.3 i.e., FSO, HAPS, and LEO. We provide the main outcomes in case of static and dynamic railway scenarios, where different ABs take place. The document details the setup and results obtained from lab/experimental assessment of the most promising ABs.

1.2 Document organization

The document is organized according to AB4Rail Grant Agreement Number 101014517 (RD-1) and AB4Rail Consortium Agreement (RD-2). The document is structured as follows.

Section 2 describes the methodology adopted to assess an experimental assessment of the eligible ABs, while Section 3 the commercial availability of selected ABs technologies through deep technological scouting. In Section 4 how the selected ABs technologies are applied to the considered railway scenarios. Section 5 details the simulations regarding the Free Space Optics (FSO), in terms of system architecture, modeling and results. Following the same structure of Section 5, Section 6 is focused on Low Earth Orbit Satellites (LEO) and Section 7 on High Altitude Platform Systems (HAPS). Finally, Section 8 draws the main conclusions and findings. Appendix A provides information about the radio propagation models used during the simulation activities.

1.3 Reference Documents

Table 1: Reference Documents.

Document Number	Document Description
RD-1	AB4Rail Grant Agreement Number 101014517 - IP/ITD/CCA - IP2
RD-2	AB4Rail Consortium Agreement

2. Adopted Methodology

The approach defined in AB4Rail regarding the simulation/emulation and experimental activities is shown in Figure 1 [1].

Figure 1. AB4Rail methodology for AB experimental assessment
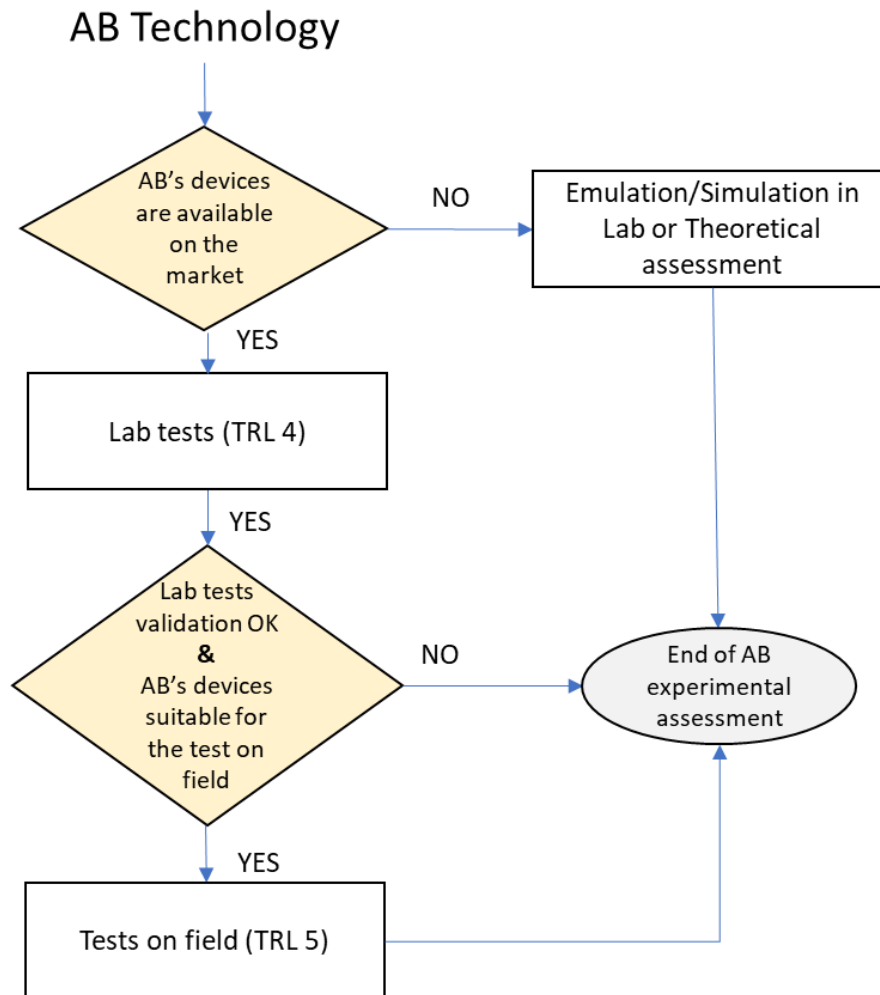
If the AB device is available in the market, the tests can be carried out in lab in order to assess them with a Technology Readiness Level (TRL) 4. After a successful validation in lab and the AB devices are ready for the field trials, the test activities on field will be arranged in order to assess the AB devices with a TRL 5.
If the AB device is not available in the market, the simulation/emulation activities with a theoretical assessment can be only performed in lab.

In particular, after the AB eligibility analysis performed in the deliverable D2.2, the results show the most promising AB are: Free Space Optics (FSO), Low Earth Orbit (LEO) and High Altitude Platform Systems (HAPS) technologies.

For this reason, the adopted methodology is described in Figure 2.

Figure 2. AB4Rail simulation/emulation methodology.

1	• Technology scouting: (i) scouting of available devices for the selected ABs, (ii) feasibility study for D2.4
2	• Simulation
3	• Result analysis
4	• Outcomes and findings
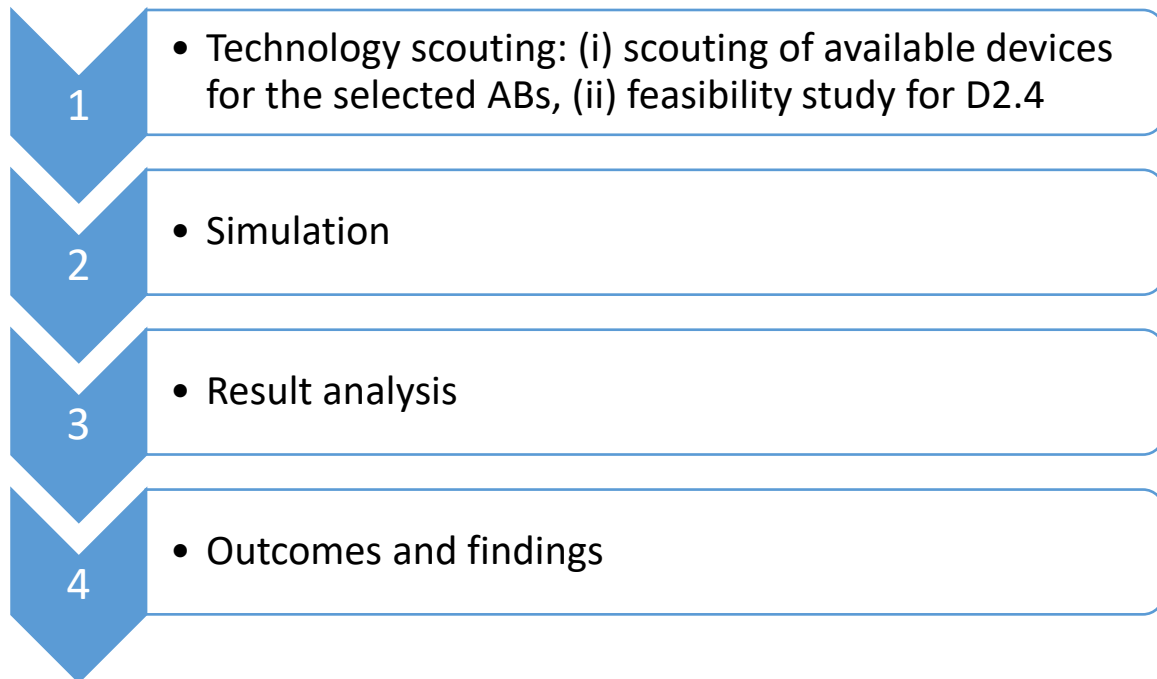
3. Commercial availability of selected ABs technologies

3.1 Free Space Optics

The manufactory world related to Free Space Optics (FSO) technologies is huge and comprised of several companies dealing with Optical Wireless Communications. Figure 3 collects the main manufactories of FSO devices available on the worldwide market. In order to identify commercial devices to be used for experimental purpose, we have selected and contacted several companies' leaders in FSO manufactory, such as CableFree, EC System, SA Photonics, and SONABEAM. As a result of this scouting activity, the FSO devices available on the market are specifically designed for applications in static scenarios only (*i.e.*, to create high-capacity fixed point-to-point links), and are not suitable for mobile transmissions. Indeed, even if the auto-tracking system is available on the most of FSO devices and compensates very slow movements of the structure on which the transmission unit is fixed, this is not capable to compensate high frequency vibrations, as occurring in case of mobile scenarios especially in railways.

Figure 3. Schematic of main manufactures of Optical Wireless Communications: [left] Infra-Red (IR)/Visible Light Communication (VLC); [Right] FSO.

For instance, CableFree uses directional beams of Infrared light for communication. It exploits the Automatic Transmit Power Control (ATPC), which is an advanced product feature allowing the transmitted optical power to be automatically adjusted to ensure that the optimum power level is received at the remote terminal. Sophisticated software within each FSO unit continuously monitors remote power levels using the unique CableFree out-of-band telemetry system and adjusts power by up to 12 dB (16x). Received Signal Strength Indicator (RSSI) variations can be caused by weather effects such as fog, heavy rain, snow or dust storms and also thermal effects, bracket movement and long-term drift. Low RSSI means degraded signal-to-noise-ratio (SNR) at the optical receiver, resulting in degraded Bit-Error-Rate (BER), in severe cases causing packet loss and reduced throughput in data networks.

ATPC enabled in identical conditions shows almost no variation in the received power. The controller automatically adjusts the transmitted power levels to ensure optimum signal received at both ends of the link.

Notice that even in case of full availability of FSO devices tailored for static scenarios, they are very expensive (*e.g.*, around 12 kEuro for the EC System EL-1G model, which provides 1 Gbps full-duplex for distances up to 4.4 km, as depicted in Figure 4) [2]. Furthermore, in order to adapt the FSO available devices to a mobile scenario, significant engineering development and testing would be needed. The cost to finalize development has been estimated (with actual technologies) in the millions of euros, which are clearly not affordable in the AB4Rail project.

From this preliminary scouting activity related to FSO technology, we have derived the following considerations:

FSO is a mature technology for static scenarios, such as fixed point-to-point connectivity links in Line of Sight (LoS) mainly used in outdoor scenarios to connect buildings at distance of a few kilometers, and more in general for Gigabit Ethernet LAN-LAN segments, last-mile network connections, Storage Area Networks, and HDTV Outside Broadcast Links.

Due to the lack of reliable and efficient auto-tracking system in mobility scenarios, FSO as AB is suitable for station and yard railway scenarios only, where mobility is very limited or absent.

FSO AB is still in its infancy for rail dynamic scenarios, such as mainline, regional, and freight, and available devices cannot be adopted in such scenarios with a guaranteed connectivity.

Leveraging on the above considerations, at the moment of this writing, we can conclude that an extended simulation campaign modeling FSO links, both in static and mobility scenarios, can be useful for our purpose of assessing the performance of FSO AB in realistic railway scenarios.

Figure 4. Data sheets of EL-1GL FSO device by EC System.

EC SYSTEM INTERNATIONAL a.s.
Na Výsluní 201/13
Telefon: +420 277 270 152
IČO 28612744
DIČ CZ28612744
www.ecsystem.cz

EC SYSTEM

EL-1GL ← up to 4400m distance →

✓ Throughput 1 Gbps
✓ Double channel technology with backup power supply voltage 48V DC (optionally)
✓ Built-in service channel
✓ Autotracking system (targeting and aiming)
✓ IP monitoring
✓ Aerodynamic protective cover

Bandwidth, Mbit/s	1250 Full Duplex
Wavelength, nm	1550
Basic interfaces	1x 1G SFP
Fade margin at a distance of 1 km,dB	40
Latency time of optical channel, ms	< 0,005
Links distance, m for availability 0,999	4400
Method of keep link direction	Autotracking system
Laser safety IEC 80625	1M
Power supply	DC 48+- 12V
Category temperature range of outdoor units, C	-40…+50
Dimensions, mm outdoor unit	480x285x300
Weight, kg outdoor unit	9,4
Management, monitoring	UDP (firm software), SNMP traps, MIB file
OU indication	Power, link signals, link direction
Service connection	10/100 Base-TX, RJ45

3.2 Low Earth Orbit (LEO) Satellites

The scouting of LEO devices is mainly focused on the available LEO constellations, such as Starlink SpaceX and Oneweb. These LEO satellite operators are already providing the LEO service, but from a rail trial point of view several issues are to be managed. Starlink SpaceX and Oneweb

constellations are going to be expanded in terms of coverage. Both LEO satellite providers offer a complete modem kit including the satellite terminal and the antenna [3][4], as shown in Figure 5. These external devices should be installed on board of the train with a direct impact on the certification procedures.

Figure 5. LEO satellite kit: SpaceX (a), OneWeb (b).

(a)   (b)
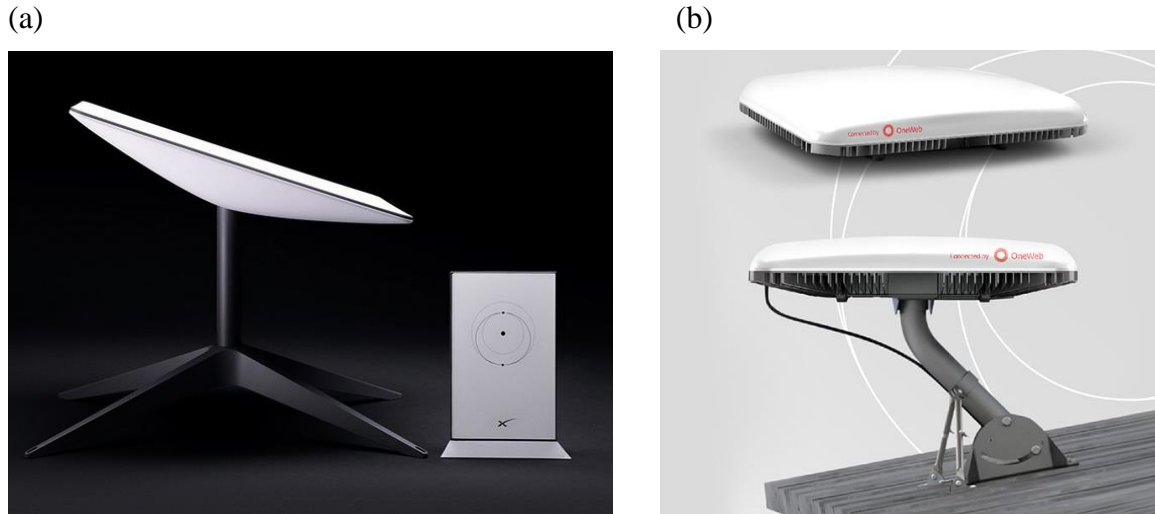
A commercial LEO service subscription is also needed. At the moment of this writing the Starlink service has not started, yet. It is envisaged it will start at the start of 2023 and we don't know if Europe will be covered due to the fact that European satellite gateways at the ground are still under construction (see after).

Finally, LEO technologies are not available in some situations, such as when the train is inside the galleries or even in some railway scenarios including stations and very large stations with roofs covering the rail tracks.

For these reasons the assessment of LEO HTS (High Throughput Satellite) technologies will be carried out using a simulated approach using well tested satellite tools as detailed in the following of this document. We would like to suggest to E2Rail to launch a new two-years (2023-2024) experimental project to evaluate on the field the feasibility of using the SpaceX constellation-based LEO satellites for railway communications.

3.3 High Altitude Platform Systems (HAPS)

In order to conduct experiments on HAPS the involvement of a third party acting as the HAPS operator is required. The HAPS are systems hosting the telco network nodes to offer backhauling links between satellite and terrestrial networks and several and different HAPS technologies have been studied and proposed up to now, as shown in Figure 6 [5].

Figure 6. Different HAPS technologies.

However, their deployment has been limited to preliminary experimental settings and no one of them has been used to realize devices that could be used by one or more HAPS operators to start a commercial service. To the best of our knowledge, at the moment, no HAPS operator and no commercial transmission services based on HAPS is available worldwide. Thus, even in the HAPS case only simulation and theoretical analysis can be performed for assessing their effectiveness in railway scenarios.

According to the HAPS Alliance [6] and to GSMA with paper [7], the HAPS systems seem to be a very promising technology offering several opportunities to the terrestrial telco operators and to unmanned aircraft use.

4. Selected ABs technologies and railway scenario

In this section, we will introduce the simulation tools, developed for the assessment of performance of eligible ABs, in case of different railway scenarios and configuration:

- Station: for railway applications in static conditions
- Mainline: for railway applications in static conditions. We identified the Rome-Florence railway line as the reference case [8].

According to the main features of the eligible ABs (FSO, LEO and HAPS), we considered two main railway scenarios, where eligible ABs can be used, and we distinguish the case of presence and absence of mobility. Specifically, we consider (*i*) a static scenario, such as station railway scenario, and (*ii*) rail dynamic scenarios, such as mainline, regional and freight.

The three eligible ABs can be applied in different contexts. FSO technology is suitable for both of station and mainline. Instead, LEO and HAPS are only eligible for dynamic railway scenarios (e.g., mainline). In the static railway scenarios, both LEO and HAPS could be not applicable because of possible obstructions of the corresponding radio links due to the shelters in the rail platforms.

In the following we illustrate several simulation results concerning the performance of FSO in both static and dynamic scenarios. For HAPS and LEO performance have been carried out only in case of dynamic scenarios. Table 2 collects the different simulated scenarios and the corresponding ABs that have been analyzed. Due to the eligibility analysis carried out in D2.3, notice that in the static scenario, we limited our simulation assessment to FSO.

Table 2: Applicability of ABs into different simulated scenarios.

Scenario	FSO	HAPS	LEO
Static (station)	✓	N/A	N/A
Dynamic (mainline, regional, and freight)	✓	✓	✓

In the static scenario, we assume no mobility occurs and connectivity links are static, with a transmitter and a receiver placed at given known positions; in rail dynamic scenarios, we assume mobility is present and can affect link performance (*i.e.*, link variability and maintenance). In the latter case, we consider dynamic radio links, with transmitter-receiver distances that can vary with time and so the path loss.

5. Free Space Optics

5.1 Considered scenarios

The Figure 7 and Figure 8 depict the system architectures of the considered scenarios that will be simulated sections. Specifically, in the station railway scenario, we assume both the FSO transmitter, and the photodetector are mounted on the top of the train and are held in fixed positions. For this scenario, we assume the FSO connectivity link is stable and does not suffer for mobility issues and no vibrations and significant thermal changes. This situation well reflects the realistic scenario of FSO connectivity links, which work efficiently for static scenarios. In case of dynamic scenario, Figure 8 describes a train moving along the railway track while it is connected to a fixed FSO transmitter. We observe that if the train is approaching the FSO transmitter, the connectivity link will show different distances and then we can expect different attenuation losses. More in detail, in the next sections, the dynamic scenario will be also enhanced through a variable deployment of multiple FSO transmitters, in order to guarantee "almost-fixed" connectivity links along the railway track.

Figure 7. System architecture for the static scenario. Both the FSO transmitter and the photodetector are in fixed positions.
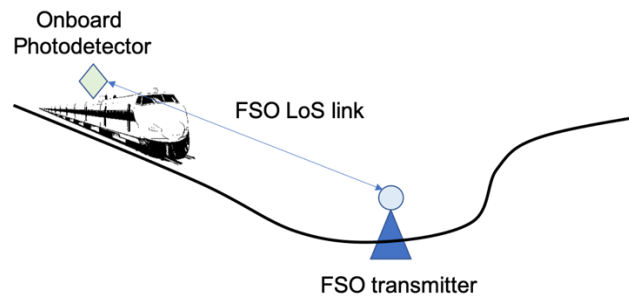
Figure 8. System architecture for the dynamic scenario. A fixed FSO transmitter is connected to a mobile photodetector mounted on a train, then causing (a-b) variable connectivity link lengths.
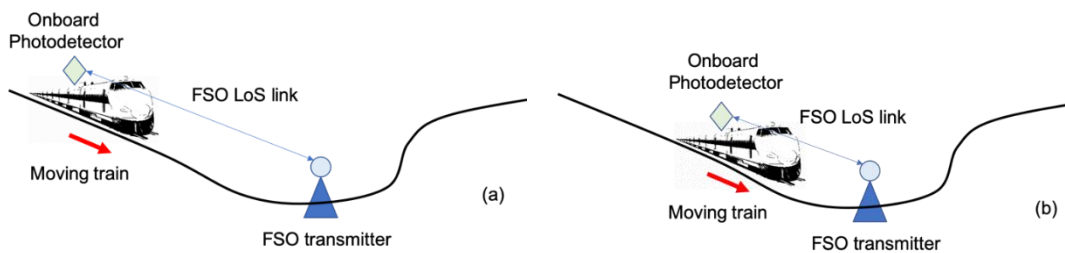
In order to render the railway scenarios more realistic we also considered the train railway-speed profile as previously introduced in AB4Rail D3.3 Deliverable. Specifically, we assume different lengths of railway segment, and for each of them we have the corresponding maximum allowed

train speed, together with the acceleration and deceleration values. Figure 9 depicts the considered train speed profile versus time along different railway segments, considering a time window of ≈ 35 minutes; specifically, we can obtain the travelled distance versus time profile as shown in Figure 10.

Figure 9. Simulated train speed profile vs. time. Railway segments are identified by markers.
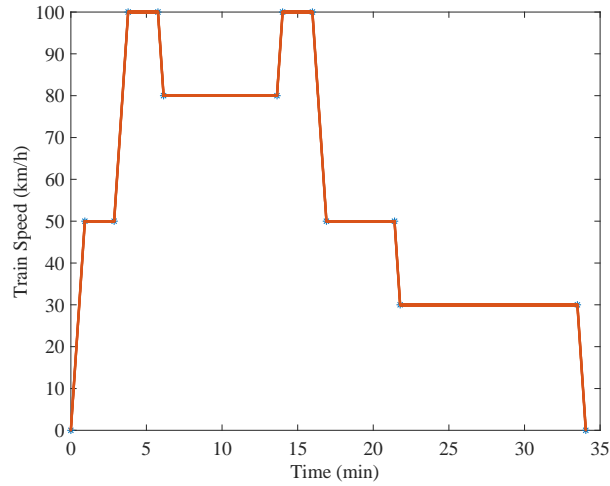
Figure 10. Distance travelled by a train vs. a given time window in accordance with the time-vs-speed profile in Figure 9.
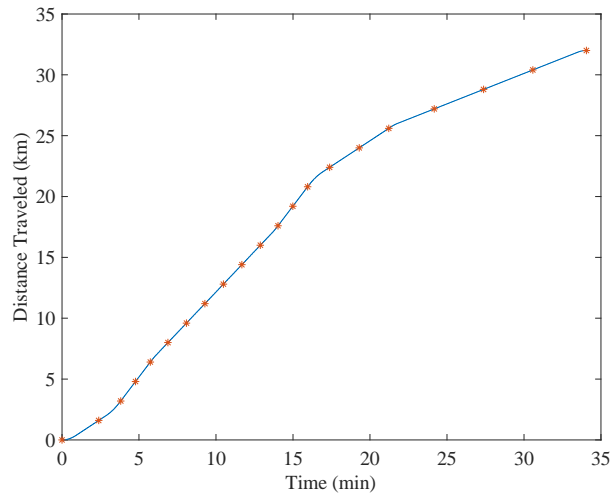
5.2 Overall System architecture

In this section, we introduce the design of our MatLab simulator for the performance evaluation of FSO connectivity links. It is comprised of different component blocks, each of them developing a task in the overall end-to-end FSO connectivity link. Specifically, we assume a laser source sending a data flow toward a photodetector receiver, at a fixed distance. The data transmission occurs along

a free space optical channel, where we can introduce different attenuation models in order to depict a realistic scenario with atmospheric attenuation loss.

The system block diagram of the simulation procedure is illustrated in Figure 11, and it includes the following blocks:

1. **Data source**: this is the first step for data transmission and considers the generation of a flow of random binary bits *i.e.*, random input data for the FSO system. The generated bits are then resampled and converted in electrical signal;

2. **Electrical/optical (E/O) converter**: Knowing the average output optical power P and extinction ratio ε, we compute the high and low power levels, corresponding to bits 1 and 0 considering the On Off Keying (OOK) modulation;

3. **Free space optical channel**: in this block, we calculate the channel coefficients, which are then multiplied by the optical power generated from step 3. The outcome is the optical received power at the receiver side. The channel coefficients depend on the given scenario modeled, such as a clean channel where no attenuation is considered or a turbulence/fog channel where atmospheric attenuation loss is introduced. We will deeply describe the different channel attenuation models in the next sections, according to the theoretical models introduced in [9];

4. **Optical to electrical (O/E) converter**: in this block, we convert the received optical power to electrical signal. We also consider the presence of additive white Gaussian noise (AWGN), modeled by means of a random normal distribution with mean value 0 and variance as the square root of noise power;

5. **Received binary bits**: A threshold level is set based on the average value of the received electrical signal. By comparing the midpoint of each received bit with the threshold, the received bit is determined to be 0 or 1.

Figure 11. System block diagram of the data transmission link from an FSO laser source to a photodetector receiver.
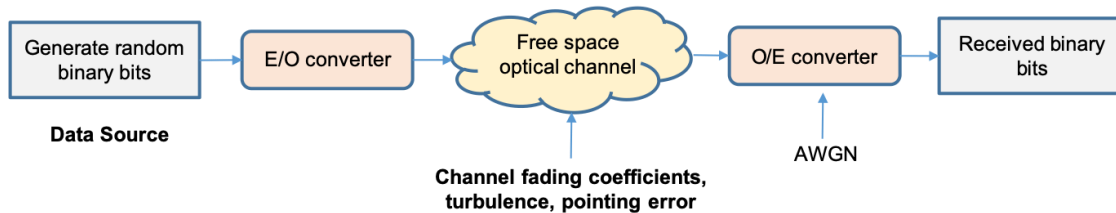
Our Matlab simulator presents a simple Graphical User Interface (GUI) where the user can set different configuration parameters. For instance, we can setup the FSO link length, the input power with OOK modulation, and define the channel fading coefficients based on (*i*) turbulence attenuation, (*ii*) pointing error, and (*iii*) fog/smoke attenuation. Specifically, for different setups, a dropdown menu is displayed, as depicted in Figure 12. In our simulator, it is possible to choose different FSO link lengths (*i.e.*, in the range [500, 1500] m). A similar approach is used for the

attenuation channel, and a warning window appears for different attenuation channel models we aim to introduce.

Figure 12. Flowchart of the simulated blocks for a FSO data link.
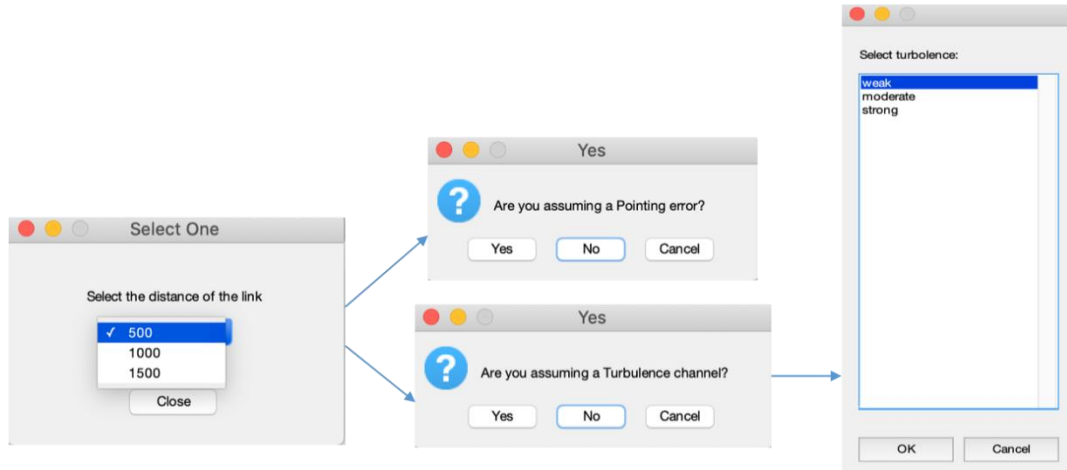
5.3 Considered models

5.3.1   The atmospheric turbulence models

There exist different atmospheric turbulence models that try to describe the attenuation loss resulting from atmospheric variations. Indeed, solar radiation absorbed by the earth's surface causes air around the earth's surface to be warmer than that at higher altitude. This warmer air layer results as less dense and rises to mix turbulently with the surrounding cooler air, then causing the air temperature to fluctuate randomly. Turbulence can cause air inhomogeneities, which can be viewed as discrete cells, namely eddies, of different temperature, acting like refractive prisms of different sizes and indices of refraction.

The Figure 13 depicts the atmospheric channel with turbulent eddies, which introduce random distortion to an input wave that is propagating along the channel [9]. Specifically, the smallest and the largest of the turbulence eddies are indicated as l_0 and L_0, typically of the order of a few millimeters and several meters, respectively. These eddies work as weak lens and result in a randomized interference effect between different regions of the propagating beam. As a result, an output wave will be affected by a randomized interference effect between different regions of the propagation beam, then causing the wavefront to be distorted in the overall process. Specifically, the interaction between the laser beam and the turbulent medium results in the scintillation effect of the optical beam, which results in fading of the received optical power, and then a system performance degradation.

Notice that the scattering effect caused by the turbulent eddies does not result in loss of energy from the beam. This assumption is valid for plane and spherical waves, considering the plane wave is generally applicable to laser beams propagating over a long distance.

In atmospheric turbulence, an important parameter for characterizing the amount of refractive index fluctuation is the index of refraction structure parameter C_n^2 introduced by Kolmogorov, as a function of the wavelength, the atmospheric altitude, and the temperature. A commonly used model to describe C_n^2 is the Hufnagel-Valley, which defines C_n^2 according to the level of turbulence $i.e.$, weak, moderate, and strong. Specifically, for the link near the ground level C_n^2 is taken to be ~1.7 $\times$ 10^{-14} and ~8.5 $\times$ 10^{-15} m$^{-2/3}$ for during daytime and at night, respectively. Also, C_n^2 typically ranges from 10^{-12} m$^{-2/3}$ to 10^{-17} m$^{-2/3}$ for the strong turbulence and weak turbulence, respectively, with a typical average value being 10^{-15} m$^{-2/3}$ for moderate turbulence level.

There exist two models for describing the probability density function (pdf) of the irradiance fluctuation in a turbulent atmospheric channel $i.e.$, (i) Log-Normal (LN) and Gamma-Gamma (GG) turbulence models.

In the region of weak fluctuations, the irradiance pdf $p(I)$ can be well modeled by means of the LN distribution, which can be expressed as

$$p(I) = \frac{1}{\sqrt{2\pi\sigma^2}}\frac{1}{I}\exp\left\{-\frac{\left[\ln\left(\frac{I}{I_0}\right) - E[l]\right]^2}{2\sigma^2}\right\},$$

where $E[l]$ denotes the expectation of l and σ^2 is the log-irradiance variance, commonly referred to as the Rytov parameter, defined as $\sigma^2 = 1.23 C_n^2 k^{7/6} L_p^{11/6}$, where k is the wavenumber and L_p is the horizontal distance travelled by the optical radiation.

The GG turbulence model is based on the modulation process where the fluctuation of light radiation traversing a turbulent atmosphere is assumed to consist of small-scale (scattering) and large-scale (refraction) effects. Both small- and large-scale eddies are assumed to be modeled by

means of Gamma distribution, and consequently, the normalized received irradiance I is defined as the product of two statistically independent random processes I_x and I_y, respectively, that is $I = I_x I_y$. They both arise from the large-scale and small-scale turbulent eddies, respectively, and both follow the gamma distribution whose pdfs are as follow:

$$p(I_x) = \frac{\alpha(\alpha I_x)^{\alpha-1}}{\Gamma(\alpha)} \exp(-\alpha I_x), \quad \text{with } I_x > 0; \ \alpha > 0$$

$$p(I_y) = \frac{\beta(\beta I_y)^{\beta-1}}{\Gamma(\beta)} \exp(-\beta I_y), \quad \text{with } I_y > 0; \ \beta > 0$$

By means of mathematical manipulation, we can derive the following GG irradiance distribution function *i.e.*,

$$p(I) = \frac{2(\alpha\beta)^{(\alpha+\beta)/2}}{\Gamma(\alpha)\Gamma(\beta)} I^{(\alpha+\beta)/2-1} K_{\alpha-\beta}\left(2\sqrt{\alpha\beta I}\right),$$

where α and β represent the effective number of large- and small-scale eddies of the scattering process, respectively. Also, $K_n(\cdot)$ is the modified Bessel function of the second kind of order n and $\Gamma(\cdot)$ is the gamma function. If the optical radiation at the receiver is assumed to be a plane wave, then the two parameters α and β that characterize the irradiance fluctuation pdf are related to the atmospheric conditions, respectively according to the following equations:

$$\alpha = \left[\exp\left(\frac{0.49\sigma^2}{(1+1.11\sigma^{12/5})^{7/6}}\right) - 1\right]^{-1},$$

$$\beta = \left[\exp\left(\frac{0.51\sigma^2}{(1+0.69\sigma^{12/5})^{5/6}}\right) - 1\right]^{-1}.$$

To summarize, we can express the channel impulse response in case of LN and GG turbulence models, respectively as follows

$$h_T = \begin{cases} h_{T,LN} \\ h_{T,GG} \end{cases}$$

where $h_{T,LN} = \exp(2I)$ and $h_{T,GG} = \frac{1}{\alpha\beta} I_x I_y$ are the channel impulse responses in case of LN and GG turbulence models, respectively.

5.3.2 Fog/smoke attenuation model

The attenuation loss due to fog particles is due to the reduction of the visibility near the ground [9]. Different types of fog result in different levels of optical losses, and these are mainly due to the distribution of the fog particles, their size, and location. Specifically, fog level varies from dense o light fog, corresponding to visibility ranging from 50 up to 770 m. In case of dense fog, the attenuation is 315 dB/km, while it decreases to 18.3 dB/km in case of light fog.

The fog/smoke attenuation model is represented according to the following equation

$$h_{FS} = \exp(-\beta L),$$

where L [m] is the link length and β is a parameter defined as

$$\beta = \frac{-\ln 0.02}{V}\left(\frac{\lambda}{550}\right)^{-q}$$

with V [m] as the visibility, λ [m] as the wavelength and q defined as

$$q = \begin{cases} 1.6 & \text{for } V > 50km \\ 1.3 & \text{for } 6km < V < 50km \\ 0.16V + 0.34 & \text{for } 1km < V < 6km \\ V - 0.5 & \text{for } 0.5km < V < 1km \\ 0 & \text{for } V < 0.5km \end{cases}$$

5.3.3 Pointing error

The pointing error occurs when there is a lack of perfect alignment of the laser transmitter and the receiver [9]. Of course, for short FSO links (*i.e.*, <1 km), this might not be an issue, but for longer link ranges, this can certainly not be neglected. The causes of misalignments are mainly due to building sway or strong wind effects on the FSO link head stand, thus affecting the FSO link performance.

Figure 14 shows the receiver aperture and a laser beam footprint at the receiver's transverse plane. We assume the laser source has a Gaussian beam profile and the photodetector is circular with aperture radius a. It follows that the power loss h_p due to an instantaneous radial displacement r between the beam centroid and the detector center is given as

$$h_p = A \exp\left(-\frac{2r^2}{w_{eq}^2}\right)$$

where w_{eq}^2 is the equivalent laser beamwidth at the receiver and A is the fraction of power collected by the detector when there is no pointing error (*i.e.*, $r = 0$).

If we consider that the elevation and horizontal displacement components of the radial displacement r are independent and identically distributed Gaussian random variables, then the radial displacement r at the receiver can be modelled according to a Rayleigh distribution, whose probability density function (pdf) is given by:

$$f(r) = \frac{r}{\sigma_s^2}\exp\left(-\frac{r^2}{2\sigma_s^2}\right)$$

where σ_s^2 is the jitter variance at the receiver. By combining the last two equations, we obtain, the pdf of power loss due to pointing error can be expressed as follows:

$$f_{h_p}(r) = \gamma^2/(A_0)^{\gamma^2}(h_p)^{\gamma^2-1},$$

with $0 \leq h_p \leq A_0$, and $\gamma = w_{eq}/2\sigma_s$ as the ratio of the equivalent beamwidth at the receiver to the pointing error displacement standard deviation.

Figure 14. Misalignment between the receiver aperture and a laser beam footprint.
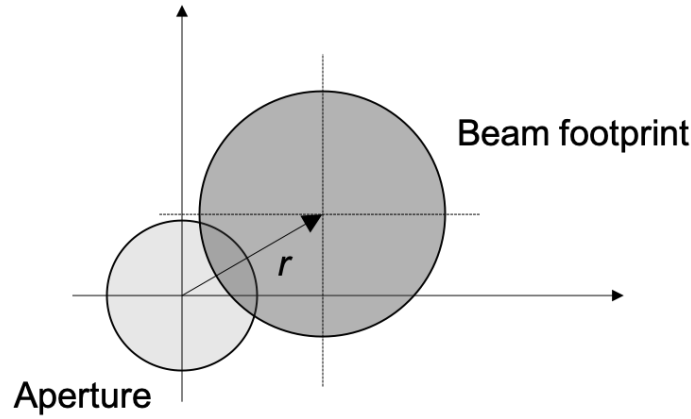
After describing the main attenuation models that introduce power loss due to atmospheric conditions, we can express the overall channel model as the production of different contributions *i.e.*,

$$h = \exp(-L)\left[h_T \cdot h_{FS} \cdot h_p\right],$$

where $h_T = 1$, $h_{FS} = 1$, and $h_p = 1$ in case of no turbulence, pointing error, and fog/smoke attenuation, respectively.

To summarize, Table 3 enlists all the channel impulse responses achievable in case of different attenuation loss models.

Table 3. Different attenuation models of FSO link and the corresponding channel impulse responses.

Attenuation model	Channel impulse response
Clear channel	$h = \exp(-L)$
Atmospheric turbulence	$h_{T,LN} = \exp(2I)$ $h_{T,GG} = \dfrac{1}{\alpha\beta} I_x\, I_y$
Fog/smoke	$h_{FS} = \exp(-\beta L),$
Pointing error	$h_p = A \exp\left(-\dfrac{2r^2}{w_{eq}^2}\right),$

5.4 Simulation Results

In this section, we will deal with the assessment of the performance of eligible ABs, in case of the previously introduced railway scenarios and configuration parameters.

As shown in Table 4, in order to assess the performance of FSO AB, mainly expressed in terms of Bit Error Rate (BER), we considered two different scenarios depicting a point-to-point LOS link *i.e.*, fixed, and mobile link, for different attenuation loss models (*i.e.*, turbulence, pointing error, fog/smoke channel, and clear channel).

Specifically, we first assumed a static point-to-point FSO LOS link for which we evaluated the BER in case of clear channel, turbulence channel, pointing error, and fog/smoke channel. Then, we also assessed the case of FSO connectivity link when the receiving photodetector is moving (*i.e.*, mobile scenario). This second scenario well depicts the case of a train moving along the track and is connected to a FSO transmitting source (*i.e.*, laser).

Table 4. Schematic of the simulated scenarios under different attenuation models, and the expected results.

Scenario	Channel model	Expected Results
• Fixed point-to-point link • Mobile point-to-point link	• Clear channel (no additional attenuation) • Turbulence channel • Pointing error • Fog/smoke channel	• BER

5.4.1   Fixed point-to-point FSO link

We first evaluated a clear FSO channel, where no attenuation is added except that of the connectivity link length. This model is not realistic in practice, as some attenuation losses are always present mainly due to atmospheric and weather conditions. However, for completeness, we evaluated the scenario of a fixed point-to-point FSO between a laser source and a receiver photodetector at a distance of $L = 1500$ m, as depicted in Figure 15. Table 5 lists the main parameters used for the simulation results.

Table 5. Main parameters used in the simulator.

Parameter	Value
Link length [m]	[500, 1500]
Wavelength [nm]	1550
Optical power [mW]	5
Background light power [mW]	0.01
Receiver aperture diameter [m]	0.005
Responsivity [A/W]	0.5

Figure 15. BER vs. SNR in case of clear channel.

clear channel, @1500m
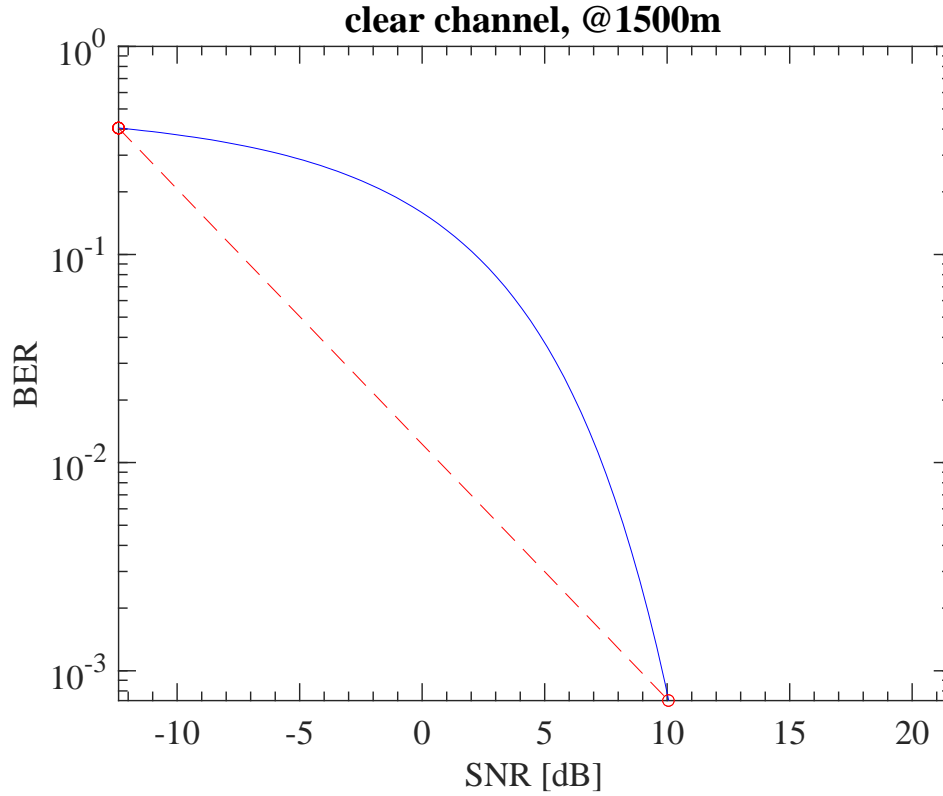
Figure 15 presents the BER vs. SNR in case of clear channel at link length of 1500 m. We observe values lower than 10^{-3} at SNR = 10 dB. In

Figure 16 (a) and (b) we present the BER versus SNR for a static FSO LoS link, considering a turbulence channel depicted according to the Gamma-Gamma model, in case of variable link length (*i.e.*, $L = 500$ and $L = 800$, respectively). We observe that, as expected, by increasing the link length the BER for a fixed SNR increases (*e.g.*, for SNR = 23dB, BER = 10^{-2} and BER = 10^{-1}, for $L = 500$ and $L = 800$, respectively) and then performance get worse. In such scenario, we also add the pointing error that causes misalignment between the laser source and the photodetector receiver (see

Figure 17). At SNR= 23dB for L = 500 m, BER = 10^{-2}, while the same value is achieved for SNR = 21dB in case of increasing link length *i.e.*, L = 800 m.

Figure 16. BER vs. SNR in case of turbulence channel for (a) L = 500 m and (b) L = 800 m. Blue and red lines refer to theoretical and simulated BER trends, respectively.

(a)   (b)
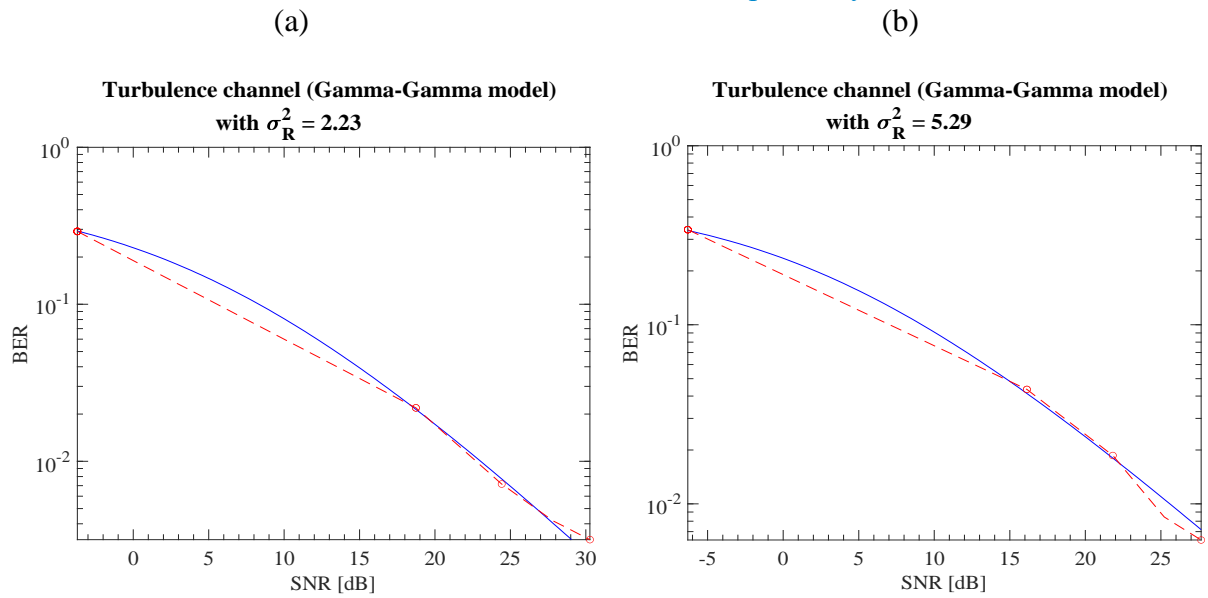
Figure 17. BER vs. SNR in case of turbulence channel and pointing error for (a) L = 500 m and (b) L = 800 m. Blue and red lines refer to theoretical and simulated BER trends, respectively.

(a)   (b)

Turbulence channel (Gamma-Gamma model) with $\sigma^2_R = 2.23$ and PE channel with $\sigma_j = 0.50$

Turbulence channel (Gamma-Gamma model) with $\sigma^2_R = 5.29$ and PE channel with $\sigma_j = 0.50$
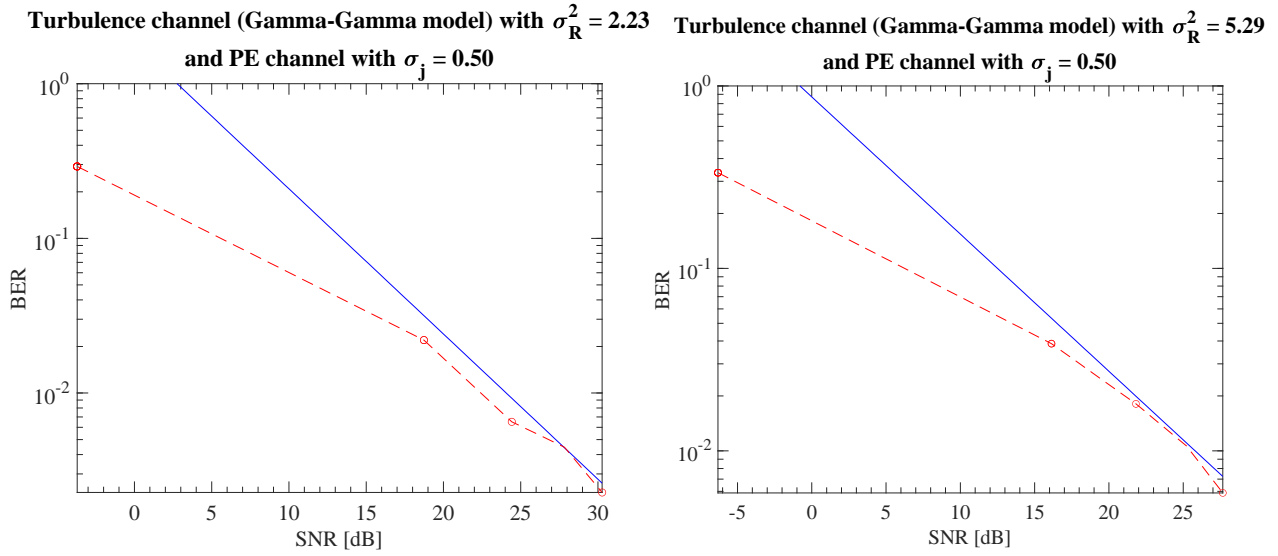
Figure 18. BER vs. SNR in case of fog/smoke channel for (a) $L = 2000$ m and (b) $L = 2400$ m. Blue and red lines refer to theoretical and simulated BER trends, respectively.

(a)

(b)
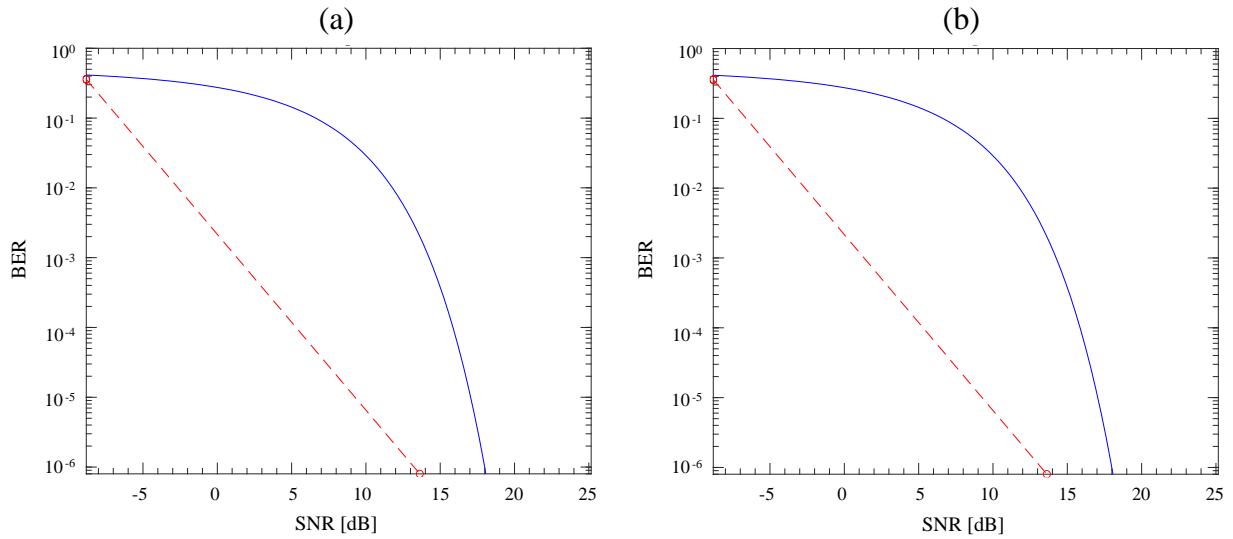
Similar results apply to the scenario of fog/smoke channel, as depicted in

Figure 18. Again, we considered BER versus SNR in case of different LOS link length. In

Figure 18 (a) and (b), BER has been obtained in case of $L = 2000$ and $L = 2400$ m, respectively. For shorter length, BER reaches lower values as compared to the case of longer distances. For instance, at SNR = 17 dB, BER reaches 10^{-5}, while for the same value at $L = 2400$m, BER is 10^{-4}.

To summarize, for comparison purpose, we selected the most significative scenarios in order to show the performance of FSO AB, in case of $L = 1500$ m and for different attenuation models *i.e.*, LN turbulence channel, and pointing error channel. In all such scenarios, we also assumed a visibility higher than 50km so that fog/smoke attenuation can be neglected. Figure 19 and Figure 20 depict the BER in case of pointing error, and turbulence channel, respectively. We can observe that for a given SNR = 10 dB, the BER is approximately 10^{-3} for the FSO link with pointing error, which is quite similar to the value obtained in case of weak turbulence, as depicted in Figure 20 (a). In case of increasing turbulence, for SNR = 10 dB the performance gets worse and the BER is lower than 10^{-1} in case of moderate and strong turbulence, as observed in Figure 20 (b) and (c), respectively.

Figure 19. BER vs. SNR [dB] in case of pointing error loss for a LOS link of $L = 1500$m.

PE channel with $\sigma_j = 0.50$, @1500m
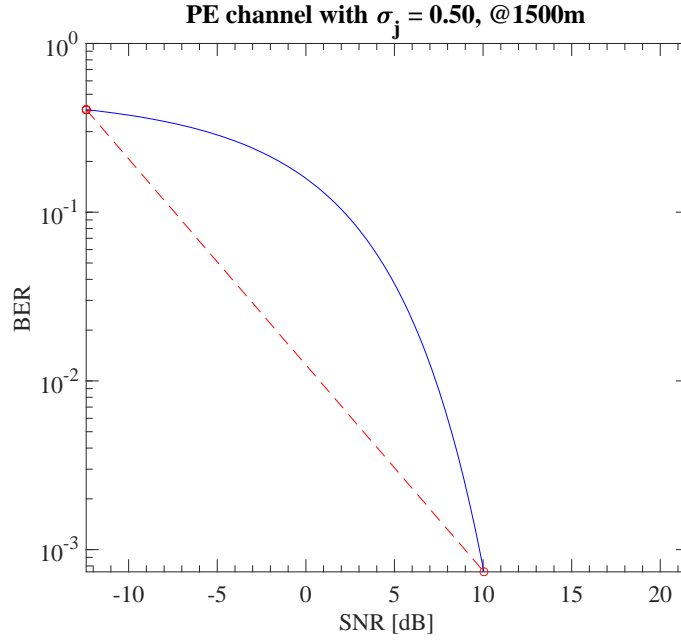
Figure 20. BER vs. SNR [dB] in case of (a) weak, (b) moderate, and (c) strong turbulence channel for a LOS link of $L = 1500$m.

(a) (b) (c)
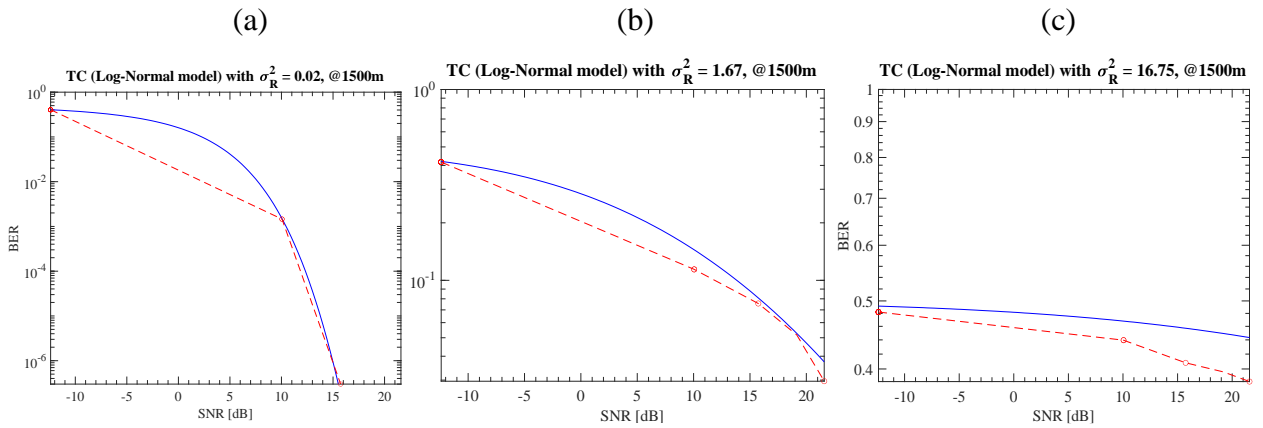
To summarize, we report the main outcomes of the simulated scenarios in the following Table 6. We have enlisted the results achieved from previous simulations, in case of different attenuation losses. We observe achievable BER in case of different SNR and communication links. As expected, for higher distances the BER will suffer from higher attenuation.

Table 6. Main simulation results expressed as BER in case of static scenario, for different attenuation models, link length, and SNR.

Static Scenario			
Link length [m]	**Attenuation model**	**BER**	**SNR**
1500	Clear channel	10^{-3}	10 dB
1500	Pointing error	10^{-3}	10 dB
1500	Moderate/strong turbulence	10^{-1}	10 dB
500	Turbulence channel	10^{-2}	23 dB
800	Turbulence channel	10^{-1}	23 dB
500	Turbulence channel w pointing error	10^{-2}	23 dB
800	Turbulence channel w pointing error	10^{-2}	21 dB
2000	Fog/smoke	10^{-5}	17 dB
2400	Fog/smoke	10^{-4}	17 dB

5.4.2 Mobile point-to-point FSO link

We are now interested in the simulation results in case of a variable link length, as occurring in case of a mobile point-to-point scenario, as early depicted in Figure 8. In this case, we present the BER variation experienced along the path, that is for variable FSO link length, in case of turbulence channel. Figure 21 depicts the behavior of BER in such scenarios. As expected for increasing lengths the BER increases; worse performance is obtained with a strong turbulence channel, followed by a moderate turbulence scenario, with BER $\approx 10^{-1}$ and BER $\approx 10^{-2}$, respectively. In Figure 21 (b), we show the BER trend along the distance variations of a receiver photodiode that is from 1000 to 2000 m, for moderate turbulence attenuation. Also in this case, we observe that for increasing connectivity link, BER shows increasing values, reaching approximately 10^{-2} at $L = 2000$ m.

Figure 21. BER variation along the path in case of (a) weak, (b) moderate and (c) strong turbulence channel, respectively.
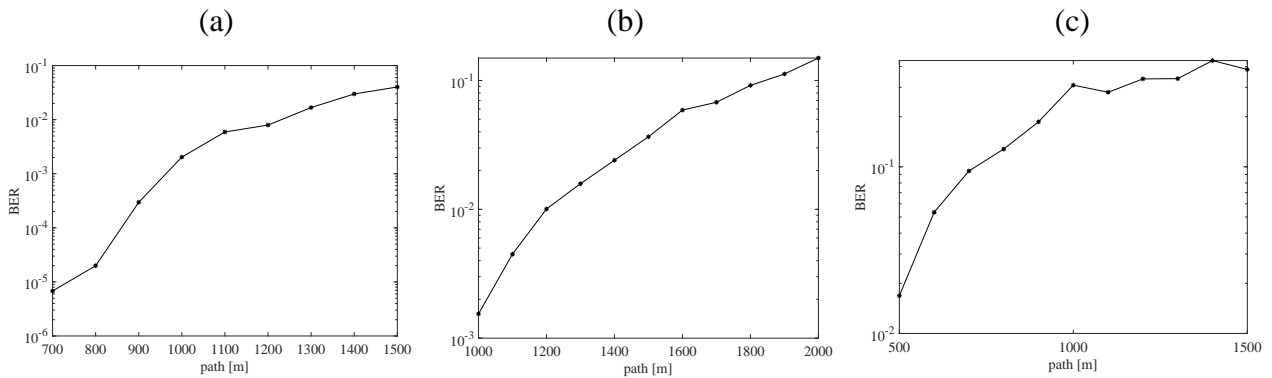
The second scenario depicts a mobile scenario where a receiver photodetector is moving along a fixed path, in case of moderate turbulence attenuation, so that the LoS connectivity link can vary from $L = 500$ up to $L = 1500$ m. In this case, we evaluated the received power along the path, as shown in Figure 22. We observe a variation from around 8×10^{-6} to 4.75×10^{-6}, obtained for $L = 500$ m and $L = 1500$ m, respectively. On the other side, increasing the link length, and considering a path from $L = 1000$ m to $L = 2000$ m, the received power is from 1.4×10^{-6} to 0.2×10^{-6}.

Figure 22. Received power with moderate turbulence along the path from a receiver photodiode to a transmitting FSO source. Link lengths are (a) from $L = 500$ m to $L = 1500$ m, and (b) from $L = 1000$ m to $L = 2000$ m

(a)   (b)
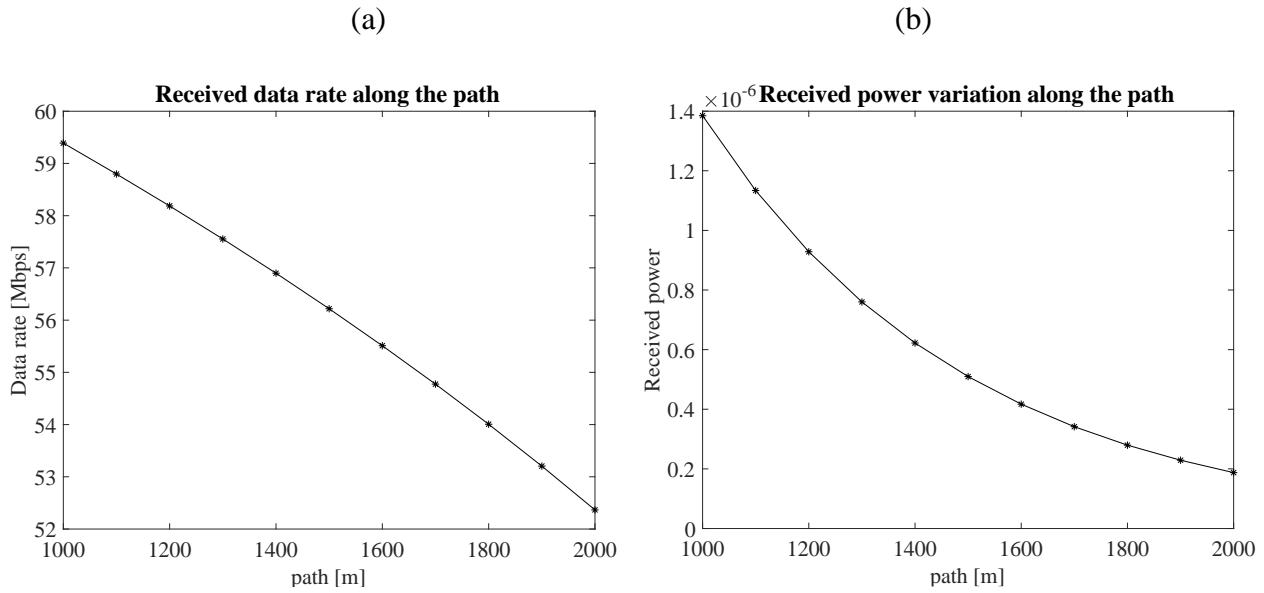
Finally, we present the achievable data rate and the received intensity in case of moderate turbulence channel for variable FSO link length.

Figure 23 presents the obtained results, where we can observe that for increasing link length the achievable data rate suffers of a slight reduction from ≈ 59 Mbps to ≈ 52 Mbps, in case of $L = 1000$ m and $L = 2000$ m, respectively. Similarly, the received intensity is lower for higher distances and smaller SNR values.

Figure 23. Data rate [Mbps] and received intensity in case of variable FSO link length for a moderate turbulence attenuation channel.

(a)   (b)
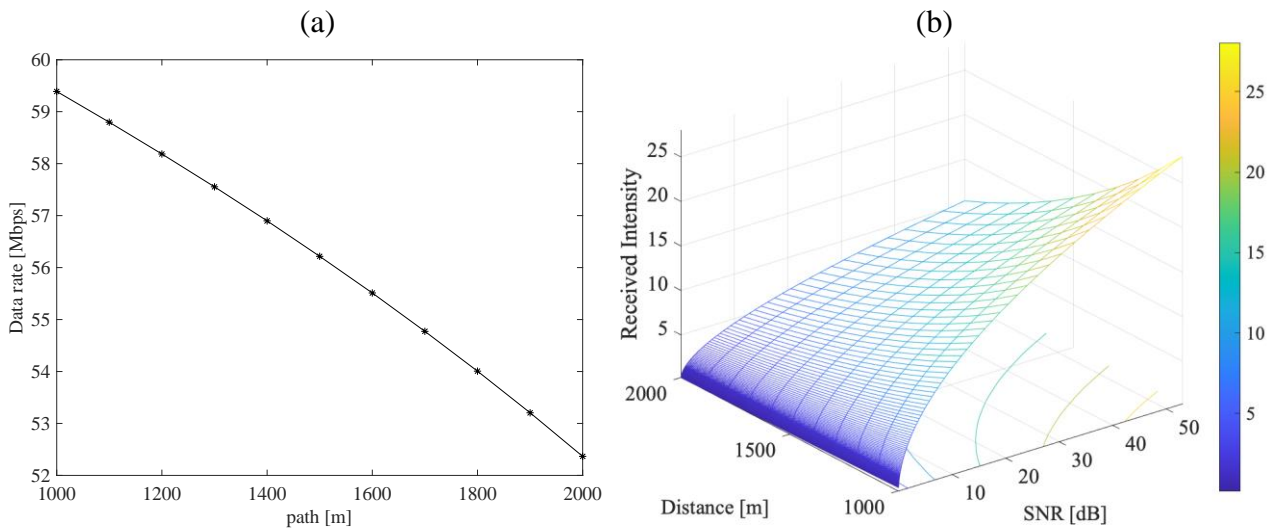
To summarize the main outcomes from the dynamic scenario, we report the values of achievable BER in the following Table 7. We have enlisted the results achieved from previous simulations, in case of different attenuation losses, considering a dynamic path of the train, so that the connectivity link length varies from 1000m to 1500m. We observe the signal propagation is more affected in case of strong turbulence, followed by moderate turbulence scenario. Also, notice acceptable performance (i.e., BER $<10^{-3}$) are for pointing error and fog/smoke attenuation model, as well weak turbulence that can reach up to BER $= 10^{-7}$.

Table 7. Main simulation results expressed as BER in case of dynamic scenario, for different attenuation models and link length.

Dynamic Scenario		
Link length [m]	Attenuation model	BER
[1000, 1500]	Moderate turbulence	$[10^{-5}, 10^{-2}]$
[1000, 1500]	Strong turbulence	$[10^{-3}, 10^{-1}]$

[1000, 1500]	Weak turbulence	$[10^{-7}, 10^{-3}]$
[1000, 1500]	Pointing error	$[10^{-6}, 10^{-4}]$
[1000, 1500]	Fog/smoke	$[10^{-5}, 10^{-4}]$

5.4.3 Alternative scenario for FSO mobile link – dual beam link

One main issue in the mobile point-to-point FSO link scenario is how to maintain LoS links, while the receiver photodetector is moving. Still in the context of dynamic railway scenario, we now introduce the scenario of single and dual-optical beams, the latter has already been described in D2.2. The importance of investigating FSO link performance achieved with this alternative dynamic scenario reflects into an interest mainly for regional and freight railway scenarios, especially the latter being characterized by long trains whose length can be even of few kms. In such a scenario, both for single and dual-optical beam schemes, we aim to deploy several BSs along the railway track, according to different BS inter-distances, so that in each position the train is connected to the closest BS, for which FSO link performance are acceptable.

Assuming the train profile vs. time early introduced in Fig. 5 and 6, in order to avoid disconnections and maintain FSO LoS links, we consider a uniform distribution of multiple FSO transmitters along the railway track, for a total distance of ≈ 35 km. As a first outcome, in case of single optical beam, we observe that for a base station (BS) inter-distance $\tilde{d} = 1000$ m, the number of BSs deployed along the rail track is 35 and it follows that FSO connectivity links are guaranteed with a minimum length of 500 m, which does not overcome 700 m, as depicted in

Figure 24. This upper bound is a good trade-off for providing effective link performance. In general,

Figure 24 shows the maximum achievable LoS FSO connectivity link lengths in case of dynamic railway scenario. For reducing the FSO inter-distance, the number of FSO transmitters increases, but the maximum achievable link length is lower bounded to 706 m. It follows that the same performance are obtained in case of 35 and 70 FSO transmitters deployed along the rail track. On the other hand, for increasing the BS inter-distance, the maximum achievable link length increases but with a following likely reduction of performance.

Table 8 collects several values of FSO inter-distance, which correspond to a different number of BSs deployed along the rail track, as well as the maximum achievable LoS FSO link length. We can conclude that in order to experience FSO connectivity links of maximum length ≈ 700 m, we can deploy 35 BSs at inter-distance $\tilde{d} = 1000$ m. Same performance are achieved for 70 BSs at shorter inter-distance $\tilde{d} = 500$ m. It follows that, as expected higher the number of FSO transmitters, lower is the inter-distance and higher the performance due to shorter FSO link lengths.

Figure 24. Single-beam approach. LoS FSO connectivity link length [km] vs. time, in case of (a)

70, (b) 35, (c) 24, and (d) 18 BS transmitters, and corresponding BS inter-distance values, respectively.

(a)

(b)

(c)

(d)
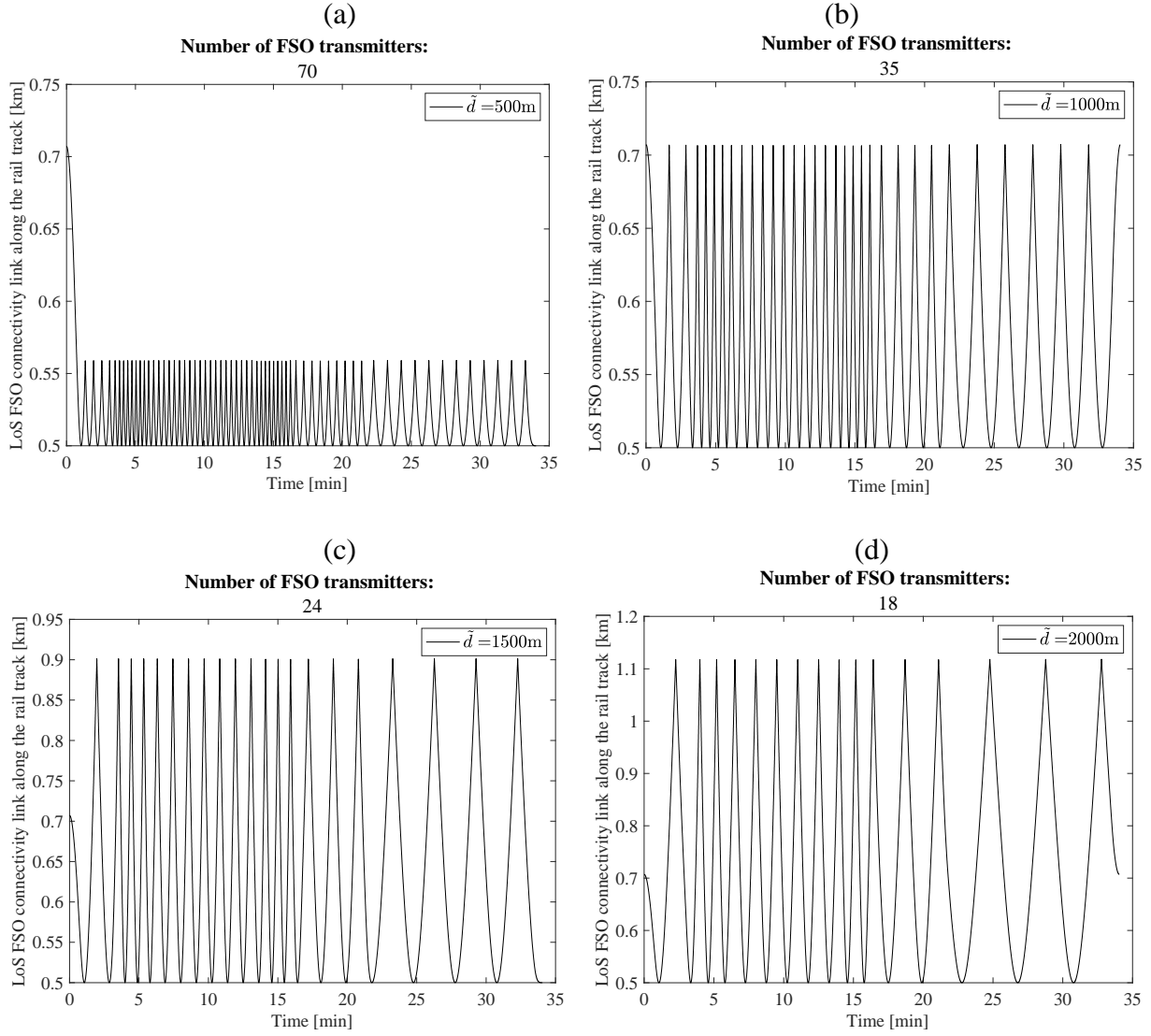
Table 8. FSO inter-distance [m] corresponding to different number of BSs and maximum achievable FSO link lengths.

BS inter-distance, $\tilde{d}$ [m]	Number of BSs	Maximum achievable FSO link length [m]
500	70	706
1000	35	706
1500	24	901
2000	18	1117

We can now extend this scheme and consider a dual-optical beam approach, that consists in equipping the train of two transceivers, one placed at the front of the train, and the second one placed at the back of the train. This approach still ensures continuous communications between the ground and train. The dual-transceivers scheme in a ground-to-train communications system has been initially presented in [10], where the single BS is equipped with two transceivers pointing to opposite directions and in particular FSO laser beams of the BS are transmitted forwardly and backwardly, so that the total coverage length of each BS is remarkably extended (doubled at least). However, the two coverage areas of the single BS's transceivers are not contiguous along the track, thus forming a *blackout area* among them. By installing two transceivers on each train, accordingly, deployed at some distance on the train i.e., respectively on the front and the back of the train, we can maintain continuous ground-to-train FSO communication links. Thanks to this strategy, it was proven that the number of the BSs is strongly reduced, while maintaining FSO stable connectivity links.

The schematic of dual-optical beam is depicted in Figure 25, where two transceivers are deployed on both the train and BSs. Each BS is equipped with two transceivers (i.e., one pointing forward and the other pointing backward), and connected to the fiber-optic core network. At the transmitter side, the geometric model of the FSO optical beam is depicted in

Figure 26, from D2.2. The height of the FSO transmitter is the same as that of the transceivers on the train, which is set as 4 m above the ground level. Here, L [m] is the length of the track covered by a laser beam of the BS, θ is the divergence angle of the laser source, which decides the radius of the optical beam, L_1 [m] is the vertical distance between the BS and the track, *i.e.*, $L_1 = 1$ m, L_2 [m] is the horizontal distance between the BS.

Figure 25. Schematic of FSO network architecture, [D2.2].
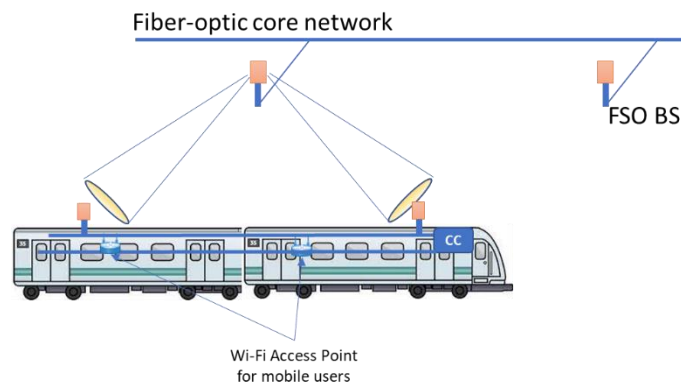
Figure 26. Geometric optical beam in an FSO link.

The dual-optical beam scheme is well represented in Figure 27, where we observe the following correspondence of parameters used, *i.e.*, $d_2 = 2L_2$ is the extension of the blackout zone of the BS, while the (half) BS coverage is $d_1 = d_3 = L$. Notice that L_t is the distance among the two antennas on the train and d_4 is the blackout distance between two adjacent BSs that is important for determining their inter-distance, which is expressed as

$$\tilde{d} = D_2 + 2d_3 + d_4,$$

where we have assumed that the blackout zone of the two BSs has the same extension.

In order to increase the inter-distance among BSs and then to reduce their number, we can include the length of the train in selecting d_4 by assuming the train is equipped with more dual beam antennas at distances L_t among each other, with the constraint $L_t > d_2$. In

Figure 28, we observe the inter-distance of BSs can be increased by an amount proportional to the length of the train by deploying more dual beam optical "antennas" on the train. Indeed, at each time instant we have at least one antenna connected to one beam of the source BSs before the train enters the coverage area of the next BS. In general, in case of long trains, one or two antennas of the same train can be connected to the left and right beams of the source BS.

Figure 27. FSO scheme in case of dual transceivers.

Figure 28. Extending the BS inter-distance by accounting for the length of the train, [D2.2].
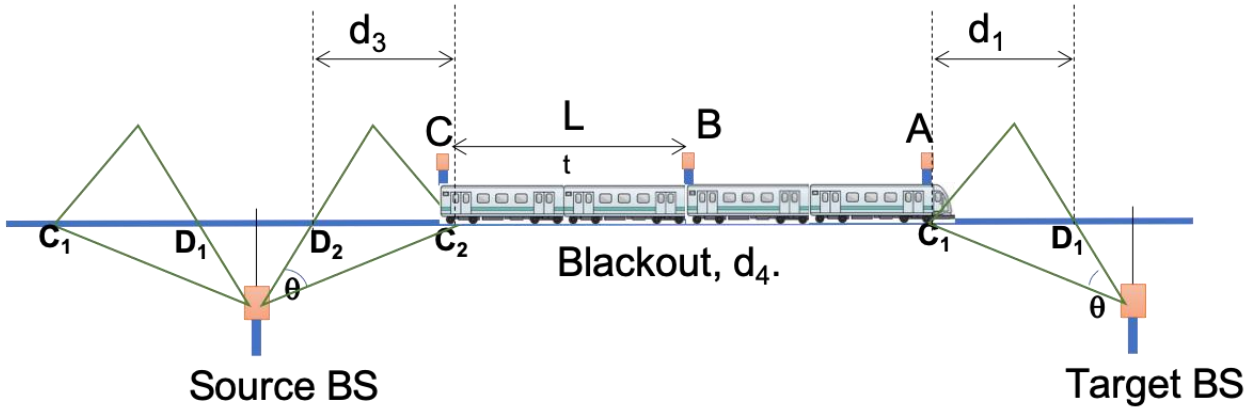
In case of dual-optical beam, we observe that the FSO connectivity links are still guaranteed, with the same maximum link length achieved with the single beam approach, and the same number of BSs. However, we notice more stability of connectivity links, due to the lower frequency of link variations. As an instance, in

Figure 29 (c) for $\tilde{d} = 1500$ m we observe 10 peaks for the maximum link length of ~ 900 m, while in

Figure 24 (c) 21 peaks are recorded corresponding to the same maximum link length. Lower is the number of peaks, higher is the link stability, meaning more stable connectivity links. Similar considerations apply to the other results in Figure 29.

Figure 29. Double-beam approach. LoS FSO connectivity link length [km] vs. time, in case of (a) 70, (b) 35, (c) 24, and (d) 18 BS transmitters, and corresponding BS inter-distance values, respectively.

(a)   (b)

Number of FSO transmitters: 70

Number of FSO transmitters: 35

(c)

(d)

Number of FSO transmitters: 24

Number of FSO transmitters: 18
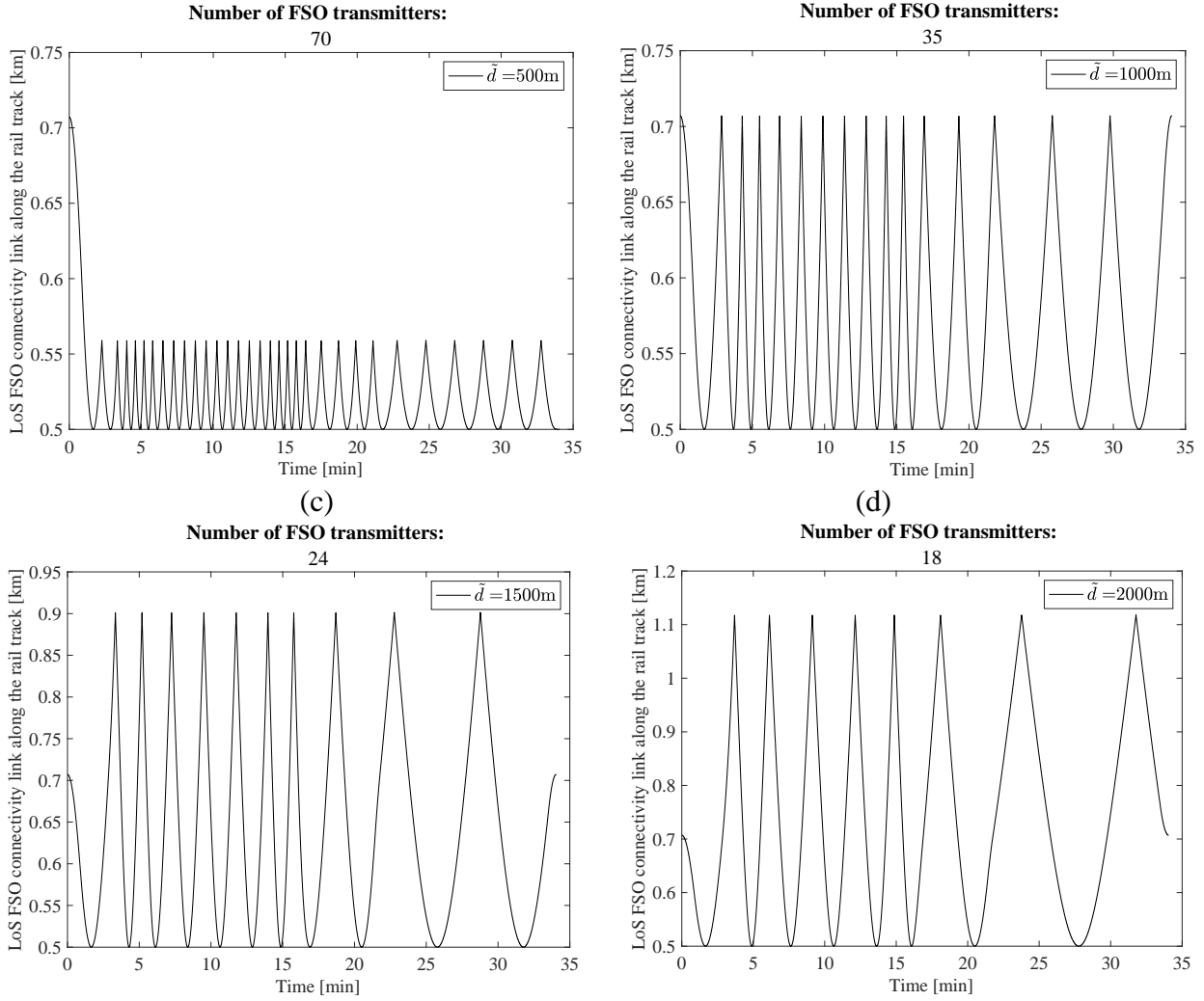
Finally, taking into account the geometrical model from

Figure 26, we aim to derive the received power level at the train transceivers. Let $\theta_{1/2}$ denote the half divergence angle (i.e., $= 2\theta_{1/2}$), and then the tilt angle of the beam, denoted by γ, can be expressed as $\gamma = \theta_{1/2} + \delta$, which is the angle between the optical axis of the beam and the horizontal axis that is parallel to the track. We can compute the estimated divergence angle of the laser beam as

$$\theta = \tan^{-1} \frac{L_1 L}{L_1^2 + L_2 L + L_2^2},$$

and the beam radius of a Gaussian beam, denoted as w, can be expressed as

$$w(z) = w_0 \sqrt{1 + \left(\frac{\lambda z}{\pi w_0}\right)^2},$$

where w_0 is the beam waist of the laser source at the transmitter and λ [m] is the wavelength of the laser beam.

According to such configuration, we can compute the received power at a given distance r [m] along the track as

$$P_{rx} = \frac{2P_{tx}A_{coll}}{\pi w^2} \exp(-2r^2/w^2),$$

where P_{tx} [W] is the transmitting power from the FSO laser source and A_{coll} [m] is the collection area at the receiver, which is modeled as

$$A_{coll} = \frac{n^2 A_{det}}{\sin^2 \psi_c},$$

where A_{det} [m^2] is the area of the photodetector, n is the refractive index of the optical concentrator, and ψ_c is the half-angle FOV of the receiver.

Figure 30 depicts the received power versus the time spent for the train to move along a given path, for different values of L_2 [m] and FSO inter-distance $\tilde{d}$ [m] i.e., $\tilde{d} = [500, 2000]$m. We observe that longer is the horizontal distance L_2, lower is the received power level. Furthermore, fluctuation of the received power are experienced in case of lower number of FSO transmitters, due to longer connectivity links and then more attenuation.

As a main result, we can observe that even if the mobile scenario is more challenging due to mobility issues and link maintainment, we observe that by accordingly deploying FSO transmitters along the railway track we can keep performance at a constant value. This can be observed from the received power level vs. the time window.

Figure 30. Received power level versus time interval.

(a)

(b)

(c)

(d)
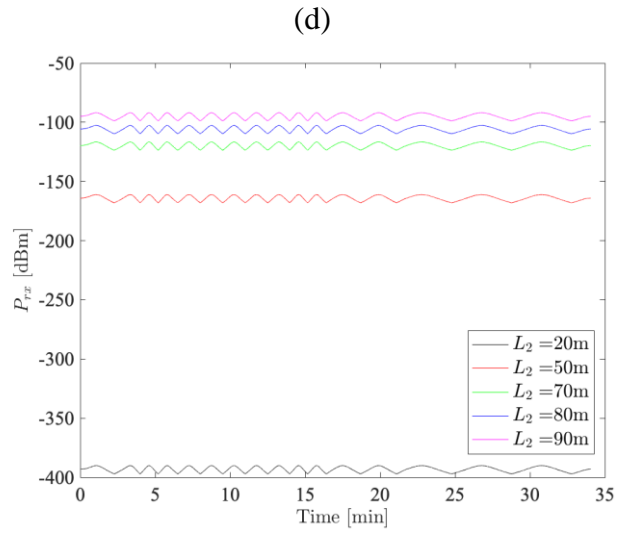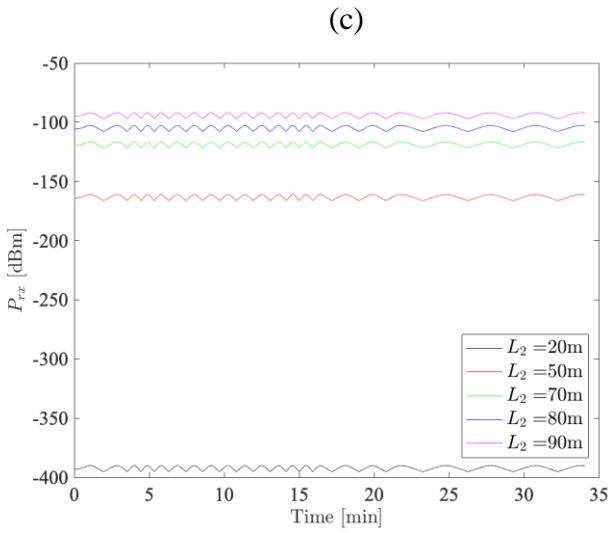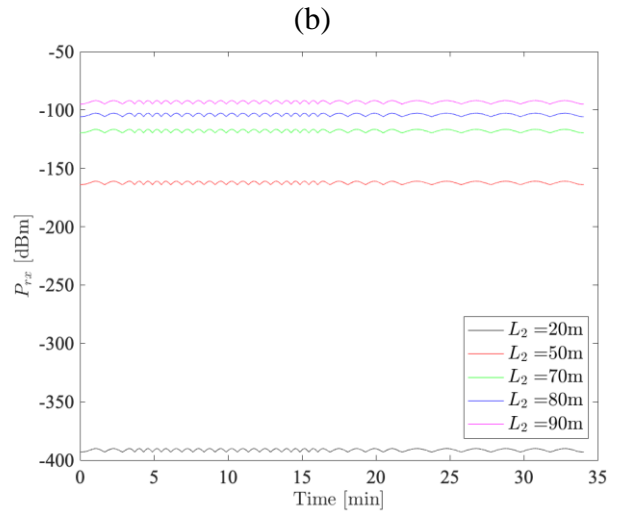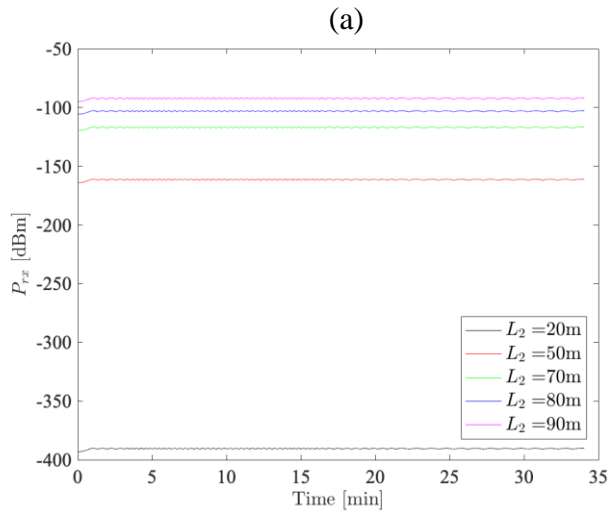
6. Low Earth Orbit Satellites

6.1 LEO System Architecture

The Figure 31 shows the overall system architecture considered in the analysis for both SpaceX and OneWeb LEO satellites.

Figure 31. LEO System architecture.
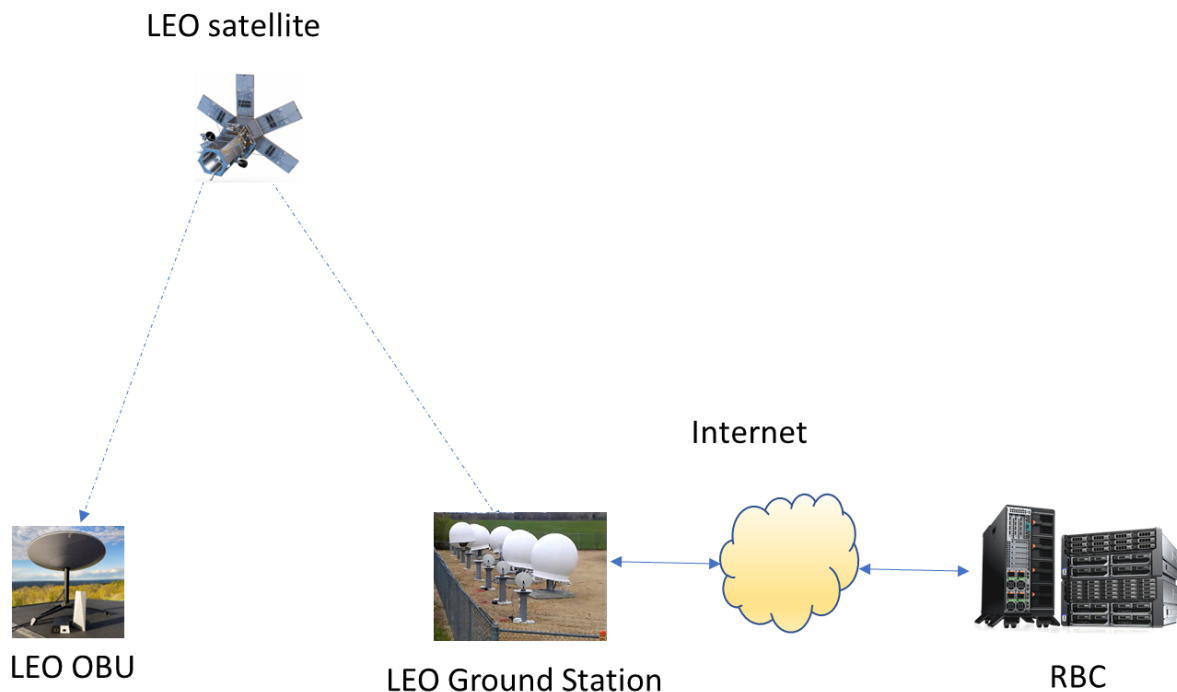
The train is equipped with the LEO terminal, called LEO On Board Unit (OBU). It allows the connection with the LEO satellite in orbit. The LEO satellite is also connected to the Radio Block Center (RBC) through an Internet connection.

The user terminal-to-satellite (upstream) and satellite-to-user terminal (downstream) paths have been analyzed separately in this document. We assume the satellite-to-earth station gateway link is managed by the LEO operator and we assume it should not be a problem in terms of link reliability and available system capacity for collecting all data from the users connected to the LEO satellites. Finally, the link from the LEO ground station to the RBC server is realized through an Internet or private link. We are not interested in the assessment of performance of this link.

The Figure 32 shows the LEO SpaceX coverage map as reported in [11].

Figure 32. LEO SpaceX coverage map.

not affiliated with
spaceX or starlink ·
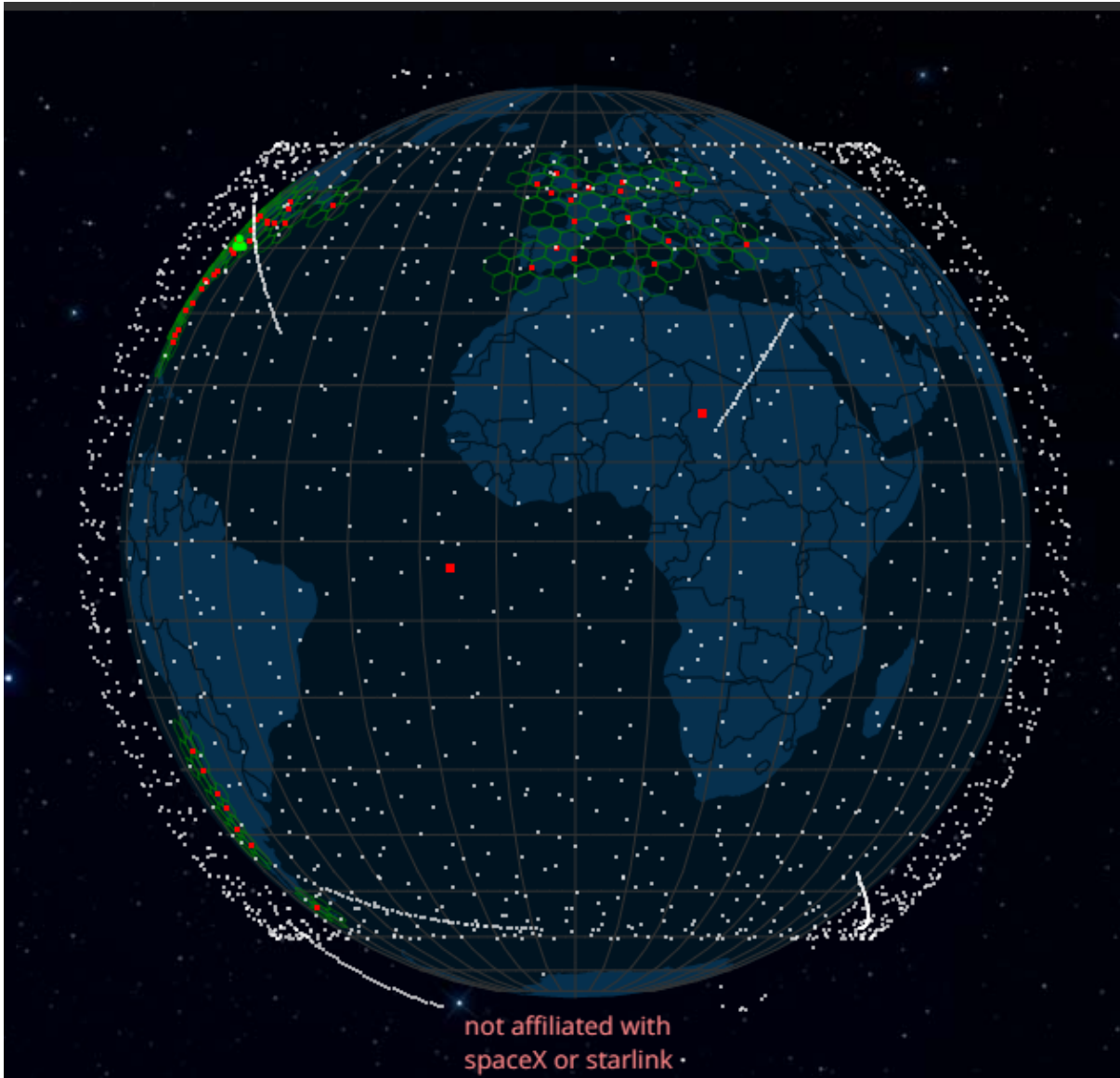
At present (12th August 2022), the only active SpaceX ground stations/gateways are installed in the United States soil. The SpaceX program is for the commissioning and realization of other satellite ground stations with gateways in Europe. In any case, no gateway is envisaged to be installed in Southern Europe (including Italy and Spain) [12] in the next future.

This fact is confirmed looking at Figure 33 showing the (actual) locations of SpaceX gateways.

Figure 33. LEO SpaceX gateway locations.

6.2 Radio propagation models

Since the SpaceX and OneWeb documentations detailing the modulation and access schemes used is reserved, to assess performance in the scientific literature the Digital Video Broadcasting DVB-S2 satellite communication system is used for link budget calculation, as in [13] [14].

The hypothesis of considering DVB-S2 transmission technology is reasonable because it is a very stable and known technology. In addition, DVB-S2 also allows two-way satellite-user terminal communications and vice versa.

Regarding the attenuation models, in addition to the free space loss characterizing the UE-to-Satellite link the atmospheric loss is used to account for link degradation due to adverse gaseous effects. The International Telecommunication Union (ITU) models considered for atmospheric attenuation are described in the recommendation ITU-R P.618-13 [15].

AS in DVB-S2 even SpaceX and OneWeb can use adaptive modulation and coding schemes (MCS) to dynamically adapt transmission in accordance with the available Signal-to-Interference plus Noise Ratio (C/(N+I)) so to maximize the spectral efficiency achievable in each situation.

6.3 Methodology

The main performance parameter to be considered in performance assessment is the signal carrier-to-interference plus noise ratio i.e. C/(N+I) which can be directly related to the $Eb/(N0+I0)$, where Eb is the energy per bit, N0 is the spectral density and I0 is the interference energy, and then to the MCS that can be selected to maximize transmission capacity for each User Equipment (UE)-to-Satellite distance. The C/(N+I) can be evaluated from link budget calculation. In the following subsections the methodology adopted for link budget calculation is described.

6.3.1   Workflow

The performance evaluation activities of SpaceX and OneWeb LEO HTS systems have been carried out in accordance with the workflow described in the Figure 34.

Figure 34. Workflow of adopted methodology.
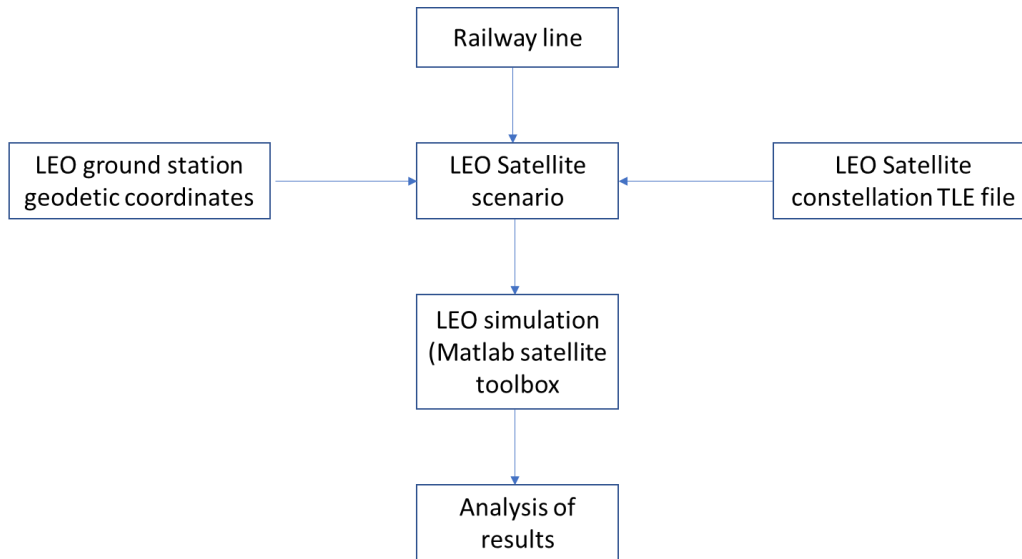
The work started with the identification of the railway line, i.e. the Rome-Florence line (Figure 35) (accommodating mainline, regional, freight railway lines), which has been considered to derive results in the previous deliverable D2.3.

Figure 35. Rome-Florence railway line.
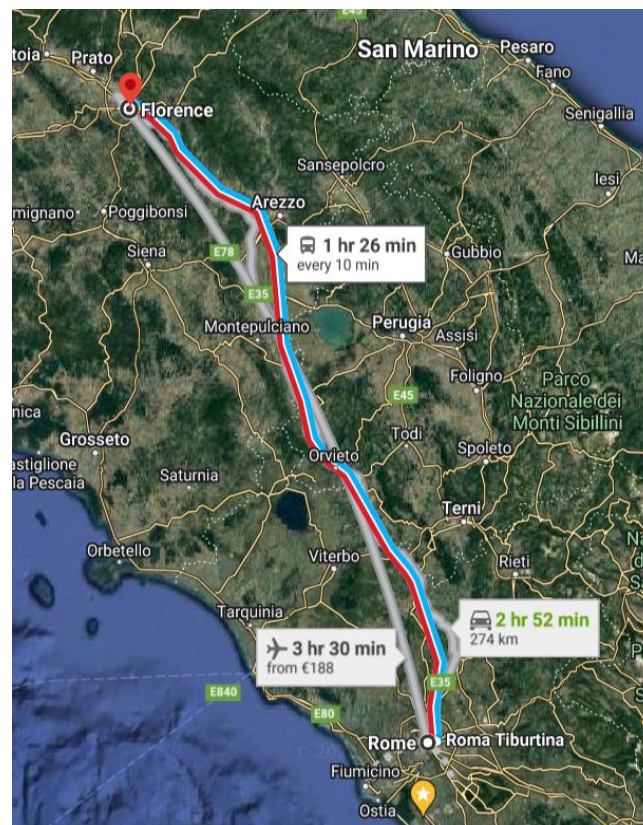
We have identified some points along the line in terms of their geodetic coordinates. The latitude/longitude coordinates of these points are shown in Table 9.

Table 9. Railway line points: list of geodetic coordinates along the Rome-Florence railway line.

Station	km	Latitude – Longitude [Degree]
Roma Termini	0	41.90134, 12.50034
GRA	10	42.02098, 12.52562
Settebagni	3	42.010617444766076, 12.521471192620652
Riano	5	42.09461901523065, 12.538950332815373
Capena	7	42.13304909449124, 12.546239722893903
Sant'Oreste	7	42.23441337468742, 12.507209805810147
Borghetto	10	42.33956298043416, 12.460174589539339
Scalo Teverina	4	42.37685648366756, 12.443351772070113
Orte Scalo	12	42.433642113880175, 12.391853361399292
Bassano in Teverina	5	42.47771690799265, 12.341384915142111
Attigliano	6	42.52716598095498, 12.300560689491748
Sant'Angelo	8	42.60369165947424, 12.24035476056048
Tordimonte	10	42.701410189222315, 12.15976718587696
Orvieto	5	42.728648129157605, 12.112174398540516
Allerona	11	42.805638772848155, 12.013125924959176
Ponticelli	13	42.91801512566852, 11.97849276939934
Chiusi Scalo	11	43.014486739925104, 11.93248752066572
Montepulciano Stazione	15	43.100591865365764, 11.88980087665434
Bettolle	8	43.233743824125156, 11.87426386159956
Castiglion Fiorentino	14	43.338361369624096, 11.86261109983031
Arezzo	15	43.47592731434826, 11.797549853039794
Montevarchi	15	43.53157022931632, 11.632469078067437
San Giovanni Valdarno	10	43.591629721992035, 11.542472871680806
Figline Valdarno	9	43.65113420132002, 11.467388305781936
Leccio	5	43.69819121622599, 11.435343211280822
Bagno a Ripoli	12	43.77116184016206, 11.330468370112502
Coverciano	4	43.777822995359124, 11.276574349730424
Le Cure	2	43.7885449870862, 11.262403228942343
Firenze S.M.	2	43.76737, 11.27318

Total distance	**238 km**

We assume the Radio Block Center (RBC) server is located in Bologna and its coordinates are listed in Table 10 [16].

RBC Location	km	Latitude – Longitude [Degree]
Bologna Centrale	300	44.3012, 11.2018

The main parameters of the SpaceX and OneWeb LEO satellite constellations are extracted from the corresponding Two-Line Element (TLE) file which can be freely downloaded in [18]. For performance assessment we assume the satellite is visible at one of the considered location points in Table 9 and Table 10 when the value of its minimum elevation angle is 15°. Below 15o we assume the satellite is obscured and cannot be used for relaying transmissions.

The Rome-Florence railway line, the geodetic coordinates of the points along the line and information on LEO satellite constellations in the TLE files are the parameters required to compose the LEO satellite scenario that can be processed with the Matlab Satellite Toolbox so to derive all the necessary data to evaluate the link budget and then the C/(N+I).

The reference Time interval considered for simulation is 1 day (24 hours). The SINR ratio is then calculated, also taking into account the interference contributions [13].

6.3.2 Details on SpaceX e OneWeb LEO constellations

The Two-Line Element (TLE) is a methodology for encoding satellite data format. It contains the list of satellite orbital elements. According to the geometric formulas, we can estimate the satellite state in terms of position and velocity. The satellite data in the TLE file are encoded according to the North American Aerospace Defense Command (NORAD) nomenclature and are allocated on two different lines [17]. The following Table 11 describes the encoded data format.

Table 11. TLE file details: Line 1 (a), Line 2 (b).

(a)

Line 1	
Column	Description
1	Line Number of Element Data
03-07	Satellite Number
8	Classification (U=Unclassified)
10-11	International Designator (Last two digits of launch year)
12-14	International Designator (Launch number of the year)
15-17	International Designator (Piece of the launch)
19-20	Epoch Year (Last two digits of year)
21-32	Epoch (Day of the year and fractional portion of the day)
34-43	First Time Derivative of the Mean Motion
45-52	Second Time Derivative of Mean Motion (Leading decimal point assumed)
54-61	BSTAR drag term (Leading decimal point assumed)

63	Ephemeris type
65-68	Element number
69	Checksum (Modulo 10)
	(Letters, blanks, periods, plus signs = 0; minus signs = 1)

(b)

Line 2	
Column	**Description**
1	Line Number of Element Data
3-7	Satellite Number
9-16	Inclination [Degrees]
18-25	Right Ascension of the Ascending Node [Degrees]
27-33	Eccentricity (Leading decimal point assumed)
35-42	Argument of Perigee [Degrees]
44-51	Mean Anomaly [Degrees]
53-63	Mean Motion [Revs per day]
64-68	Revolution number at epoch [Revs]
69	Checksum (Modulo 10)

Example: Starlink SpaceX

```
1 44713C 19074A   22213.84145833  .00010689  00000+0  71603-3 0  2138
2 44713  53.0562 333.6845 0001336  83.9430 132.6542 15.06394655    12
```

The cited TLE files on Starlink SpaceX and OneWeb are available on Celestrak repository [18] and can be imported in the Satellite toolbox to simulate the movement of satellites over their orbits.

6.3.3 Satellite Toolbox

The Satellite Toolbox is the Matlab toolbox specifically designed for satellite simulations and analysis. It can import the satellite TLE files, and it allows to analyse the satellite data with high accuracy. Given one point on earth (e.g., a reference point), *the toolbox allows to derive the azimuth, the elevation angle and the range of any one of the satellites in the constellation with respect to the selected reference point*. In addition, the Satellite Communications Toolbox implements the ITU-R propagation models P.618 [19].

The Figure 36 gives a graphical representation of satellite orbits simulated and analyzed using Satellite Toolbox.

Figure 36. Satellite Toolbox Graphic User Interface.
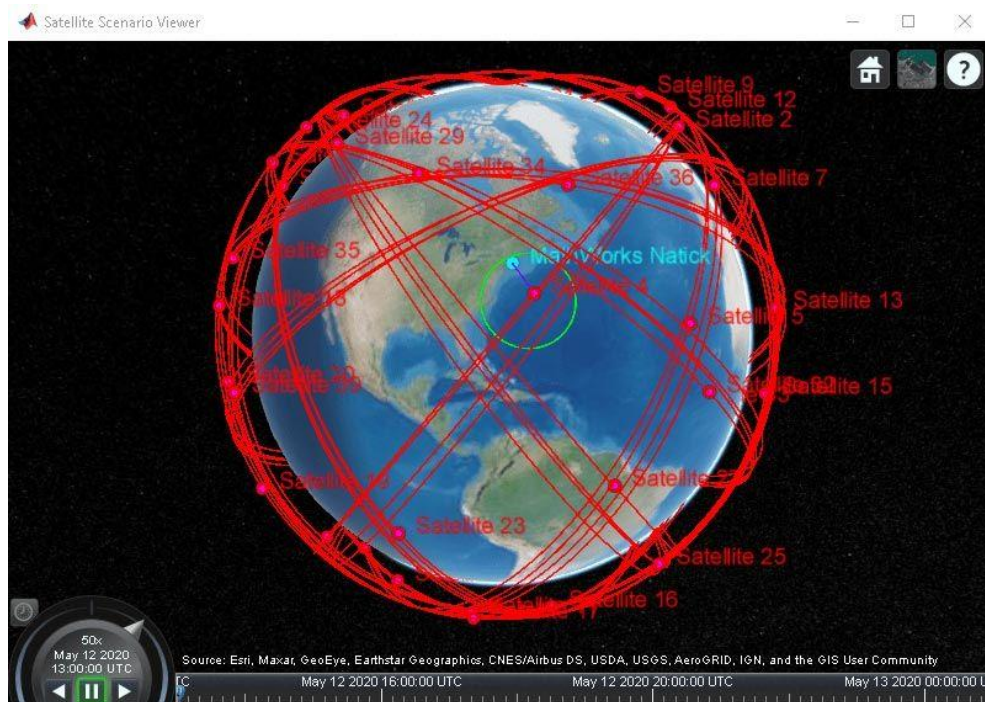
6.3.4 LEO constellations' simulation: aim and Key Performance Indicators (KPI)

The main scope of simulations for the considered LEO HTS satellite constellations is the calculation of the C/(N+I) along the Rome-Florence railway line in the considered reference points.

Starting from the SpaceX and OneWeb TLE files, we have considered the distribution of the satellites covering the considered railway line during an entire day (24 hours). Satellite data (see after) are calculated considering a sampling time (i.e., the distance between two consecutive time instants) of about 2min.

The main satellite parameters are then calculated to proceed with the link budget estimation.

The C/(N+I) is related to the available Bit Rate by means of the best MCS that can be selected in the upstream or downlink. The following Key Performance Indicators (KPIs) are considered for analysing the behaviour of the satellite constellation with time and for achieving the link budget analysis. All the parameters listed below can be obtained starting from the calculation of the: *azimuth*, *elevation* and *range* of each satellite with respect to each one of the selected reference points (RPs).

1. Trend over time of the elevation angle range, pathloss in free space and the visibility range of each satellite and for each RP;
2. Best case and worst case for LEO satellite
   - Range of the best satellite with time over the entire day (24 hours); the best satellite is the visible satellite at minimum range from the reference point at each time instant;
   - Best satellite propagation delay statistics
   - Worst satellite delay statistics (the worst satellite is the visible satellite with the highest range from the considered reference point (RP) at the ground)
3. Distribution of visibility intervals of all satellites for each RP; the visibility interval is evaluated for each satellite and it is the duration of the time interval starting when the single satellite becomes visible (i.e., its elevation is above or equal to 15o) and ending when the satellite returns below the minimum elevation angle (i.e., below 15°);
4. Distribution of the visibility intervals of the best satellite for each RP (this interval is evaluated considering at each time instant the best satellite with respect to the considered RP)
5. Link budget used for the assessment of the C/(N+I)
   For each RP we have evaluated the link budget considering at each time instant: the best satellite, the worst satellite and one "*persistent*" satellite. As persistent satellite we mean the satellite with the longest duration of its visibility time interval with respect to the RP. In practice we assume the satellite modem at the RP remains connected to the same satellite for the entire duration of its visibility time. At the end of the visibility time interval the modem selects another satellite and remains connected to it for the entire duration of its visibility time and so on.

6.3.5 link budget calculation and Modulation and Coding Scheme (MCS)

The link budget calculation is based on the following formula [20] [21]:

$$P_{RX}[\text{dBm}] = P_{TX} + G_{TX} - L_{TX} - FSPL - L_M + G_{RX} - L_{RX}$$

Where:

P_{RX} [dBm]: received power

P_{TX} [dBm]: transmitter output power

G_{TX} [dBi]: transmitter antenna gain

L_{TX} [dB]: transmitter loss

FSPL [dB]: path loss, usually free space loss

L_M [dB]: losses: fading, body loss, atmospheric loss etc.

G_{RX} [dBi]: receiver antenna gain

L_{RX} [dB]: receiver losses

From the previous formula, the calculation of minimum Bit Rate is based on the steps summarized in Figure 37:

Figure 37. Minimum Bit rate calculation methodology.

1. • Calculation of SINR

2. • Calculation of $E_s/(N0+I0)$ ratio

3. • Calculation of $E_b/(N0+I0)$ ratio

4. • Selection of Modulation and Coding Scheme (MCS) for DVB-S2 communication

5. • Calculation of minimum Bit Rate
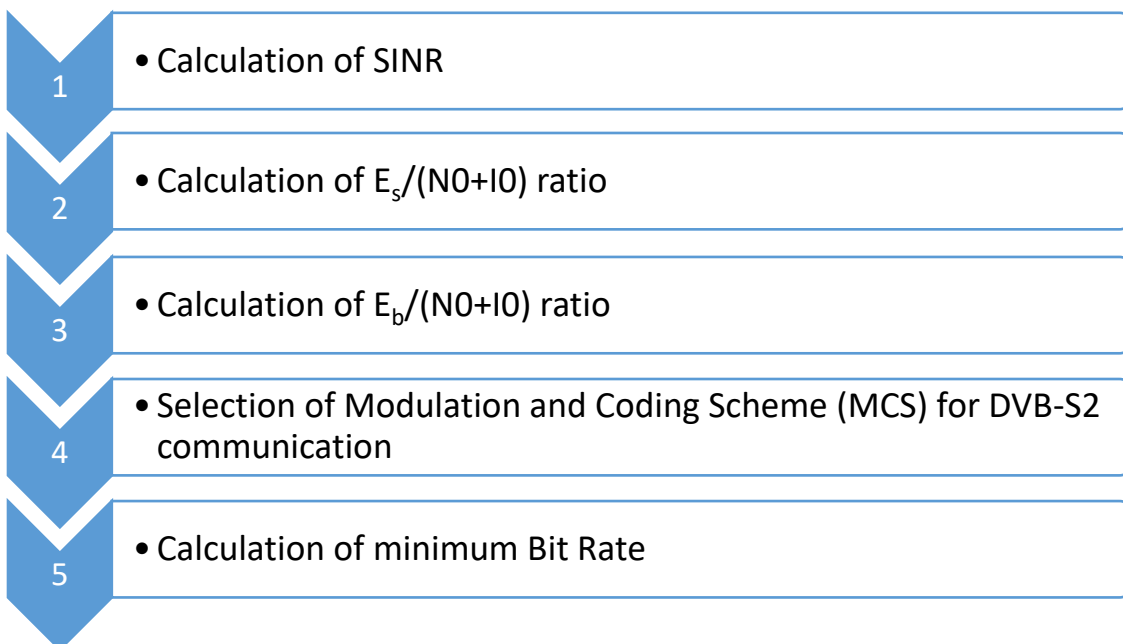
As shown in the previous Figure, starting from the C/(N+I) calculation, we proceed with the calculation of ratio between the energy per transmitted symbol and single sided noise power spectral density (Es/(N0+I0)) and Es is the energy per useful symbol and Eb=Es-10*log10(spectral efficiency). After, we calculate ratio between the energy per information bit and single sided noise power spectral density (Eb/(N_0+I_0)).

According to [22] we selected the modulation and coding scheme (MCS) based on the target margin (in dB) (see after). Given the spectral efficiency (i.e., the MCS) and the transmission bandwidth the available bit rate is:

Spectral efficiency * bandwidth = Available Bit Rate

To better clarify these concepts, we consider the following example.
- From the link budget calculation, we obtain a C/(N+I) ratio of 13.5 dB
- According to the values listed in the Table 12Table 12 with the reference values of Es/N0 and Eb/N0 corresponding to the C/(N+I) value of 13.5 dB, we observe:
  o If we select the 16APSK 2/3 MCS, Eb/(N0+I0) is equal to 9.4 dB and in the same column we observe that 5.9 dB is the minimum value of Eb/(N0+I0) ratio necessary to select this MCS. This implies that the obtained link margin is given by the following calculation: (9.4-5.9) dB = 3.5 dB
  o Still considering C/(N+I) = 13.5 dB, we could select other MCSs, although the resulting margin is going to decrease. Example. In case of 16 APSK 5/6 MCS, the minimum requested value of Eb/(N0+I0) ratio is 7.5 dB. The value of Eb/(N0+I0) corresponding to the considered C/N value is 8.4 dB. It means the margin decreases and it given by the following calculation: (8.4-7.5) dB = 0.9 dB

The Table 12 shows a graphical representation of this example.

Table 12. C/N values in case of DVB-S2 SNR 16APSK and 32APSK.

Spectral Efficiency Normal Block Mode Pilots ON ▶		16APSK						32APSK				
		2.574613	2.896320	3.090495	3.221863	3.439530	3.482680	3.623332	3.866247	4.030589	4.302894	4.356875
	Code Rate ▶	2/3	3/4	4/5	5/6	8/9	9/10	3/4	4/5	5/6	8/9	9/10
(Co+No)/No	C/N = Es/No	Eb/No	Eb/No	Eb/No	Eb/No	Eb/No	Eb/No	Eb/No	Eb/No	Eb/No	Eb/No	Eb/No
9.8	9.3	5.2	4.7	4.4	4.2	4.0	3.9	3.7	3.4	3.3	3.0	2.9
10.1	9.7	5.5	5.0	4.8	4.6	4.3	4.2	4.1	3.8	3.6	3.3	3.3
10.4	10.0	5.9	5.4	5.1	4.9	4.6	4.6	4.4	4.1	3.9	3.6	3.6
10.7	10.3	6.2	5.7	5.4	5.2	4.9	4.9	4.7	4.4	4.3	4.0	3.9
11.0	10.6	6.5	6.0	5.7	5.6	5.3	5.2	5.0	4.8	4.6	4.3	4.2
11.3	11.0	6.9	6.3	6.1	5.9	5.6	5.5	5.4	5.1	4.9	4.6	4.6
11.6	11.3	7.2	6.7	6.4	6.2	5.9	5.9	5.7	5.4	5.2	5.0	4.9
11.9	11.6	7.5	7.0	6.7	6.5	6.2	6.2	6.0	5.7	5.6	5.3	5.2
12.2	11.9	7.8	7.3	7.0	6.8	6.6	6.5	6.3	6.1	5.9	5.6	5.5
12.5	12.2	8.1	7.6	7.3	7.2	6.9	6.8	6.7	6.4	6.2	5.9	5.9
12.8	12.6	8.5	7.9	7.7	7.5	7.2	7.1	7.0	6.7	6.5	6.2	6.2
13.1	12.9	8.8	8.3	8.0	7.8	7.5	7.5	7.3	7.0	6.8	6.5	6.5
13.4	13.2	9.1	8.6	8.3	8.1	7.8	7.8	7.6	7.3	7.1	6.9	6.8
13.7	13.5	9.4	8.9	8.6	8.4	8.1	8.1	7.9	7.6	7.5	7.2	7.1
14.0	13.8	9.7	9.2	8.9	8.7	8.5	8.4	8.2	8.0	7.8	7.5	7.4
14.3	14.1	10.0	9.5	9.2	9.1	8.8	8.7	8.5	8.3	8.1	7.8	7.7
14.6	14.4	10.3	9.8	9.5	9.4	9.1	9.0	8.9	8.6	8.4	8.1	8.1
14.9	14.8	10.7	10.1	9.9	9.7	9.4	9.3	9.2	8.9	8.7	8.4	8.4
15.2	15.1	11.0	10.4	10.2	10.0	9.7	9.6	9.5	9.2	9.0	8.7	8.7
15.5	15.4	11.3	10.8	10.5	10.3	10.0	10.0	9.8	9.5	9.3	9.0	9.0
15.8	15.7	11.6	11.1	10.8	10.6	10.3	10.3	10.1	9.8	9.6	9.3	9.3
16.1	16.0	11.9	11.4	11.1	10.9	10.6	10.6	10.4	10.1	9.9	9.7	9.6
16.4	16.3	12.2	11.7	11.4	11.2	10.9	10.9	10.7	10.4	10.2	10.0	9.9
16.7	16.6	12.5	12.0	11.7	11.5	11.2	11.2	11.0	10.7	10.6	10.3	10.2
17.0	16.9	12.8	12.3	12.0	11.8	11.5	11.5	11.3	11.0	10.9	10.6	10.5
17.3	17.2	13.1	12.6	12.3	12.1	11.9	11.8	11.6	11.3	11.2	10.9	10.8
17.6	17.5	13.4	12.9	12.6	12.4	12.2	12.1	11.9	11.7	11.5	11.2	11.1
17.9	17.8	13.7	13.2	12.9	12.7	12.5	12.4	12.2	12.0	11.8	11.5	11.4
18.2	18.1	14.0	13.5	13.2	13.1	12.8	12.7	12.5	12.3	12.1	11.8	11.7
18.5	18.4	14.3	13.8	13.5	13.4	13.1	13.0	12.8	12.6	12.4	12.1	12.0
18.8	18.7	14.6	14.1	13.8	13.7	13.4	13.3	13.2	12.9	12.7	12.4	12.4
19.1	19.0	14.9	14.4	14.1	14.0	13.7	13.6	13.5	13.2	13.0	12.7	12.7
19.4	19.3	15.2	14.7	14.4	14.3	14.0	13.9	13.8	13.5	13.3	13.0	13.0
19.7	19.7	15.5	15.0	14.8	14.6	14.3	14.2	14.1	13.8	13.6	13.3	13.3
20.0	20.0	15.8	15.3	15.1	14.9	14.6	14.5	14.4	14.1	13.9	13.6	13.6

6.4 Starlink and OneWeb LEO constellation performance assessment and link-budget calculation

The following Table 13 summarizes the main parameters used to calculate the LEO satellite link budget in case of SpaceX and OneWeb, both in uplink and downlink.

The paper [13] is based on a constellation dating back to 2018, while our analysis is based on a constellation updated in July 2022 (we have used the most recent TLE files), where the number of SpaceX satellites has been increased and also low orbit and polar satellites have been added.

Table 13. Parameters used for the link budget calculation in case of SpaceX and OneWeb LEO constellations: downlink (a), uplink (b).

(a)

Parameter	OneWeb	SpaceX	Unit
Frequency	12.7	12.7	GHz
Bandwidth	0.250	0.125	GHz
EIRP	34.6	36.7	dBW
MCS	16 APSK 2/3	16 APSK 3/4	-
Roll-off Factor	0.1	0.1	-
Atmospheric loss	0.41	0.53	dB
LEO Rx Antenna Diameter	0.7	0.7	m
LEO RX antenna gain	38.3	37.7	dBi
System Temperature	350.1	362.9	K
Rx C/ASI	25	25	dB
Rx C/XPI	20	22	dB
HPA C/3IM	30	25	dB
Rx Eb/(N0+I0)	5.9	6.7	dB
Req. Eb/N0	5.2	5.9	dB
Link Margin		0.82	dB
Shanno Limit		1.46	dB
Data rate		674.3	Mbps

(b)

Parameter	OneWeb	SpaceX	Unit
Frequency	14.25	14.5	GHz
Bandwidth	0.25	0.125	GHz
Tx antenna Diameter	0.48	0.48	m
EIRP	39.4	39.4	dBW
MCS	256 APSK 32/45	256 APSK 3/4	-
Roll-off Factor	0.1	0.1	-
Atmospheric loss	2.9	2.9	dB
LEO Rx Antenna Diameter	0.48	0.7	m
LEO RX antenna gain	37.8	40.9	dBi
System Temperature	350.1	535.9	K
Rx C/ACI	27	27	dB
Rx C/ASI	27	27	dB
Rx C/XPI	25	25	dB
HPA C/3IM	30	30	dB

6.5 SpaceX and OneWeb performance assessment: simulation results

Results presented in this Section refer to LEO satellites flying over the Italian area during the day. The RPs are selected along the Roma-Firenze railway line.

The Figure 38 shows the number of visible SpaceX and OneWeb LEO satellites during the day when considering the RP located in Rome. We have observed that this number remains practically unchanged when considering the other RPs along the line.

Figure 38. Number of LEO Satellites visible during the day: SpaceX (a), OneWeb (b).

(a)   (b)
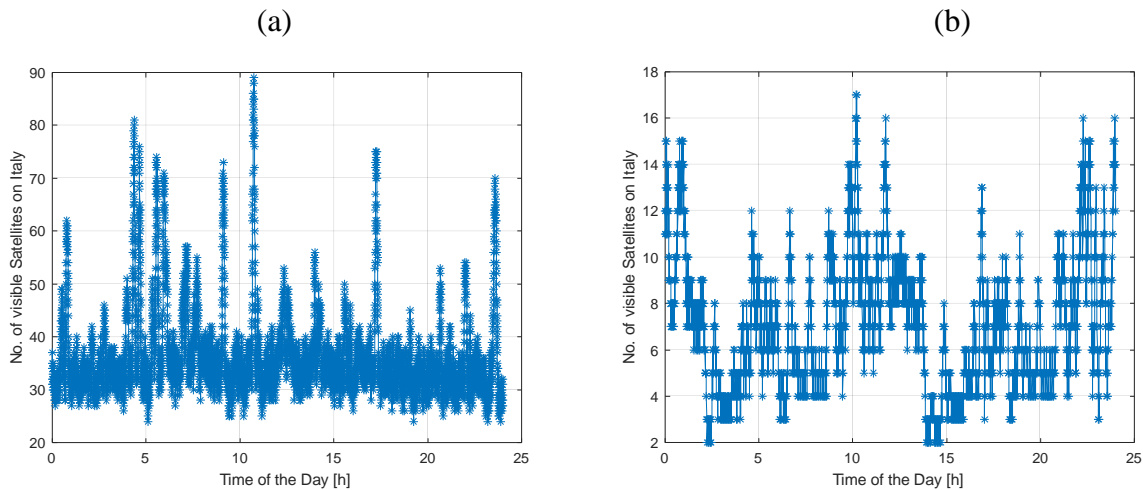
As from Figure 38, during the day the visible satellites are those above 15o degree of elevation angle. During their daily movement, the satellites pass from a low elevation angle to a maximum and then the elevation angle starts to decrease. In both cases, SpaceX and OneWeb, for the Rome-Florence section, there is a rather constant trend in the average number of satellites visible throughout the day, with 30-40 satellites in the first case, and 8 in the second case. The numbers of the two operators depend on the satellite launch plans and their relative operations in orbit. For this reason, the number of visible OneWeb satellites is lower than SpaceX. This difference will be reduced with time when the number of satellites of OneWeb will increase.

In Figure 39 shows the range (km) of a pair of LEO Satellites visible in a certain time interval of the day from one RP in Rome. Both SpaceX and OneWeb constellations have been considered.

Figure 39. Range distance of a couple of LEO Satellites visible during the day from each Ground Station: SpaceX (a), OneWeb (b).

(a)   (b)
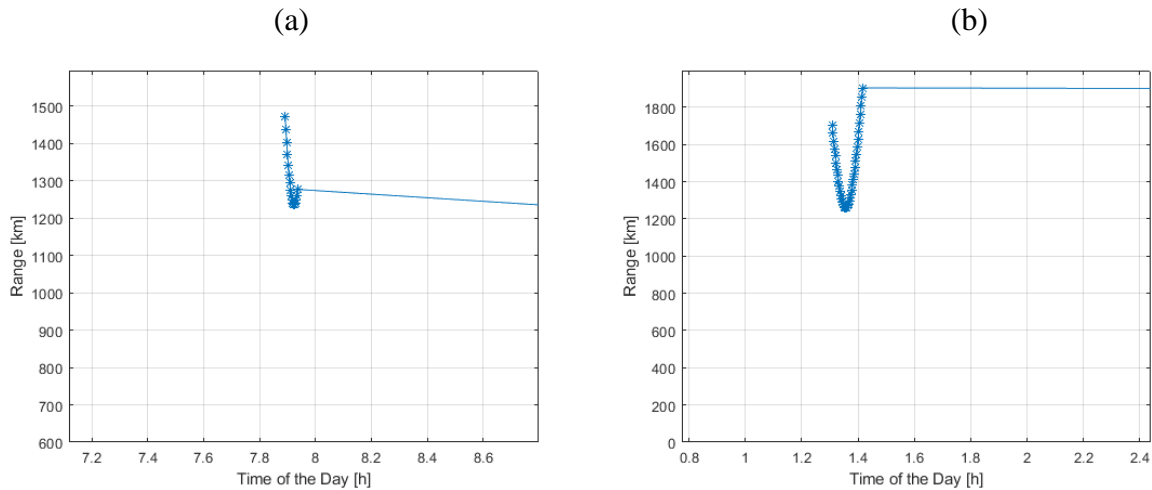
It should be observed that distances can vary between a maximum distance of about 1,500 km (SpaceX) or 1,900 km (OneWeb) and a minimum distance of 500 km (SpaceX) and about 1,200 km (OneWeb). The orbits of SpaceX satellite are closer to the earth.

In Figure 40 we show the Elevation angle of a couple of LEO Satellites visible during the day for the RP in Rome corresponding to the range situation in Figure 37. Both for SpaceX and OneWeb have been considered.

Figure 40. Elevation angle of a couple of LEO Satellites visible during the day from each Ground Station: SpaceX (a), OneWeb (b).

(a)   (b)
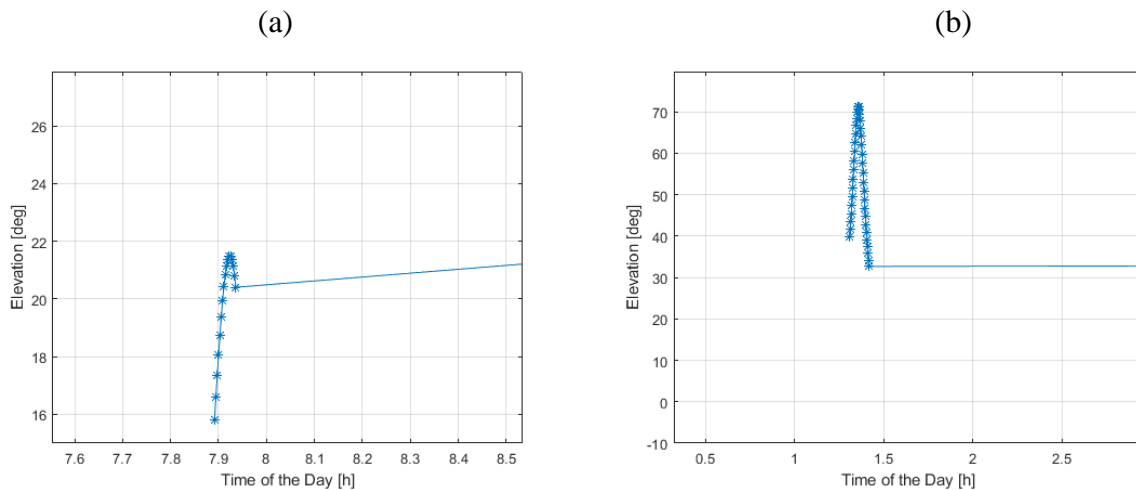
As expected, elevation angles vary from a minimum of 15 ° (below which the satellite is not visible)

(in the case of Spacex, otherwise 30 ° in the case of OneWeb) up to a maximum of 60° or 70°, in the case of from SpaceX or OneWeb respectively. The maximum elevation angle corresponds to the minimum distance of the satellite from the ground.

In Figure 41 we plot the Range of a single LEO Satellite visible at the same time of the day from the RP in Rome and another RP in Bologna. Both SpaceX and OneWeb constellations have been considered.

Figure 41. Range distance of the same LEO Satellite visible during the day from two different Ground Stations (Rome and Bologna): SpaceX (a), OneWeb (b).

(a)

(b)
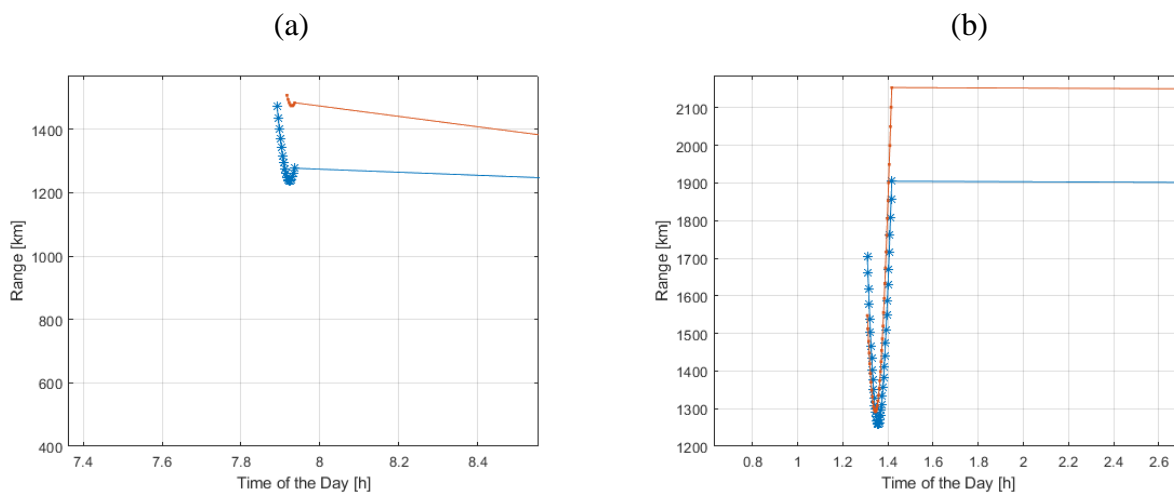
From the figure it emerges that the same satellite is seen by the two considered RPs almost at the same range. In fact, since the distance between Rome and Bologna is about 400 km, the same satellite is visible, for example, at 8 am at 1500 km in Bologna and 1200 km in Rome in the case of SpaceX, while it is visible at 1900 km In Rome and at 2150 km in Bologna in the case of OneWeb between 1:30 and 2:00 am.

In Figure 42 we plot the Elevation angle of the LEO Satellite corresponding to the situations in Figures 39a and 39b.

(a)   (b)

From these Figures it can be seen that the same satellite is visible, for example, at 8 am the elevation angle of the satellite has a value of about 22 ° in Rome and about 15 ° in Bologna in the case of SpaceX, while it is visible at about 32° in Rome and at 26° in Bologna in the case of OneWeb at a time between 1.30 am and 2 am. This derives from the fact that the distance between the two RPs is not very large as compared to the range of the satellite.

The calculated range with time of the single visible satellite can be used to evaluate the propagation delay τ as

$$\tau = range/c$$

and c is the light speed resulting in propagation delays in the order of some ms for the UE-to-Satellite link and vice versa.

In Figure 43 we plot the range of the best and worst LEO visible satellites during the day for SpaceX and in a limited time interval for OneWeb.

(a)   (b)
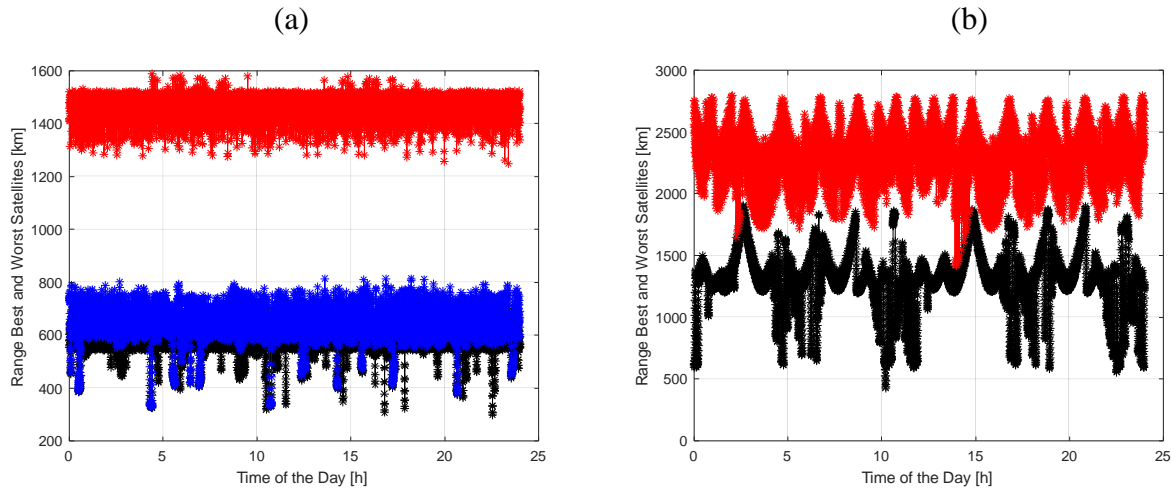
In Figure 43 shows the ranges of the best satellite are indicated in black while the worst satellite is indicated in red. In blue we have indicated the distance of the second-best available satellite for SpaceX i.e., the second satellite which is closer to the RP. In the case of SpaceX, the closest satellite (best) during the day is located at a variable distance between 300 km and 600 km, the farthest satellite (worst) between 1,300 km and 1,550 km (and in some cases even 1,600. The range of the second "best" satellite varies between 300 and 800 km.

In the case of OneWeb, the farthest satellite (worst) is around 2,200 km, while the closest one (best) is between 500 km and 1600 km.

In Figure 44 we plot the Cumulative Density Function (CDF) of the one-way propagation delay corresponding to the visibility time of the best and of the worst LEO satellite during the day. Both SpaceX and OneWeb constellations have been considered.

Figure 44. Cumulative Density Function (CDF) of the propagation delay in the case of the best and worst LEO satellite visible during the day: SpaceX (a), OneWeb (b).

(a)   (b)
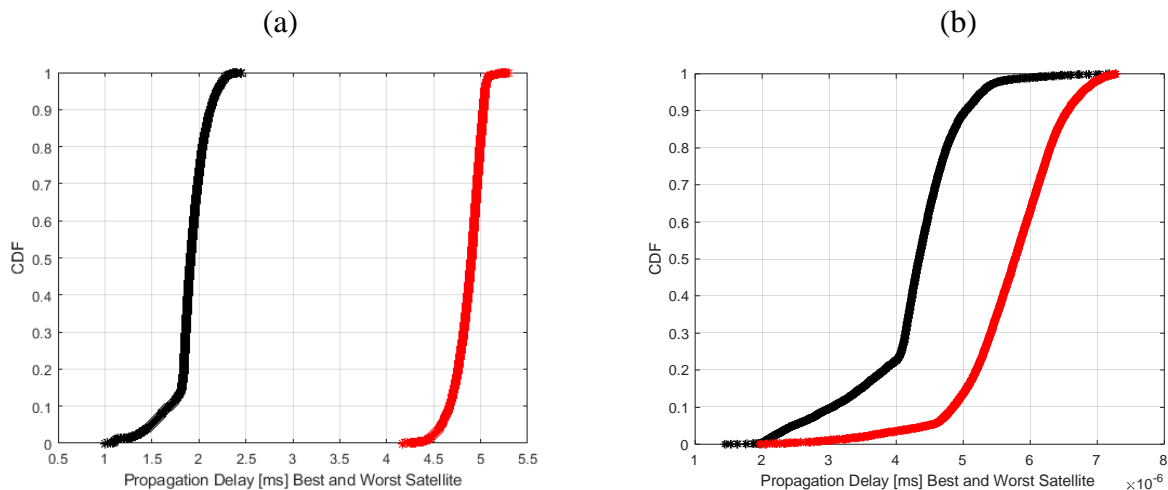
In the case of SpaceX, in 50% of cases, the LEO satellite provides a propagation delay of about 1.8 ms (in the best case) and of 5 ms (in the worst case). In 80% of cases, the propagation delay is about 2 ms (in the best case) and 5 ms (in the worst case).

In the case of OneWeb, in 50% of cases, the LEO satellite provides a propagation delay of about 4.2 ms (in the best case) and of about 5.6 ms (in the worst case). In 80% of cases, the propagation delay reaches over 4.5 ms (in the best case) and over 6 ms (in the worst case).

Even in the worst-case scenario for SpaceX the propagation delay never exceeds 5.5 ms and 7 ms for OneWeb. Instead, when considering the satellite modem always connect (and search for) the best satellite these maximum delays fall below 2.5 ms for SpaceX and to 5ms for OneWeb. This reveals that the two considered LEO HTS constellations are very attractive for supporting relatively low delay transmissions and that they can be serious competitors for terrestrial radio access systems in sub-urban areas and especially in rural areas where older terrestrial radio technologies (e.g., GSM-R) are present (e.g., rural areas) or are not available at all. Starting from this very encouraging data we believe a trial in 2023 should be started in another EU2Rail project to test on the field the potentials of SpaceX LEO for railway communications and, in the future, of OneWeb opening the possibility of using the two satellite constellations together and one as backup of the other.

In Figure 45 we plot the Cumulative Density Function (CDF) of the elevation angle in the case of the best and worst LEO satellite visible during the day, both for SpaceX and OneWeb.

Figure 45. Cumulative Density Function (CDF) of the elevation angle in the case of the best and worst LEO satellite visible during the day: SpaceX (a), OneWeb (b).
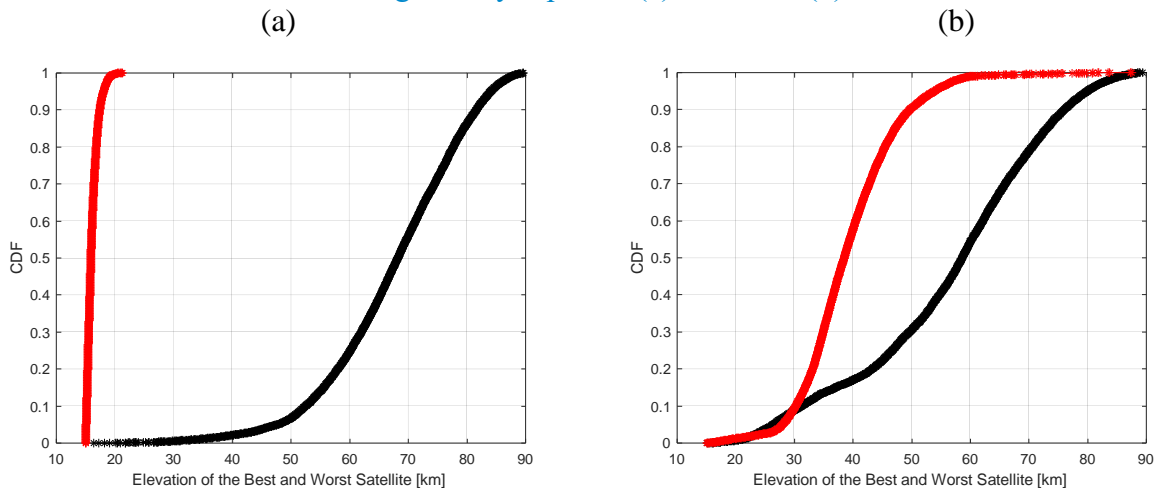
In the case of SpaceX, in 50% of cases, the worst satellite provides an elevation angle of about 15° in 50% of cases and about 17° in 80% of cases, while the best satellite provides an elevation angle of about 65° in 50% of cases and 75% in 80% of cases

In the case of OneWeb, however, in 50% of cases, the worst satellite provides an elevation angle of about 35° in 50% of cases and 40° in 80% of cases, while the best satellite provides an elevation angle of about 60° in 50% of cases and 70° in 80% of cases.

In Figure 46 we plot the Complementary Cumulative Distribution Function (CCDF) of the range of both the best and of the persistent satellite considering the two RPs in Rome and Bologna for both for SpaceX and OneWeb LEO constellations.

Figure 46. Complementary cumulative distribution Function (CCDF) of the visibility range of both the best and persistent in visibility, seen from two different Ground Stations (Rome and Bologna): SpaceX (a), OneWeb (b).

(a)   (b)
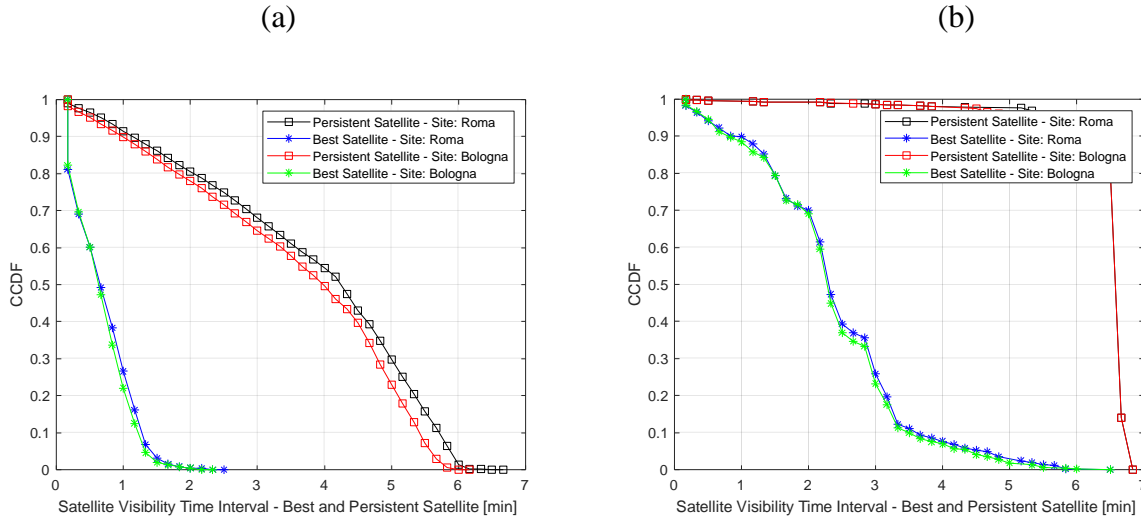
In the case of SpaceX, the red and black curves refer to the satellite in visibility for the whole day (persistent) and which has an elevation angle greater than 15°. Beyond this value, the satellite is no longer visible. The visibility time interval of this satellite is about 1.5 minutes in 80% of cases and 4 minutes in the case of 50% of cases. The blue and green curves refer to the best satellite seen by the two different GSs. The visibility time interval of the best satellite is less than 30 seconds in 80 of cases and less than one minute in 50% of cases.

In the case of OneWeb, the persistent satellite visibility time interval is about 6.8 minutes in 80% of cases and about 6.5 minutes in 50% of cases. The blue and green curves refer to the best satellite seen by the two different GSs. the visibility time interval of the best satellite is between 1 and 2 minutes in 80% of cases and between 2 and 3 minutes in 50% of cases.

The fact that OneWeb satellites have visibility time longer than SpaceX satellites is due to their higher orbits. The visibility time interval is always significantly shorter than the time of the persistent satellite. Obviously, and as also demonstrated in the next of this Section, best performance are achieved when selecting the best satellite every time but this would require a more complicated satellite modem able to rapidly switch from one satellite to another one. This could be difficult to achieve especially in the SpaceX case where the visibility time of the best satellite could be below one minute (see Figure 46a).

In Figure 47 we report the cumulative Distribution Function (CDF) of the achievable C/(N+I) of the best, worst and persistent satellites. The CDF has been obtained by collecting data from all the RPs considered along the Roma-Firenze railway line. The case in Figure 47 refers to downlink, for both SpaceX and OneWeb.

Figure 47. Cumulative Distribution Function (CDF) of the SINR interval of the best, worst and persistent satellites, visible by all Ground Stations, in downlink: SpaceX (a), OneWeb (b).

(a)   (b)
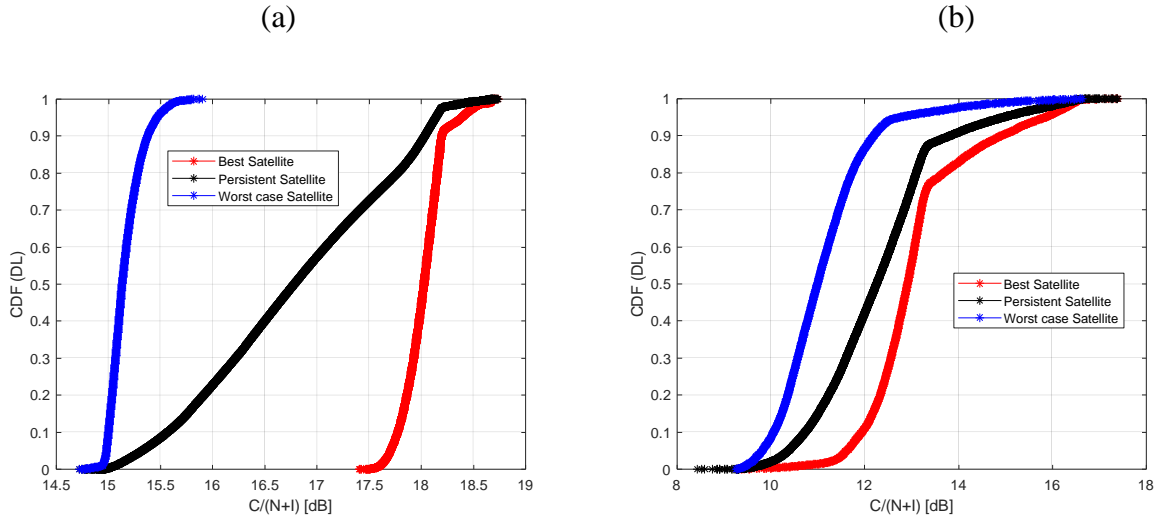
From all figures, it can be observed that the range of variations of the C/(N+I) is limited within about 5dB for SpaceX and 9 dB for OneWeb. The reduced performance of OneWeb is due to the higher range of satellites with respect to SpaceX and to the reduced number of satellites which are available up to now. OneWeb performance are however destined to improve with the launch of the new satellites.

In the case of SpaceX, the best satellite provides a C / (N + I) value of almost 18 dB and 17.7 dB respectively in 80% and 50% of cases. The worst satellite provides a value of 15.4 dB and 15.2 dB respectively in 80% and 50% of cases. Finally, the persistent satellite provides a C / (N + I) value of almost 17.7 dB and 16.7 dB respectively in 80% and 50% of cases.

In the case of OneWeb, the best satellite provides a C / (N + I) value of almost 13.8 dB and 12.5 dB respectively in 80% and 50% of cases. The worst satellite provides a value of 11.5 dB and 10.5 dB respectively in 80% and 50% of cases. Finally, the persistent satellite provides a value of C / (N + I) equal to almost 12.5 dB and 12 dB respectively in 80% and 50% of cases.

As expected in all case, the adaptive selection of the best available satellites allows to improve performance and to render the available C/(N+I) practically independent of the RP position as shown in the SpaceX case (see Figure 47a red curve). The possibility of tracking the persistent satellite allows to simplify the on-board satellite modem but it may lead to variation in the available C/(N+I) while the train is moving along the railway line thus causing variable performance.

In Figure 48 we plot the Cumulative Distribution Function (CDF) of the uplink C/(N+I) interval of the best, worst and persistent satellites, obtained by collecting all C/(N+I) evaluated for each visible satellite in every one of the RPs for both for SpaceX and OneWeb.

Figure 48. Cumulative Distribution Function (CDF) of the SINR interval of the best, worst and persistent satellites, visible by all Ground Stations, in uplink: SpaceX (a), OneWeb (b).
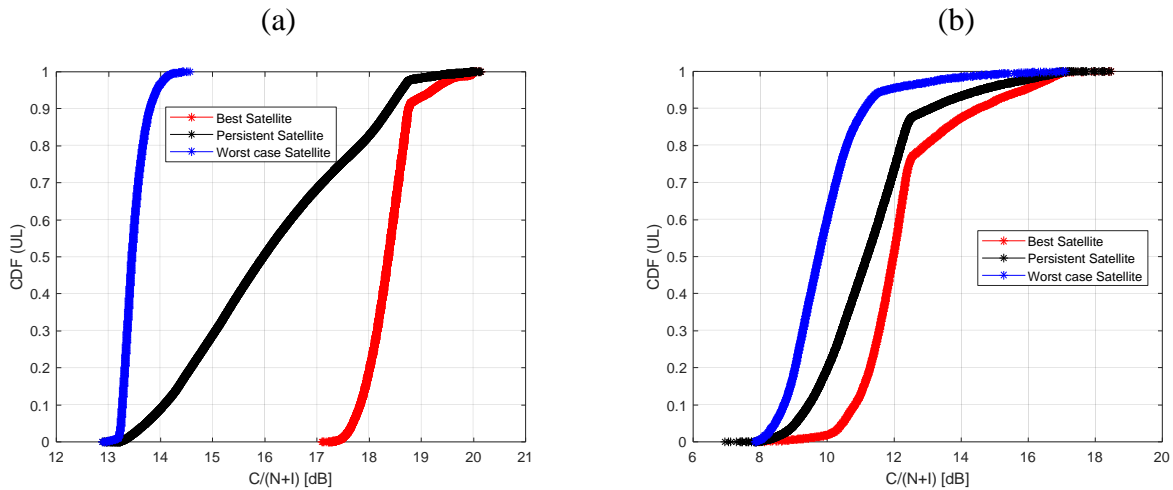
In the case of SpaceX, the best satellite provides a C / (N + I) value of almost 18.5 dB and 18 dB respectively in 80% and 50% of cases. The worst satellite provides a value of 13.5 dB and 13.2 dB respectively in 80% and 50% of cases. Finally, the persistent satellite provides a value of C / (N + I) equal to almost 17.5 dB and 16 dB respectively in 80% and 50% of cases.

In the case of OneWeb, the best satellite provides a C / (N + I) value of almost 12.5 dB and 12 dB respectively in 80% and 50% of cases. The worst satellite provides a value of 10 dB and 9.5 dB respectively in 80% and 50% of cases. Finally, the persistent satellite provides a value of C / (N + I) equal to almost 12 dB and 11 dB respectively in 80% and 50% of cases.

Same considerations for downlink still apply to uplink when considering the selection of the best and of the persistent satellite.

7. High Altitude Platform System (HAPS)

7.1 HAPS System Architecture

The HAPS is considered as an important asset to extend the terrestrial Radio Access Network (RAN) based on one or more transmission standards such as LTE or 5G.

The generic HAPS system architecture is illustrated in Figure 49.

Figure 49. Overall HAPS system architecture.
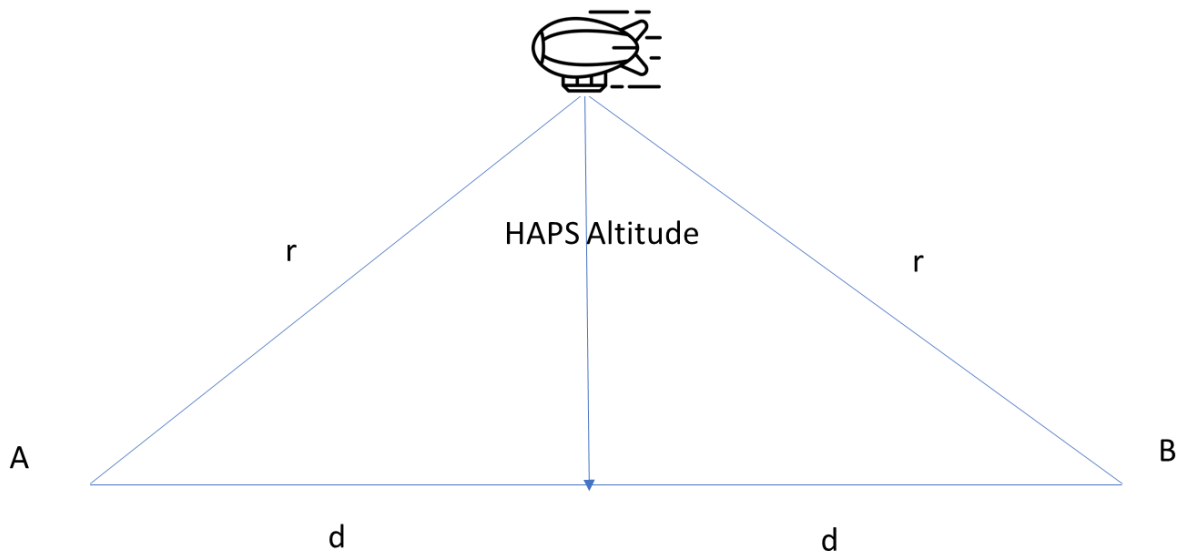
Due to most favorable atmospheric conditions, the HAPS is usually positioned at an altitude of 19 km-20km [23]. The single HAP can host one eNB or gNB. In the following we assume the HAP hosts an eNB. This is in line with the ongoing experimentation activities in different countries.

We further assume that the HAP is visible when the elevation angle is greater than 15°. This leads to a maximum horizontal distance for visibility of 74.64 x 2 = 150 km with the HAP at the height of 20km. However, as shown in the following, the HAP radio coverage on the ground can be significantly larger than d=74.64 km (d is the horizontal distance in Figure 49). This depends on the characteristics of the UE and of the on-board radio equipment. We implicitly assume that for elevation below 15° obscuration phenomena prevent the possibility to communicate with the HAPS due to radio link outage.

7.2 Methodology for performance evaluation

Starting from the HAPS system architecture in Figure 49, the scope of the simulation is to analyze the system performance of HAPS in terms of:

- Available radio coverage on the ground from a single HAP

- Evaluation of available system capacity per single HAPS and then of the modulation and coding scheme (MCS) that can selected depending on the (horizontal) distance of UE from the vertical projection of the HAPS on the ground (i.e. the point x in Figure 49);

The selected performance parameters depend on the User Equipment (UE) Sensitivity and on path loss (PL). Concerning the PL two models have been considered for evaluation purposes: the ITU-R P.528 aeronautical channel model and the Free Space Path Loss (FSPL).

Similarly, to LEO HTS satellite performance evaluation, the main aim of the simulation for the HAPS is the calculation of the C/(N+I) for uplink and downlink transmissions. For simplicity, to account for the different types of interference introduced in the LEO case, we assume the HAPS on-board equipment has the same C/ACI, C/3MI etc. characteristics of the LEO equipment. Interference among different beams of the HAPS is difficult to evaluate since the antenna radio patterns are unknown and because it is not clear if the HAPS will partition the available band among beams using a frequency reuse pattern maybe similar to that adopted for the initial planning of the cellular radio systems.

In

Figure 50 we depict the workflow adopted for evaluating the HAPS performance.

Figure 50. HAPS system simulation workflow.
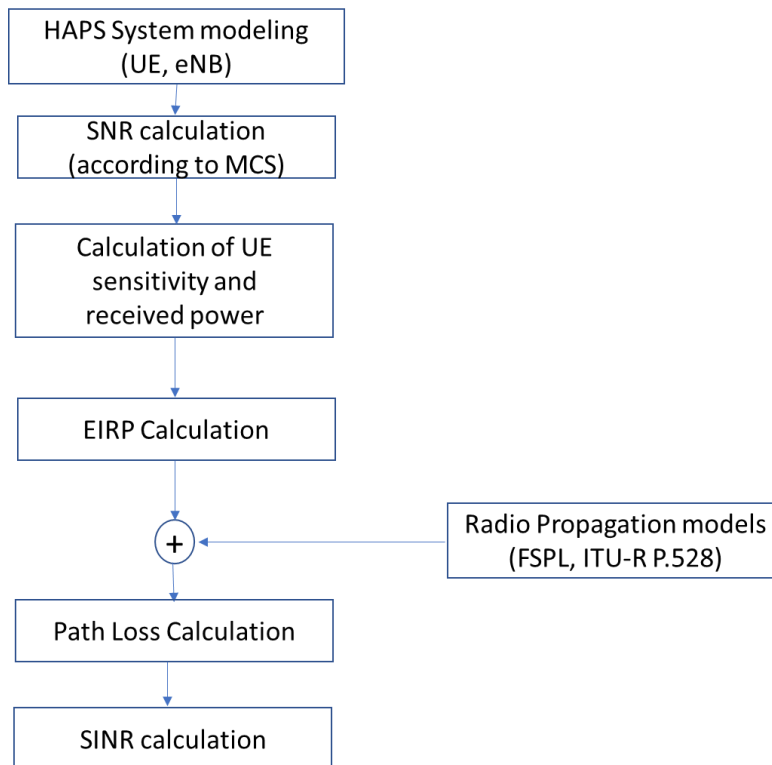
As previously outlined, we assume the HAPS is equipped with an eNB which is connected to the Evolved Packet Core (EPC) using a dedicated link. In the following analysis we are interested in the performance evaluation of the radio links connecting the UE to the eNB in the HAPS (uplink) and vice versa (downlink) assuming that the HAPS to EPC link is designed properly to accommodate for all the traffic generated by terminals in the HAPS coverage on the ground.

In the HAPS system modeling we account for all the radio parameters characterizing the UE and the eNB i.e., the UE sensitivity, the power that can be transmitted by the UE and the eNB (i.e., the available EIRP for uplink and the downlink). The path loss is accounted for using the Free Space Path Loss (FSPL) [24] and ITU-R P.528 [25] radio propagation models.

To render the evaluation more realistic we also account for the different MCSs that can be selected by the UE and the eNB in accordance with the achieved C/(N+I), which is a function of the distance between the eNB on the HAPS and the UE at the ground.

In principle, HAPS coverage and transmission parameters should be selected so that the radio coverage area under the HAPS is partitioned into concentric circles, each one allowing the UE to transmit with an MCS ranging from QPSK 1/3 up to 64QAM 4/5 as indicated in the LTE standard. In particular, it should be expected that UE which is in close proximity of the HAPS vertical could use the 64 QAM 4/5 while at the edge of the cell the QPSK 1/3 MCS. In the following of this Section, we prove that in certain circumstances this could not be possible to achieve if the transmitter/receiver parameters are not properly selected. Figure 51 gives a graphical illustrative representation of the MCS dependence from HAPS and the corresponding influence on the horizontal distance.

Figure 51. HAPS system modeling: influence of Modulation and Coding Scheme (MCS) (a), coverage a single beam (b).

(a)
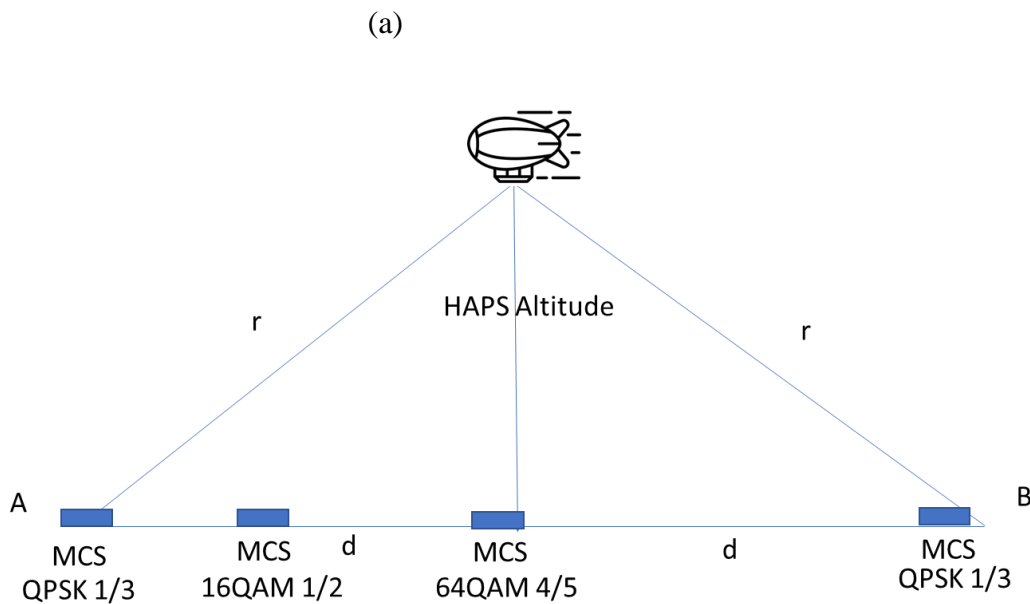
(b)
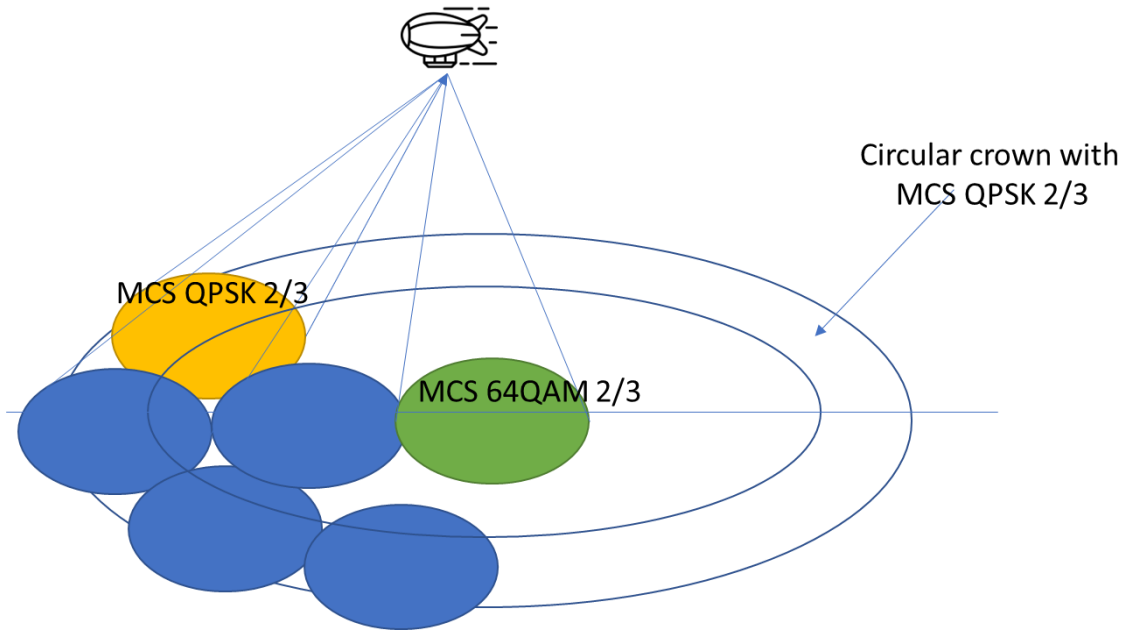
If the HAPS antenna is of multi-beam type and for each beam the transmitter/receiver parameters remain unaltered i.e., same antenna gains and the same transmission parameters, as shown in Figure 52 some beams may cover cell areas characterized by low efficiency MCSs while others can cover cell areas with more efficient MCS. This means that the available transmission capacity per beam can be different, and some beams could be penalized in terms of performance especially when the beam covers the cell border. Instead, by varying the radio link parameters within each beam (e.g., the antenna gain, and the transmitter power are adjusted at single beam level) equalization of performance among beams could be achieved allowing for example the beams at the cell edge to adopt a more spectral efficient MCS. Our evaluation focuses on the analysis of the achievable radio coverage on the ground disregarding the presence of multi-beams. The considered procedure is general and can be reused to evaluate the coverage characteristics at the single beam level given its specific transmission parameters e.g., beam antenna gain, EIRP etc.

Finally, in our analysis we would like to put into evidence the importance of the selection of the transmission frequency range for guaranteeing the required radio coverage.

7.2.1   Considered radio propagation models for path loss calculation

The main radio propagation models considered in simulations are:

- Free Space Path Loss (FSPL)

- ITU-R P.528

The ITU-R P.528 Recommendation provides the guidelines to compute the transmission loss within the VHF, UHF and SHF bands (from 100 to 30,000 MHz) reserved to the aeronautical services.

According to ITU-R P.528 model, three different frequency bands are considered [25]:

- Band 1 (694–960 MHz)

- Band 2 (1710–1885MHz, 1885-1980 MHz, 2010–2025 MHz, 2110–2170 MHz)

- Band 3 (2500–2690 MHz)

The differences in path loss calculation between the free space model and the ITU-R P.528 are evidenced in Appendix A.

7.2.2   Transmit/receive parameters

The simulations are carried out considering different UE terminals of the LTE type i.e., OFDM modulation type and the MCSs are considered in the evaluation. The UE and the HAPS can operate in different frequency bands (indicated in the following with B1, B2 and B3). The radio propagation model ITU-R P.528 has been considered to achieve a more realistic evaluation of the PL which account for the height of the HAPS above the ground [25].

The UE terminal is ranging from (i) a traditional LTE UE, (ii) an intermediate enhanced LTE UE, and (iii) the enhanced LTE UE. The difference among the three types of UE lies in the modem and the eNB parameters including transmission power, transmitter and receiver antenna gains.

The following input parameters are considered for downlink performance evaluation:

- Noise Power Density N_0: -174 dBm/Hz for both UE and the eNB at the HAP. The noise system temperature of the HAP should be different (few Kelvins) with respect to the UE but we neglect this aspect.

- Number of OFDM subcarriers (Nc) in 1.4 MHz LTE band: 72

- Number of OFDM subcarriers (Nc) in 5 MHz LTE band: 300

- Number of OFDM subcarriers (Nc) in 10 MHz LTE band: 600

- Number of OFDM subcarriers (Nc) in 20 MHz LTE band: 1200

The EIRP is calculated in accordance with the formula [26]:

$$EIRP\ [dBm] = GTx + PTx_{eNB} - Loss\ Tx - 10 * log10(Nc)$$

where:

- EIRP: is the Effective Isotropic Radiated Power

- GTx: is the Transmitter Antenna Gain

- PTx: is the Transmitter Antenna Power

- Loss Tx: is the Transmission Loss

- Nc: Number of OFDM subcarriers (depending on the LTE bandwidth)

The following geometric parameters are considered for the UE and the eNB mounted at the HAPS:

- UE antenna height: 1.5 m
- HAPS height: 19 km

Since the HAPS is at height of several km, the adoption of the ITU-R P.528 propagation model is mandatory in place of the free space model. The differences between the estimated path loss with the ITU-R P.528 and the free space model are outlined in Appendix A.

7.3 Simulation results

7.3.1 HAPS Link Budget calculation

The Table 14 summarizes the simulations cases concerning the link budget calculation for the modelled HAPS system in Figure …

Table 14. Simulated cases for HAPS link budget calculation.

No. of the Simulation case	UE terminal	Frequency band	Note
1	Traditional LTE UE	B1 [DL: 960 MHz, UL: 694 MHz]	-
2	Intermediate enhanced LTE UE	B1 [DL: 960 MHz, UL: 694 MHz]	UE Terminal with higher antenna gains
3	Intermediate enhanced LTE UE	B2 [DL: 2000 MHz, UL:1900 MHz]	UE Terminal with higher antenna gains
4	Intermediate enhanced LTE UE	B3 [DL: 2500 MHz, UL:2400 MHz]	UE Terminal with higher antenna gains
5	Full enhanced LTE UE	B1 [DL: 960 MHz, UL: 694 MHz]	UE Terminal with higher antenna gains and TX power
6	Full enhanced LTE UE	B2 [DL: 2000 MHz, UL:1900 MHz]	UE Terminal with higher antenna gains and TX power
7	Full enhanced LTE UE	B3 [DL: 2500 MHz, UL:2400 MHz]	UE Terminal with higher antenna gains and TX power

As described in the next sections, full enhanced LTE UE and Intermediate enhanced LTE UE terminals are considered, together with the traditional UE. It depends on their different technical features that enhance the HAPS performance, in terms of LTE radio coverage.

The main outputs of the simulation are the achievable radio coverage expressed in terms of the horizontal distance of the terminal from the vertical projection of the HAPS on the ground for different MCSs and the calculation of the achievable C/(N+I) as a function of the same horizontal distance. To this purpose we have considered the C/(N+I) requirements of the MCSs specific of the LTE system that are reported in Table 15.

Table 15. C/(N+I) requirements of the MCSs for LTE networks.

MCS		C/(N+I) [dB]
QPSK	1/3	-1
	1/2	2
	2/3	4.3
	3/4	5.5
	4/5	6.2
16 QAM	1/2	7.9
	2/3	11.3
	3/4	12.2
	4/5	12.8
64 QAM	2/3	15.3
	3/4	17.5
	4/5	18.6

As expected, the MCS corresponding to the QPSK 1/3 corresponds to the lower sensitivity which is obtained at the expense of a significant reduction in the spectral efficiency. The 64QAM 4/5 corresponds to the highest spectral efficient MCS and this is achieved at the expense of a higher reference C/(N+I).

7.5.1.1. HAPS Simulation with Traditional LTE UE

The following Table 16 summarizes the main parameters considered in the simulation activities performed in B1 frequency band (694–960 MHz), for both DL and UL. We considered a traditional LTE UE at the following frequencies: 750 MHz in downlink and 690 MHz in uplink. The transmitter/receiver link budget parameters have been set to those which are typical for the handheld LTE devices.

Table 16. HAPS Simulation parameters in considering a traditional LTE UE in downlink and uplink.

Parameter	HAPS Downlink	HAPS Uplink	Unit
Bandwidth	1.4; 5; 10; 20	-	MHz
TX power (eNB)	36.65; 42.9; 45.9; 48.88	29	dBm
TX gain	18	0	dB
Noise figure	7	2	dB
RX gain	3	18	dB
Shadow Margin	6.45	4.5	dB
Body Loss	2	2	dB
TX Loss	2	2	dB
RX Loss	2	2	dB
Interference Margin	5	5	dB
Builging penetration loss	0	0	dB
Number of subcarriers	-	12	-
Number of Physical Resource Block (PRB)	-	6	-

In Table 17 we report the calculated maximum horizontal distance d that can be reached when using a specific MCS in B1 frequency band.

The horizontal distance d is evaluated as:

$$d = \sqrt{r^2 - h^2} \;\; (*)$$

and r in (*) is the UE-HAPS range corresponding to a specific MCS and h is the height of the HAPS from the ground (e.g., 19 km in the considered case).

The horizontal extension of the circular crown where one UE can transmit to the HAPS using the i-th MCS is given by d, where d is the maximum distance at which the UE can transmit using the i-th MCS. As an example, from data in Table 16 the horizontal extension of the circular crown where the UE can transmit using the QPSK 2/3 MCS is given by 36.535-30.088=6.45 km.

Frequency band B1 (694–960 MHz)

Table 17. Horizontal UE-HAPS distance in DL/UL in B1 (694–960 MHz) considering a traditional LTE UE.

MCS	Horizontal Distance [km]				
	DL: 1.4 MHz	DL: 5 MHz	DL: 10 MHz	DL: 20 MHz	UL
QPSK 1/3	72.45	72.874	72.79	72.542	72.834
QPSK 1/2	50.417	50.761	50.693	50.493	50.6
QPSK 2/3	36.535	36.829	36.771	36.6	35.687
QPSK 3/4	30.088	30.363	30.309	30.149	30.229
QPSK 4/5	26.751	26.987	26.94	26.803	26.871
16QAM 1/2	18.947	19.187	19.139	19	19.068
16QAM 2/3	N/A	N/A	N/A	N/A	N/A
16QAM 3/4	N/A	N/A	N/A	N/A	N/A
16QAM 4/5	N/A	N/A	N/A	N/A	N/A
64QAM 2/3	N/A	N/A	N/A	N/A	N/A
64QAM 3/4	N/A	N/A	N/A	N/A	N/A
64QAM 4/5	N/A	N/A	N/A	N/A	N/A

From Table 17 we report the calculated maximum horizontal distance d that can be reached when using a specific MCS in B1 frequency band. It can be observed that the best MCS the typical handheld LTE terminal can use to transmit to the HAPS is the 16 QAM 1/2 and the horizontal extension of the corresponding circular crown is around 19 km. The results in Table 16 evidence that a traditional LTE UE terminal is not able to use MCSs with higher spectral efficiency to communicate with HAPS, thus leading to a reduction on the achievable spectral efficiency. It should be observed that results have been obtained considering LTE transmission in the UHF band and even in this case it is not possible to improve the achievable spectral efficiency. In addition, the horizontal radio coverage is below 100 km, which is the limit foreseen for HAPS applications [23].

For this reason, in order to better exploit the available band improved LTE terminals should be considered for transmission to the HAPS. In the following analysis we have varied some transmitter/receiver parameters of the UE and eNB as well as the transmission frequency so to improve link budget. We talk about full enhanced LTE UE and intermediate enhanced LTE UE. These terminals are characterized by higher antenna gain and radio features even including beamforming if necessary. From a practical point of view, when considering the UE mounted on the train, it should be equipped with: one transmitter amplifier providing more RF power and an antenna with a relatively high gain that in principle should be adaptively oriented to the eNB antenna mounted on the HAPS while the train is moving. The possibility of improving the noise figure (NF) of the receiver at the HAPS or at the UE on the train should be considered so to improve link budget.

7.5.1.2.HAPS Simulation with Intermediate enhanced LTE UE

In this section we consider an Intermediate enhanced LTE UE. We have varied the transmitter and receiver antenna gains while leaving the UE and eNB transmitter powers unchanged. We have also varied the transmitter frequency in the other frequency bands, as shown in Table 18.

Table 18. HAPS simulation parameters considering an Intermediate enhanced LTE UE (in downlink and uplink).

ITU-R P.528 frequency band	HAPS frequency (downlink)	HAPS frequency (uplink)	Unit
B1	750	690	MHz
B2	2,000	1,900	MHz
B3	2,500	2,400	MHz

In the following Table 19 the main parameters are listed, according to the simulation activities performed considering Intermediate enhanced LTE UE both in DL and UL.

Table 19. HAPS simulation parameters considering an Intermediate enhanced LTE UE (in downlink and uplink).

Parameter	HAPS Downlink	HAPS Uplink	Unit
Bandwidth	1.4; 5; 10; 20	-	MHz
TX power (eNB)	36.65;42.9; 45.9; 48.88	28.8	dBm
TX gain	18	6	dB
Noise Figure	7	2	dB
RX gain	6	18	dB
Shadow Margin	4	4	dB
Body Loss	2	0	dB
TX Loss	2	2	dB
RX Loss	2	2	dB
Interference Margin	4	4	dB
Builging penetration loss	0	0	dB

The following tables summarizes the horizontal UE-HAPS distance in B1, B2 and B3 frequency bands respectively for each LTE bandwidth (both DL/UL).

Frequency band B1 (694–960 MHz)

Table 20. Horizontal UE-HAPS distance in DL/UL in B1 (694–960 MHz) considering a Intermediate enhanced LTE UE.

MCS	Horizontal Distance [km]				
	DL: 1.4 MHz	DL: 5 MHz	DL: 10 MHz	DL: 20 MHz	UL
QPSK 1/3	200.9	202.09	201.86	201.16	201.58
QPSK 1/2	145.79	146.62	146.46	145.98	144.17
QPSK 2/3	113.19	113.85	113.72	113.34	111.87
QPSK 3/4	99.6	100.15	100.04	99.722	98.575
QPSK 4/5	92.488	92.994	92.894	92.6	91.555
16QAM 1/2	76.989	77.436	77.347	77.087	76.152
16QAM 2/3	51.407	51.755	51.685	51.483	50.6
16QAM 3/4	45.618	45.945	45.88	45.691	44.86
16QAM 4/5	41.987	42.294	42.234	42.055	41.26
64QAM 2/3	28.382	28.624	28.576	28.436	27.807
64QAM 3/4	18.25	18.494	18.446	18.304	17.664
64QAM 4/5	12.704	12.987	12.931	12.767	N/A

As from Table 20, almost all the MCSs can be used in B4. They are ranging from QPSK 1/3 (at edge cell, around 200 and 201 km) up to 64 QAM 3/4 (at the minimum horizontal distance from the HAPS, around 18 km in downlink and 17 km in uplink).

The 64 QAM 4/5 MCS is only available in downlink. In uplink it cannot be used.

Also in this case, the analysis results evidence that an intermediate enhanced LTE UE can guarantee higher performance than traditional LTE UE.

Frequency band B2 (2,000–1,900 MHz)

Table 21. Horizontal UE-HAPS distance in DL/UL in B2 (2,000–1,900 MHz) considering a Intermediate enhanced LTE UE.

MCS	Horizontal Distance [km]				
	DL: 1.4 MHz	DL: 5 MHz	DL: 10 MHz	DL: 20 MHz	UL
QPSK 1/3	77.52	77.952	77.866	77.615	74.357
QPSK 1/2	55.476	55.81	55.744	55.549	52.982
QPSK 2/3	41.656	41.953	41.894	41.722	39.397
QPSK 3/4	34.959	35.244	35.188	35.022	32.782
QPSK 4/5	31.21	31.482	31.428	31.27	29.125
16QAM 1/2	23.174	23.411	23.364	23.226	21.326

16QAM 2/3	2.5397	3.5191	3.3478	2.7851	N/A
16QAM 3/4	N/A	N/A	N/A	N/A	N/A
16QAM 4/5	N/A	N/A	N/A	N/A	N/A
64QAM 2/3	N/A	N/A	N/A	N/A	N/A
64QAM 3/4	N/A	N/A	N/A	N/A	N/A
64QAM 4/5	N/A	N/A	N/A	N/A	N/A

The possibility of increasing the transmitter and receiver antenna gains allow to improve radio coverage and the spectral efficiency thus compensating the propagation effects due to higher transmission frequency. As from Table 21, only the MCSs available in B2 are ranging from QPSK 1/3 (at edge cell, around 148 and 150 km) up to 16 QAM 2/3 (at the minimum horizontal distance from the HAPS, around 2.7 km). In uplink it cannot be used.

However, even in this case the UE is not able to use MCSs with higher spectral efficiency, as the other 16 QAM and 64 QAM MCSs.

Frequency band B3 (2,500–2,400 MHz)

Table 22. Horizontal UE-HAPS distance in DL/UL in B3 frequency band (2,500–2,400 MHz) considering an Intermediate enhanced LTE UE.

MCS	Horizontal Distance [km]				
	DL: 1.4 MHz	DL: 5 MHz	DL: 10 MHz	DL: 20 MHz	UL
QPSK 1/3	62.121	62.493	62.419	62.202	58.839
QPSK 1/2	43.442	43.737	43.679	43.507	40.732
QPSK 2/3	31.001	31.273	31.219	31.61	28.52
QPSK 3/4	25.269	25.509	25.462	25.322	23.014
QPSK 4/5	22.07	22.312	22.264	22.124	19.803
16QAM 1/2	13.946	14.22	14.166	14.007	11.19
16QAM 2/3	N/A	N/A	N/A	N/A	N/A
16QAM 3/4	N/A	N/A	N/A	N/A	N/A
16QAM 4/5	N/A	N/A	N/A	N/A	N/A
64QAM 2/3	N/A	N/A	N/A	N/A	N/A
64QAM 3/4	N/A	N/A	N/A	N/A	N/A
64QAM 4/5	N/A	N/A	N/A	N/A	N/A

As from Table 22, the effect of increasing frequency is that of coverage and spectral efficiency reduction. In fact, only the MCSs available in B3 are ranging from QPSK 1/3 (at edge cell, around 120 km) up to 16 QAM 1/2 (at the minimum horizontal distance from the HAPS, around 14 km in downlink and 19 km in uplink).

Also in this case, the analysis results evidence that the intermediate UE LTE like terminal is not able to use MCSs with higher spectral efficiency, as the other 16 QAM and 64 QAM MCSs.

7.5.1.3. HAPS Simulation with full enhanced LTE UE

In the following, we have repeated all the simulations considering a full enhanced UE LTE like terminal where we have increased the transmitter/receiver antenna gains and the UE transmitter power. The frequencies considered are the same of the intermediate LTE UE case, as shown in Table 18. Table 23 summarizes the main HAPS simulation parameters in case of a full enhanced LTE UE

Table 23. HAPS Simulation parameters considering a full enhanced LTE UE: downlink (a), uplink (b).

Parameter	HAPS Downlink	HAPS Uplink	Unit
Bandwidth	1.4; 5; 10; 20	-	MHz
TX power (eNB)	36.65;42.9; 45.9; 48.88	29.3	dBm
TX gain	21	9	dB
RX gain	9	21	dB
Shadow Margin	4	4	dB
Noise Figure	7	2	dB
Body Loss	2	0	dB
TX Loss	2	2	dB
RX Loss	2	2	dB
Interference Margin	4	4	dB
Builging penetration loss	0	0	dB
Number of sub carriers	-	12	-
Number of Physical Resource Block (PRB)	-	6	-

Frequency band B1 (694–960 MHz)

Table 24 summarizes the UE-HAPS horizontal distance in case of B1 band (694–960 MHz) and for each LTE bandwidth (both DL/UL).

Table 24. Horizontal UE-HAPS distance in DL/UL in B1 (694–960 MHz) considering a full enhanced LTE UE.

MCS	Horizontal Distance [km]				
	DL: 1.4 MHz	DL: 5 MHz	DL: 10 MHz	DL: 20 MHz	UL
QPSK 1/3	344.96	345.4	345.31	345.06	347.47
QPSK 1/2	267.65	268.46	268.32	267.84	277.7
QPSK 2/3	218.65	220.1	219.81	218.97	236.52
QPSK 3/4	190.37	191.39	191.19	190.59	201.58
QPSK 4/5	176.83	177.81	177.61	177.04	184.81
16QAM 1/2	147.38	148.22	148.05	147.57	153.85
16QAM 2/3	101.73	102.29	102.18	101.85	106.15
16QAM 3/4	92.488	92.994	92.894	92.6	96.526
16QAM 4/5	86.753	87.242	87.145	86.86	90.581
64QAM 2/3	65.79	66.183	66.106	65.877	68.826
64QAM 3/4	50.086	50.431	50.363	50.162	52.611
64QAM 4/5	43.173	43.49	43.428	43.243	45.477

As from Table 24, all the MCSs can be used in B1 with a full LTE terminal. They are ranging from QPSK 1/3 (at edge cell, around 345 and 347 km) up to 64 QAM 4/5 (at the minimum horizontal distance from the HAPS, around 43 km in downlink and 52 km in uplink). The analysis results evidence that a full enhanced LTE UE can guarantee higher performance.

Frequency band B2 (2,000–1,900 MHz)

Table 25 summarizes the UE-HAPS horizontal distance in case of B2 (2,000–1,900 MHz) and for each LTE bandwidth (both DL/UL).

Table 25. Horizontal UE-HAPS distance in DL/UL in B2 (2,000–1,900 MHz) considering a full enhanced LTE UE.

MCS	Horizontal Distance [km]				
	DL: 1.4 MHz	DL: 5 MHz	DL: 10 MHz	DL: 20 MHz	UL
QPSK 1/3	148.78	149.56	149.41	148.95	150.54
QPSK 1/2	108.17	108.79	108.67	108.3	109.43
QPSK 2/3	83.569	84.039	83.946	83.672	84.571
QPSK 3/4	73.457	73.873	73.791	73.549	74.357
QPSK 4/5	68.004	68.397	68.32	68.091	68.846
16QAM 1/2	56.122	56.462	56.395	56.197	56.853
16QAM 2/3	36.049	36.332	36.277	36.112	36.58
16QAM 3/4	31.21	31.482	31.428	31.27	31.71
16QAM 4/5	28.219	28.461	28.413	28.272	28.664
64QAM 2/3	16.656	16.911	16.861	16.712	17.124
64QAM 3/4	N/A	N/A	N/A	N/A	N/A
64QAM 4/5	N/A	N/A	N/A	N/A	N/A

As from Table 25, almost all the MCSs can be used in B2 with a full LTE terminal. They are ranging from QPSK 1/3 (at edge cell, around 149 and 150 km) up to 64 QAM 2/3 (at the minimum horizontal distance from the HAPS, around 16 km in downlink and 17 km in uplink). 64 QAM ¾ and 64 QAM 4/5 MCSs cannot be used. The analysis results evidence that a full enhanced LTE UE can guarantee higher performance.

Frequency band B3 (2,500–2,400 MHz)

Table 26 summarizes the UE-HAPS horizontal distance in case of B3 (2,500–2,400 MHz) and for each LTE bandwidth (both DL/UL).

Table 26. Horizontal UE-HAPS distance in DL/UL in B3 (2,500–2,400 MHz) considering a full enhanced LTE UE.
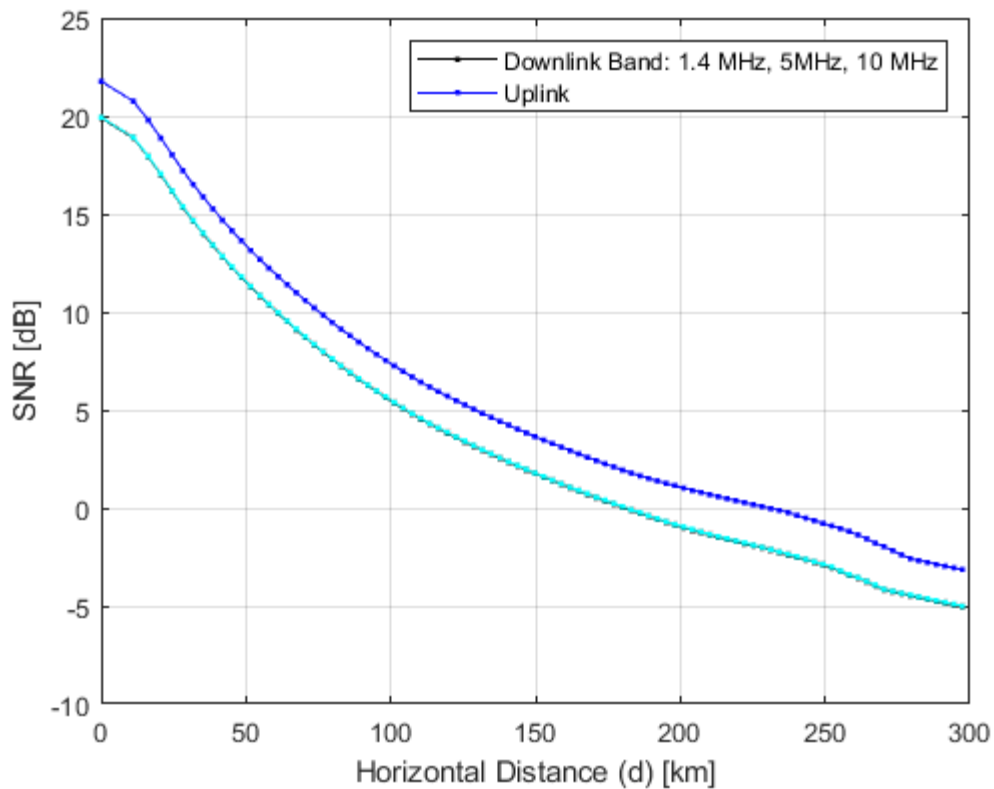
MCS	Horizontal Distance [km]				
	DL: 1.4 MHz	DL: 5 MHz	DL: 10 MHz	DL: 20 MHz	UL
QPSK 1/3	120.8	121.47	121.34	120.95	120.98
QPSK 1/2	86.657	87.172	87.069	86.77	86.769
QPSK 2/3	67.201	67.589	67.512	67.287	67.335
QPSK 3/4	58.714	59.062	58.993	58.791	58.839
QPSK 4/5	54.146	54.482	54.415	54.22	54.252
16QAM 1/2	44.008	44.302	44.244	44.073	44.087
16QAM 2/3	26.186	26.422	26.376	26.238	26.208
16QAM 3/4	22.07	22.312	22.264	22.124	22.093
16QAM 4/5	19.309	19.555	19.506	19.363	19.332
64QAM 2/3	36.541	43.979	42.607	38.303	37.284
64QAM 3/4	N/A	N/A	N/A	N/A	N/A
64QAM 4/5	N/A	N/A	N/A	N/A	N/A

As from Table 26, the MCSs to be used in B3 with a full LTE terminal are ranging from QPSK 1/3 (at edge cell, around 120 km and 121 km) up to 64 QAM 2/3 (at the minimum horizontal distance from the HAPS, around 38 or 43 km in downlink and 37 km in uplink). Also in this case, 64 QAM ¾ and 4/5 MCSs cannot be used. The analysis results evidence that a full enhanced LTE UE can guarantee higher performance.

7.3.2 C/N and C/(N+I) calculation

In Figure 52 we plot the C/(N+I) ratio vs the horizontal distance d in downlink (with 1.4 MHz, 5 MHz and 10 MHz bandwidth) and uplink, depending on the horizontal distance. The intermediate terminal case has been considered for evaluation purposes.

Figure 52. C/N calculation for the HAPS in uplink and downlink.

In downlink, the C/N is around 20 dB at the minimum horizontal distance. It decreases to 5 dB at 100 km and -5 dB at 300 km. in uplink, the SNR is around 22 dB at the minimum horizontal distance, 7 dB at 100 km, and -2 dB at 300 km.

The curves of the downlink C/N are super-imposed in all cases. This fact is not surprising since the link budget parameters have always been selected to provide a balanced coverage between uplink and downlink and to guarantee that coverage is independent of the bandwidth for DL.

Figure 53 shows the SINR ratio trend in downlink (with 1.4 MHz, 5 MHz and 10 MHz bandwidth) and uplink, depending on the horizontal distance.

Figure 53. C/(N+I) calculation for the HAPS in uplink and downlink.

The C/(N+I) has been evaluated taking into account for the several interference effects in DL and UL including the ACI and the 3rd order intermodulation (3IM).
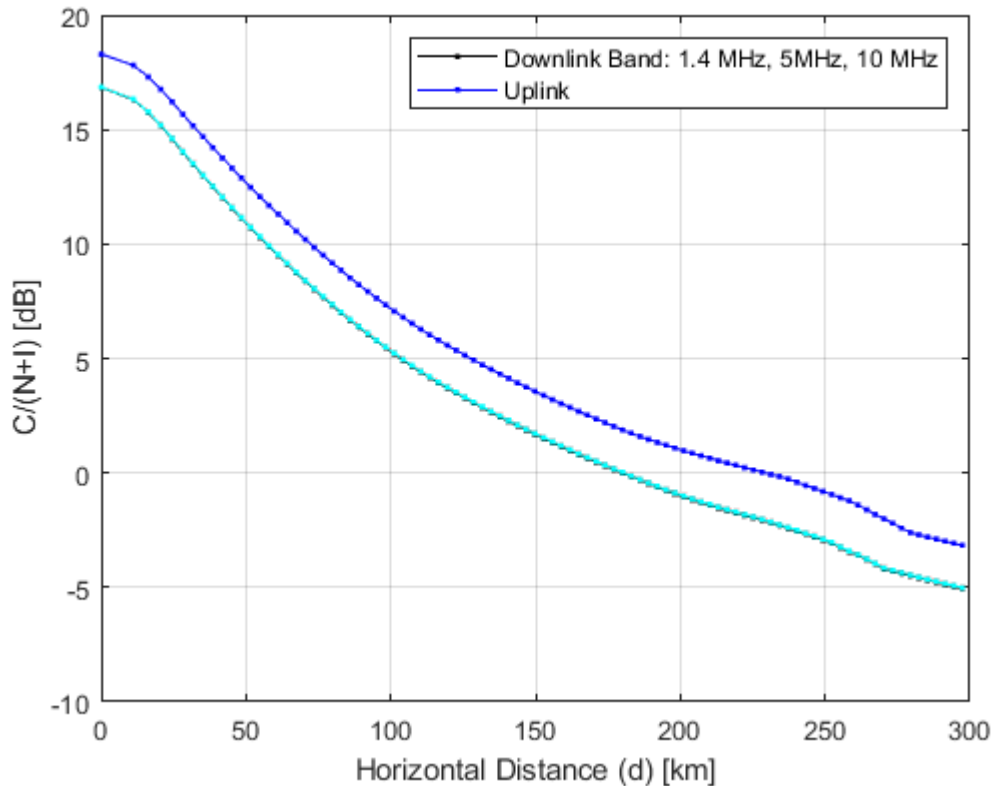
In downlink, the C/(N+I) is around 16 dB at the minimum horizontal distance. It decreases to 5 dB at 100 km and -5 dB at 300 km. In uplink, the C/(N+I) is around 18 dB at the minimum horizontal distance, 7 dB at 100 km, and -2 dB at 300 km.

8. Conclusions

In this deliverable, we have presented the main results related to the assessment of selected ABs i.e., FSO, HAPS, and LEO, in case of static and dynamic railway scenarios.

We provide the main outcomes in case of static and dynamic railway scenarios, where different ABs take place. The document details the setup and results obtained from simulation and emulation of the eligible ABs using the tools in our labs.

Specifically, FSO technology is the sole one that well fits into the static scenarios (i.e., within the train stations) due to its technology features and the impact on the railway sector. The assessment of FSO technology has been carried out through extensive simulations. For this aim, we developed our own simulator that allows to simulate FSO connectivity links both in static and dynamic scenarios. In order to better simulate realistic FSO links, we considered different attenuation models mainly due to atmospheric turbulence, pointing error, and fog/smoke attenuation. Simulation results have been obtained in terms of BER for different connectivity links and attenuation models. As a main outcome, we can observe that shorter FSO links allow to achieve lower BER, as well as adding attenuation losses provides a degradation of link performance. In case of dynamic scenarios i.e., mainline, regional, and freight, we considered a fixed FSO source and the receiver PD moving, so that variable link lengths are achieved. A more realistic dynamic scenario is comprised of a single and double beam model, where multiple FSO transmitters are properly deployed along the railway track. With this scheme, we can achieve more stable connectivity links that do not overcome fixed lengths, thus guaranteeing stable link performance.

Regarding the LEO constellations, we considered the Starlink SpaceX and OneWeb constellations. When the LEO satellite is visible from the ground station (the minimum required elevation angle is 15°), from the carried simulations a quite constant satellite service level is evidenced in all situations. A minimum performance targeted in terms of SINR and corresponding offered Bit Rate is present. It is fully compliant with the Network-as-a-Service (NaaS), already discussed in the previous D2.3 deliverable. For each LEO satellite beam, a very considerable aggregated traffic capacity is provided: from 800 Mbps to the Gbps as an aggregate stream, depending on the Modulation and Coding Scheme (MCS). We considered the DVB-S2 modulation schemes for the Bit Rate calculation. We can also identify the best DVB-S2 modulation format and the maximum Bit Rate value, according to the formula: (spectral efficiency * Bandwidth) = minimum Bit Rate. This considerable amount of capacity is very important to manage huge amount of data, as foreseen in specific ACS traffic class, especially in the tomorrow situation (e.g., for video data application in uplink). This makes the LEO technology as a very interesting and competitive AB with the terrestrial communication technologies (e.g., 5G). The high data rate capacity provided by the LEO technologies it is also important for assuring a greater reliability of the connections and for reducing the re-transmissions in case of failures. In this way, the transmission of mission-critical applications can be guaranteed in terms of communication link reliability, although the communication delay must be always verified with the required target. The QoS / QoE aspects are to be managed carefully by the LEO operator according to the ACS service requirement. The DL and UL link are basically balanced because they almost reach the same SINR values. It evidences a sufficient level of LEO constellation coverage radio planning.

The HAPS is currently used as a physical asset hosting the LTE eNB, and in the future the 5G gNB. HAPS has a reduced altitude from the ground (at about 20 km), and it can be assumed almost a static system (affected by a few oscillations). In the three different frequency bands (identified by the ITU-R P.528 propagation model), the traditional UE gives a poor performance in the band B1 (694–960 MHz) in terms of MCS adoption and the corresponding available spectral efficiency. In this band, it can only use MCS ranging from QPSK 1/3 (at edge cell) up to 16QAM 1/2 (at the minimum horizontal distance from the HAPS, around 26 km). Other 16QAM and 64QAM MCS cannot be implemented. A quite similar result is present in the other frequency band B2 (1710–1885MHz, 1885-1980 MHz, 2010–2025 MHz, 2110–2170 MHz) and band B3 (2500–2690 MHz). 64QAM ¾ and 64QAM 4/5 MCSs guaranteeing higher spectral efficiency cannot be used by a traditional UE terminal. Full-enhanced LTE UE and intermediate LTE UE provide higher performance in B1 than a traditional UE in terms of coverage, MCS and corresponding spectral efficiency to be offered. These results allow confirming that the HAPS system hosting an LTE eNB cannot include a traditional UE terminal for ACS communications. The performance in terms of coverage and spectral efficiency are very poor. Several ACS traffic classes cannot be supported. The involvement of full-enhanced LTE UE and intermediate LTE UE terminals are only to be assumed for ACS applications. As described in D2.3, both in the case of LEO and HAPS, the Infrastructure Manager (IM) need to sign a cooperation model with the LEO and HAPS network operators, based on specific target requirements for ACS applications.

The results evidence the applicability of FSO, LEO, and HAPS to be used as ABs for ACS applications in railway scenarios. Their technical feasibility allows having a huge capacity for data transmission. This is very important, especially for the bandwidth-consuming ACS applications in tomorrow's railway scenarios.

The challenges related to the FSO devices mainly regard the necessity to deploy an FSO network considering the atmospheric issues and the mobility of the train. A dedicated system for managing the FSO TX-RX coupling in a dynamic scenario is to be provided. On LEO and HAPS, the main challenges are related to the specific agreements to be signed in cooperation with LEO and HAPS network providers.

This deliverable D2.4 is compliant with the planned objectives. It provides not only simulation results on FSO, LEO, and HAPS but also some useful considerations on network deployment. The main findings and results contained in this deliverable will be described and illustrated within the dissemination and exploitation activities, including the final meeting and the final report on dissemination and exploitation.

Future works to be proposed can be focused on the performance analysis in the lab and in the field using physical devices and prototypes. These activities need a specific memorandum of understanding (MoU) to be signed with LEO and HAPS network providers, while concerning FSO it is suggested to investigate research companies which are developing equipment and devices related to dynamic scenarios.

Appendix A

The Path Loss is calculated considering both the Free Space Path Loss (FSPL) and ITU-R P.528. Figure 54 shows the Path Loss trend where both models are applied in each frequency band B1 (694–960 MHz), B2 (2,000–1,900 MHz) and B3 (2,000–1,900 MHz), depending on the distance between UE and the eNB on the HAPS.

Figure 54. Path Loss calculation for the HAPS: Free Space Path Loss and ITU-R P.528 propagation models.
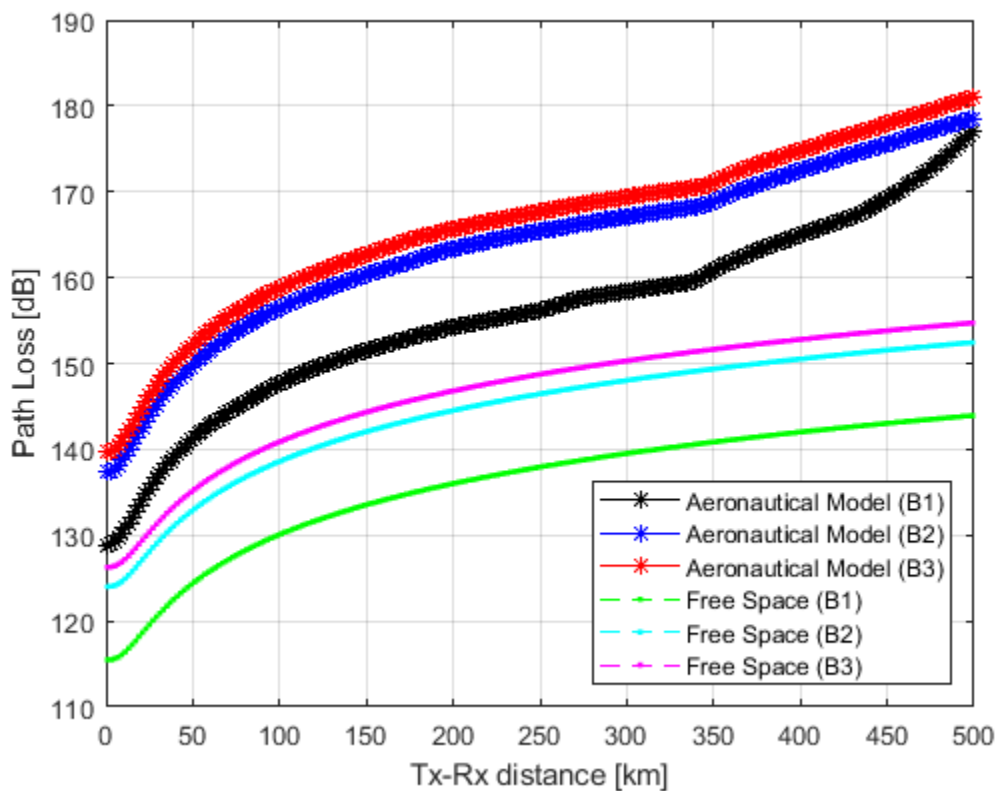
In case of ITU-R P.528 radio propagation model, in B1 frequency band the Path Loss is around 140 dB if the TX - RX distance is around 50 km, 148 dB at 100 km, and over 150 dB at 200 km. At 500 km, it overcomes 175 dB. In B2 and B3 frequency bands, the Path Loss has a trend quite similar. With a TX-RX distance of 50 km, the Path Loss is around 150 dB, overcomes 160 dB at 150 km and 180 dB at 500 km.

If the Free Space Path Loss (FSPL) radio propagation model is applied, the Path Loss has a decreasing trend from B1 to B3 frequency band. In B3 frequency band, it is around 141 dB with a TX-RX distance of 100 km, 150 dB at 300 km, and 155 dB at 500 km. In B2 frequency band, the Path Loss is 132 dB at 50 km, over 140 dB at 150 km, and around 152 dB at 500 km. Finally, in B1 the Path Loss assumes the lowest values: at 50 km it is around 125 dB, at 200 km around 135 dB, and at 500 km it is under 145 dB.

Within the 200 km of horizontal UE-HAPS distance, the performance is considerable due to the path loss and the SINR provided by the HAPS. While the final BR offered to the end user (4G LTE user in our simulations) depending on the MCS, values of Path Loss and SINR around 140 (FSPL model) or 160 dB (ITU-R P.528 model), and 0 dB respectively, evidence an acceptable system performance in the considered railway scenario.

References

[1] AB4Rail Project Deliverable 2.2, "Assessment of ABs benefits challenges and impact on infrastructure", 2021

[2] EC SYSTEM, EL-1GL FSO device datasheet (URL:http://www.ecsystem.cz/en/products/free-space-optic-equipment/free-space-optics-1-gbps)

[3] Starlink Kit description (URL: https://www.starlink.com/kit)

[4] OneWeb kit description (URL: https://oneweb.net/resources/hardware/user-terminals)

[5] THE HAPS ALLIANCE, "Unlocking the potential of the stratosphere, Q2 2022 (URL: https://hapsalliance.org/wp-content/uploads/formidable/16/HAPS_Alliance_Pitch_Deck_-_2022-Q2_FINAL.pdf)

[6] THE HAPS ALLIANCE, The HAPS Alliance Commends the GSMA for White Paper on HAPS Opportunities (URL: https://hapsalliance.org/blog/the-haps-alliance-commends-the-gsma-for-white-paper-on-haps-opportunities/

[7] GSMA, "High Altitude Platform System – A point of view from the mobile operators" (URL: https://www.gsma.com/futurenetworks/latest-news/high-altitude-platform-system-a-point-of-view-from-the-mobile-operators/#.Yhzgl8GEVvI.twitter)

[8] Rete Ferroviaria Italiana (RFI), "Rome-Florence 'Direttissima' High Speed line" (URL: https://www.italferr.it/content/italferr/en/proejct-studies/italia1/alta-velocita---alta-capacita/firenze-roma.html)

[9] "Optical Wireless Communications", System and Channel Modelling with MATLAB®, Z. Ghassemlooy, W. Popoola, S. Rajbhandari, 2nd Edition 2018, CRC Press

[10] Q. Fan, N. Ansari, J. Feng, R. Rojas-Cessa, M. Zhou and T. Zhang, "Reducing the Number of FSO Base Stations With Dual Transceivers for Next-Generation Ground-to-Train Communications," in IEEE Transactions on Vehicular Technology, vol. 67, no. 11, pp. 11143-11153, Nov. 2018, doi: 10.1109/TVT.2018.2870065.

[11] SpaceX LEO Satelllite coverage Map (URL: https://satellitemap.space/)

[12] SpaceX gateway station list (URL: https://www.are.na/block/11941813)

[13] del Portillo Barrios, Inigo & Cameron, Bruce & Crawley, Edward., "A technical comparison of three low earth orbit satellite constellation systems to provide global broadband", 2019. Acta Astronautica. 159. 10.1016/j.actaastro.2019.03.040.

[14] ETSI EN 302 307, "Digital Video Broadcasting (DVB), 2014, Second generation framing structure, channel coding and modulation systems for broadcasting; Part2: DVB-SE extensions (DBVS2X)".

[15] P.618-13 (12/2017) ITU Recommendation: Propagation data and prediction methods required for the design of Earth-space telecommunication systems

[16] G. Bonafè, F. Senesi, "Applicazioni ERTMS / ETCS su linee convenzionali RFI URL: http://www.cifi.it/UplDocumenti/CIFI%20ERTMS%20ETCS%20%20BOLOGNA.pdf)

[17] North American Aerospace Defense Command (NORAD) (URL: https://www.norad.mil/)

[18] Celestrak repository (URL: https://celestrak.org/)

[19] Satellite Communications Toolbox (URL: https://it.mathworks.com/products/satellite-communications.html)

[20] J. Ko et al., "Millimeter-Wave Channel Measurements and Analysis for Statistical Spatial Channel Model in In-Building and Urban Environments at 28 GHz," in IEEE Transactions on Wireless Communications, vol. 16, no. 9, pp. 5853-5868, Sept. 2017, doi: 10.1109/TWC.2017.2716924.

[21] Cotton SL, D'Errico R, Oestges C. A review of radio channel models for body centric communications. Radio Sci. 2014 Jun;49(6):371-388. doi: 10.1002/2013RS005319. Epub 2014 Jun 12. PMID: 26430285; PMCID: PMC4579845.

[22] ETSI EN 302 307 V1.1.2 (2006-06)

[23] L. C. Alexandre, A. Linhares, G. Neto and A. C. Sodre, "High-Altitude Platform Stations as IMT Base Stations: Connectivity from the Stratosphere," in IEEE Communications Magazine, vol. 59, no. 12, pp. 30-35, December 2021, doi: 10.1109/MCOM.001.2100477.

[24] Recommendation ITU-R P.525-4 (08/2019) "Calculation of free-space attenuation"

[25] Recommendation ITU-R P.528 "A propagation prediction method for aeronautical mobile and radionavigation services using the VHF, UHF and SHF bands"

[26] Distributed Computer and Communication Networks, 23rd International Conference, DCCN 2020, Moscow, Russia, September 14–18, 2020.